Experimental and Modeling Studies of Oil Shale Oxy-fuel Combustion

CAN RÜSTÜ YÖRÜK

TALLINN UNIVERSITY OF TECHNOLOGY
Faculty of Chemical and Materials Technology
Laboratory of Inorganic Materials

This dissertation was accepted for the defense of the degree of Doctor of Philosophy in Chemical and Materials Technology on September 15, 2016.

Supervisor: Professor Andres Trikkel, Laboratory of Inorganic Materials, Tallinn University of Technology

Co-Supervisor: Ph.D. Rein Kuusik, Senior Research Scientist, Laboratory of Inorganic Materials, Tallinn University of Technology

Opponents: Professor Ron Zevenhoven, Thermal and Flow Engineering Laboratory, Åbo Akademi University

Ph.D. Indrek Aarna, Head of the Research and Development Department of Eesti Energia

Defense of the thesis: October 27, 2016, at 11:00, Lecture hall: SOC–311
Tallinn University of Technology, Ehitajate tee 5, Tallinn, Estonia

Declaration:
Hereby I declare that this doctoral thesis, my original investigation and achievement, submitted for the doctoral degree at Tallinn University of Technology has not been submitted for any academic degree.

Can Rüstü Yörük

Põlevkivi hapnikus põletamise eksperimentaalne uurimine ja modelleerimine

CAN RÜSTÜ YÖRÜK

TABLE OF CONTENTS

LIST OF PUBLICATIONS

I   Meriste, T.; Yörük, C.R.; Trikkel, A.; Kaljuvee T.; Kuusik, R. TG–FTIR Analysis of Oxidation Kinetics of Some Solid Fuels Under Oxy-fuel Conditions. Journal of Thermal Analysis and Calorimetry 2013, 114(2), 483-489. doi: 10.1007/s10973-013-3063-x

II   Yörük, C.R.; Meriste, T.; Trikkel, A.; Kuusik, R. Thermo-oxidation Characteristics of Oil Shale and Oil Shale Char Under Oxy-fuel Combustion Conditions. Journal of Thermal Analysis and Calorimetry 2015, 121(1), 509-516. doi: 10.1007/s10973-015-4484-5

III Yörük, C.R.; Trikkel, A.; Kuusik, R. Oxy-fuel Combustion of Estonian Oil Shale: Kinetics and Modeling. Energy Procedia 2016, 86, 124–33. doi:10.1016/j.egypro.2016.01.013

IV   Yörük, C.R.; Trikkel, A.; Kuusik, R. Prediction of Flue Gas Composition and Comparative Overall Process Evaluation for Air and Oxy-fuel Combustion of Estonian Oil Shale using Aspen Plus Process Simulation. Energy&Fuels 2016. doi:10.1021/acs.energyfuels.6b00022 (available online)

Copies of these publications are included in APPENDIX A.

Other publication related to the research:

Yörük, C.R.; Normann, F.; Johnsson, F.; Trikkel, A.; Kuusik, R. Applicability of the FB reactor of Aspen Plus for CFB Oxy-fuel Combustion of Estonian Oil Shale: Gas and Solid Hydrodynamics. 22nd International conference on fluidized bed conversion 2015, Turku, Finland. Ed. D. Bankiewicz, M. Mäkinen, P. Yrjas. VTT, 150−159. (Peer reviewed conference paper)
Online source:
https://www.researchgate.net/publication/306504231_Applicability_of_the_FB_reactor_of_Aspen_Plus_for_CFB_Oxy-fuel_Combustion_of_Estonian_Oil_Shale_Gas_and_Solid_Hydrodynamics

THE AUTHOR´S CONTRIBUTION

The contribution of the author to the papers listed below is as follows:

I   The author participated in the experimental work and contributed the writing of manuscript. The applicant performed the kinetic analysis and he has minor role in writing of the paper.

II   The author carried out the experimental work and participated in the interpretation of results. He has major role in writing of the paper.

III   The author participated in planning of work. He performed the experimental and process modeling work. He was responsible for writing the manuscript and is the corresponding author.

IV   The author had the lead role in planning and performing the process modeling. He wrote the paper and is the corresponding author. He was responsible for analyzing and interpretation of the results.

INTRODUCTION

Carbon dioxide (CO_2) is a major greenhouse gas (GHG) emitted to the atmosphere mainly by human activities, such as burning of fossil fuels, which causes the atmospheric CO_2 concentrations to increase. Different options have been proposed to achieve a sustainable reduction of CO_2 emissions, e.g., fuel switching to lower C/H ratios, energy generation from non-fossil sources (nuclear power and renewables), increases in energy efficiency, direct flue gas cleaning, and carbon dioxide capture and storage (CCS). There is no doubt that renewables, nuclear power and improvements in energy efficiency are important for a low carbon economy, and these options will play an even more significant role in the near future. However, the usage of fossil fuels must also be considered to obtain a complete solution, especially for developing countries. As long as fossil fuels are a major feature of meeting global energy demands (fossil fuels will account for around 40% of primary energy use in 2050) [1], long term climate goals cannot be reached without their usage.

According to this global portfolio, power generation by firing fossil fuels with low carbon emissions is a key aspect, and CCS is the only technology that allows continued use of fossil fuels while also substantially reducing GHG emissions. The three main CO_2 capture technologies are: pre-combustion, post-combustion, and oxy-fuel (OF) combustion. Additionally, chemical looping is another CO_2 capture technology that is competitive and increasingly studied for CCS. Although the choice of capture technology depends on several factors, capture technologies are more efficient if the concentration of CO_2 in the flue gases is increased. A possible technology for achieving this is OF combustion which enables an increase of the CO_2 concentration in exhaust gas. In this technology, nitrogen (N_2) is separated from air in an air separation unit (ASU), and the combustion process is carried out using oxygen (O_2) and recycled combustion products, which are mainly CO_2 and water (H_2O) vapor.

OF combustion can easily be applied to pulverized combustion (PC) and fluidized bed (FB) combustion technologies. Over the last few years, laboratory studies and pilot-scale experiments have indicated that OF combustion is a favorable option for retrofitting conventional coal and coal-biomass firing systems. OF combustion with CCS is already part of the CO_2 mitigation solution, as the first generation of circulating fluidized bed (CFB) boilers with OF combustion has been demonstrated (CIUDEN 30 MWth) to be a reliable and feasible technology, and full-scale commercialization is expected from several projects, such as Compostilla–Spain, FutureGen–USA, and White Rose–UK [2].

These developments have also been one of the main fields of interests in the energy sector of Estonia, and fundamental research has progressed together with the pilot-scale study on OF combustion at Tallinn University of Technology.

Power stations in Estonia use a non-conventional local fossil fuel, Estonian oil shale (EOS), to meet thermal power demands and provide over 90% of the electricity in Estonia. Both PC and CFB boilers operate in the power stations.

Based on operating experience since 2004, CFB boilers appear to be more suitable for low-rank, high-sulfur, and high-ash fuels like EOS in terms of combustion efficiency and reduced emissions, including CO_2 emissions. However, owing to the extensive usage of EOS in electricity production, the reduction in CO_2 emissions remains a great challenge, and future cuts in CO_2 emissions require the application of CCS.

In this context, OF combustion technology could be a new strategy for Estonia, which would reduce the impact of CO_2 emissions and give more freedom to energy policies by maintaining the usage of local primary energy supplies. However, the complicated composition of organic and mineral matter in EOS increases the importance of investigating its use under different combustion conditions such as OF combustion, on which there is limited knowledge and almost no experience. Thus, obtaining technical knowledge about design to progress CFB OF combustion operations, which is the topic of this present study, is crucial. The research in this thesis includes experimental investigations and process modeling to understand and analyze the complex combustion behavior of EOS under various conditions with the aim of generating a fundamental knowledge base for OF combustion of EOS that could possibly lead to its integration in the electricity infrastructure of Estonia.

LIST OF ABBREAVIATIONS

ASU	Air separation unit
CFB	Circulating fluidized bed
CFBC	Circulating fluidized bed combustion
CCS	Carbon dioxide capture and storage/sequestration
DTA	Differential thermal analysis (heat effects)
DTG	Differential/derivative thermogravimetry (mass change rate)
EGA	Evolved gas analysis
FB	Fluidized bed
FGC	Flue gas condensation
FGD	Flue gas desulfurization
FTIR	Fourier transform infrared spectroscopy
GHG	Greenhouse gas
HHV	Higher heating value
IGCC	Integrated gasification combined cycle
MDEA	Methyldiethanolamine
MEA	Monoethanolamine
OF	Oxy-fuel
OS (EOS)	Oil shale (Estonia oil shale)
PC	Pulverized combustion
PSD	Particle size distribution
RFG	Recycled flue gas
TA	Thermal analysis
TG	Thermogravimetry (mass change)
UOS	Utah oil shale

1. LITERATURE REVIEW

In this chapter, a short overview of the three main CO_2 capture technologies used for CCS is given, with an emphasis on OF combustion. Further, the literature review provides insight into the characteristics of solid fuel (coal, biomass, and oil shale (OS)) combustion in various atmospheres by discussing selected experimental and modeling studies for OF combustion.

1.1 Overview of CO_2 capture

The text in this section, which is based on Ref. [3-8], summarizes and explains the CO_2 capture technologies. There are three main types of CO_2 capture systems: post-combustion, pre-combustion, and OF combustion. In general, the concentration of CO_2 in the gas stream, the pressure of the gas stream, and the fuel type (solid or gas) are important factors in selecting the capture system.

1.1.1 Post combustion

Post-combustion capture refers to the removal of CO_2 from the flue gas of conventional fossil-fuel-fired power plants. This process is typically performed via chemical absorption with amine-based chemical solvents, such as monoethanolamine (MEA) and methyldiethanolamine (MDEA). This technology is attractive owing to the ease of retrofitting and, as the operations have reached a commercial stage, it operates in a mature market. The configuration of a post-combustion capture system is shown in Fig. 1.
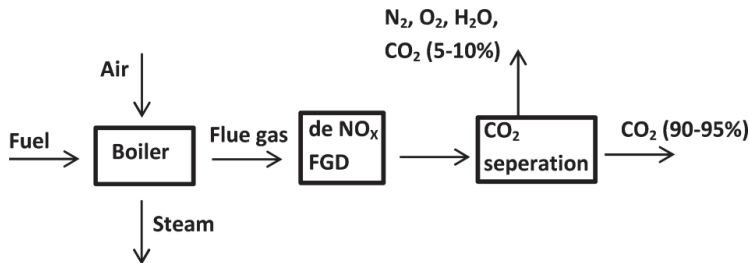
Figure 1. Configuration of post combustion capture

The low concentration of CO_2 in the flue gas (normally <15 vol%), high energy requirement for solvent regeneration, and costly absorption process (owing to the required equipment and large volume of absorbents) are the main drawbacks of this technology, which also cause an efficiency penalty for the overall power plant.

1.1.2 Pre-combustion

The pre-combustion process typically involves the conversion of a carbonaceous fuel, such as coal, biomass, natural gas, or oil, into a gaseous mixture that primarily consists of H_2 and CO, called syngas. This process is performed in an integrated gasification combined cycle (IGCC) with a shift reactor to convert CO to CO_2, followed by a CO_2 capture process. A simplified diagram of the pre-combustion process is shown in Fig. 2.
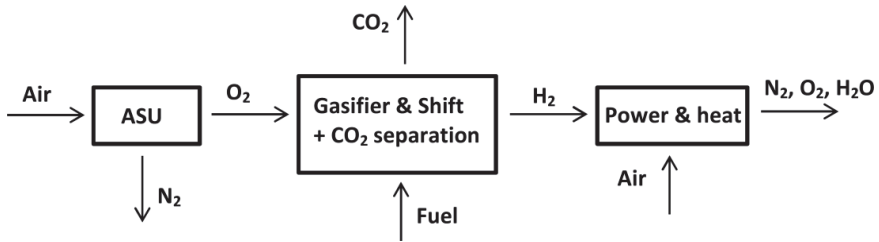
Figure 2. Configuration of pre-combustion capture

Pre-combustion capture is a promising process in terms of plant efficiency characteristics, as high concentrations of CO_2 can be obtained and high pressures (70–80 bar) are favorable for the separation. However, the pre-combustion capture method is more complex and has higher capital costs than the post-combustion method because it incorporates a greater number of process steps, including gasification of the fuel, water-gas shift, and CO_2 separation, which requires the combustion system to be redesigned for possible retrofitting applications.

1.1.3 OF combustion

OF combustion is performed using a mixture of almost pure O_2 (purity >95%) and recycled flue gas (RFG) (60–80% of the total flue gas) instead of air as a combustion oxidizer. A simplified configuration for OF combustion is shown in Fig. 3.
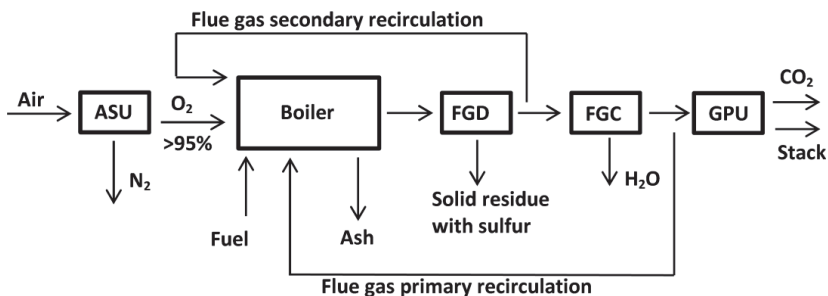
Figure 3. Configuration of OF combustion process

N_2 is separated from air in an ASU and the produced O_2 is mixed with RFG and then fed into the boiler. Thus, combustion occurs in an atmosphere of O_2 and RFG, with combustion in O_2 leading to very high temperatures. The RFG, which can be wet or dried, compensates for the reduced volume of gas owing to the removal of N_2. The N_2-free and O_2-enriched atmosphere of OF combustion increases the content of CO_2 (typically between 60 and 85%) in the flue gas compared with that obtained using conventional combustion (12–16%). The main drawback of this technology is the ASU, which uses cryogenic separation technology and causes the most significant efficiency penalty for the plant (7–9% of overall efficiency), although it is commonly used [6].

1.2 Overview of OF combustion

This chapter focuses on a technical overview of the fundamental differences between air and OF combustion, combustion characteristics studied by thermal analysis (TA) methods, and selected modeling carried out with Aspen Plus process simulation software.

1.2.1 Fundamental differences (Air vs OF) and key aspects

A number of studies on the OF combustion of coal and biomass have been carried out and reviewed in Ref. [6-9], where detailed descriptions of OF combustion technology and its current industrial status can be found. More specifically, the characteristics of the OF combustion process and its differences from air combustion have been elucidated, while the main issues regarding fuel ignition, devolatilization and char burnout, flame stability and gas phase temperature, heat transfer, handling of flue gas recycle (FGR), gas emissions (SO_x and NO_x), boiler design and gas–solid hydrodynamics, and ash handling and formation have been clarified. The different physical properties of CO_2 and N_2 (Table 1), including thermal conductivity, density, specific heat capacity, gas emissivity, and O_2 diffusivity, are the main cause of differences between conventional air and OF combustion.

Table 1: Physical properties of CO_2 and N_2 at 1 atm and 1273 K [9]

Physical Property	CO_2	N_2
Density, ρ (kg m^{-3})	0.4213	0.2681
Specific heat capacity, C_p (J kg^{-1} K^{-1})	1292	1213
Thermal conductivity, k (W m^{-1} K^{-1})	0.0849	0.0793
Mass diffusivity of O_2 in X, $D_{02,X}$ (m^2 s^{-1})	2.133 x 10^{-4}	2.778 x 10^{-4}
Emissivity and absorptivity (radiation heat transfer)	>0 (participating)	0 (non-participating)
Thermal diffusivity, α (m^2 s^{-1})	1.560 x 10^{-4}	2.440 x 10^{-4}

This change in the combustion medium has a significant influence on the flame characteristics, as the RFG is used to control the temperature in the boiler and to insure that there is enough gas volume for heat transfer. Furthermore, the absence of N_2 significantly increases the partial pressures of CO_2 and H_2O in the gas, which leads to enhanced radiative heat transfer owing to increased gas emissivity [10]. It has been reported that the change of the combustion environment from O_2/N_2 to O_2/CO_2 results in considerably lower temperatures in the flame zone, decreased gas temperatures, and delayed ignition of fuel particles. This is caused by the higher specific heat capacity of CO_2 and the lower diffusivity of O_2 in CO_2 than in N_2 [11-14].

The existing extensive studies on OF combustion technology are mainly related to PC units, which are also partially valid for CFB combustion, as the main phenomena that affect the combustion of solid fuels are similar. Thereby, it has been shown that the change from air to OF combustion conditions decreases CFB furnace temperatures by about 100°C owing to the higher heat capacity of the gas in OF combustion [7]. As a result, researchers have established that by increasing the O_2 concentration to around 24–32%, depending on the type of RFG process, fuel, and combustion technology, it is possible to obtain ignition properties, as well as flame and gas phase temperature profiles, that are similar to those for air combustion, which allows the required heat transfer profile of an air-fired boiler to be maintained [7, 8, 11-14]. In other words, similar heat transfer profiles can be achieved for air and OF combustion as long as the gas temperatures are similar, which is controlled by the RFG rate and O_2 concentration [10, 14]. This is an important finding for air to OF transition processes in flexi-burn systems. Moreover, several small-scale units have proven that similar temperature profiles are achievable, and the transition from air to OF combustion is feasible and safe [7, 15-18].

In OF combustion, as fuel combustion with pure O_2 results in very high combustion temperatures, part of the flue gas is recycled to the combustion chamber to act as an inert stream and lower the temperature. Handling of the RFG during OF combustion is an important design parameter (considering the temperature, burner aerodynamics, residence time, etc.). As conventional air combustion has been usually considered as a reference for OF combustion, a fraction of the RFG must be set to reach similar temperatures inside the combustor to achieve a similar heat flux compared with the air combustion case. Several studies have proposed that approximately two-thirds of the boiler exit flue gas mass flow should be recirculated, which is typically between 60 and 80% of the total flue gas [5-8]. Recycling can take place before or after the flue gas condenser (FGC), depending on whether wet or dry recycle is required for the combustion process. The wet (hot) FGR is thermodynamically favorable compared with the dry (cold) FGR. Locating the recycling location further from the boiler (after FGC) results in cooler flue gas, and reheating of this gas is an energy penalty.

Compared with dry recycle, higher RFG temperatures can be achieved with wet recycle. However, an additional dry recycle stream would be required if there are any restrictions on the level of moisture or SO_2 to prevent low- and high-temperature corrosion. For this reason, primary and secondary streams have been considered for the FGR system for the OF combustion process [19, 20]. Additionally, as some excess O_2 in the flue gas is recycled to the boiler with the RFG, this excess O_2 level has to be controlled and considered as part of the RFG handling process. An excess O_2 level in the flue gas of around 3% (<5%) is considered desirable [7, 8]. According to heat and mass balance process calculations, OF and air combustion show similar furnace radiative heat transfer at 3.3–3.5% excess O_2 for the OF case and 20% excess air for air combustion [20]. In brief, the RFG ratio is a key operational parameter that affects the level of excess O_2, burner design, combustion efficiency, heat transfer performance, gaseous components, and emissions.

Although CO_2 and H_2O are the main gaseous components resulting in the fundamental differences of OF combustion, other gases such as SO_x and NO_x also have an impact on the design of the boilers, as any problems should be prevented and their emissions into the environment controlled. Recycling SO_x and NOx with the RFG could enrich the concentration of these gases in the furnace and SO_x/NO_x may have higher ppmv concentrations in flue gases owing to the reduced volume. These impurities are controlled in various parts of the combustion process (in the furnace, in the FGR loop, and during and after CO_2 separation) [19].

The sulfur chemistry in OF combustion includes the release of sulfur from fuel, formation of different sulfur species (SO_2, SO_3, and H_2S), and capture of sulfur by the sorbent injected into the furnace via direct and indirect sulfation reactions [7]. SO_2 emissions in OF combustion are proportional to the sulfur content of the fuel, as the SO_2 concentration depends on the change of the volume of the combustion medium, which is lower at higher O_2 concentrations, and therefore the SO_2 concentration increases [21]. The SO_2 concentration can be reduced when a sulfur capture process is applied by injecting sorbents, such as limestone ($CaCO_3$) or dolomite ($CaMg(CO_3)_2$), into the furnace. The furnace temperatures in CFB boilers are much lower than those in PC boilers, and the partial pressure of CO_2 over $CaCO_3$ becomes higher than the equilibrium CO_2 pressure during OF combustion in CFB boilers, which prevents the calcination of limestone. As a result, sulfur capture could occur via direct sulfation (Eq. 1) [7, 22].

$$CaCO_{3(s)} + SO_{2(g)} + 1/2O_{2(g)} \rightarrow CaSO_{4(s)} + CO_{2(g)} \tag{1}$$
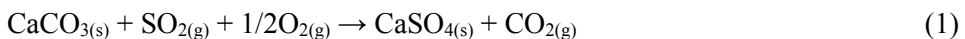
However, considering the general conclusions about sulfur capture in CFB boilers and the results from various small- to large-scale tests, it has been reported that both direct and indirect sulfation can contribute to sulfur capture, depending on the process parameters, including operation temperature and

pressure. High sulfur capture efficiencies (>95%) can be achieved with no specific difficulties, as confirmed at the CIUDEN power plant [7, 16, 21-25].

The control of NO_x emissions (NO and NO_2) is also influenced by changes in the OF combustion process, primarily decreased concentrations of N_2, RFG, residence times, increased concentrations of combustion products, and temperature profiles [19]. Most reported experiments have shown that a significant reduction of the NO_x emission rate can be achieved with OF combustion compared with air combustion, as thermal NO_x formation is eliminated owing to the absence of air-N_2. Moreover, fuel-N is the main source of NO_x formation, which facilitates the reduction of NO into N_2 via the reverse Zeldovich mechanism [19]. It is expected that the conversion of fuel-N to NO_x increases with increasing O_2 fraction, which also causes higher combustion temperatures. However, according to Ref. [16, 17, 23, 26], fuel-N to NO conversion during CFB OF combustion is generally lower than that during air combustion owing to destruction mechanisms (NO_x reburn mechanism in the gas phase), which are dominant and enhanced in OF combustion by flue gas recirculation [27]. Considering the above mentioned mechanisms, OF combustion in CFB boilers usually shows similar or higher concentrations of NO_x emissions than CFB air combustion when volumetric units are considered. NO_x concentrations can be given in different units: ppm and mg N^{-1} m^{-3} (volumetric) or in energy-based units: mg NO_x $(MJ)^{-1}$ and fuel-N to NO_x. However, when the concentration is considered in energy-based units, NO_x is lower during OF combustion, which is a clear benefit of the OF combustion technology [6, 7, 14, 21, 28, 29].

1.2.2 Experimental studies based on conventional fuels

The analysis of the combustion process for OF technology, including different solid fuels and their properties, pyrolysis behavior, volatile and char burn out, and gasification reactions, has been an elementary and key research area, as this knowledge is important for the development of OF combustion systems. The main interest of these studies is derived from the need to understand the effect of a CO_2-rich environment in OF combustion, as the changed gas composition influences both heat transfer and combustion kinetics. In studies based on TA methods with a specific focus on the pyrolysis behavior [30-35], it has been reported that during the pyrolysis tests with coal and biomass samples from different regions under N_2 and CO_2 ambient conditions, the main stages were removal of moisture content, volatile release, and char gasification. According to these experiments, although the replacement of N_2 by CO_2 slightly influenced the devolatilization process in terms of fuel reactivity, there were no major differences observed at low temperatures up to 700°C. The main difference detected in all these studies was at high temperatures (above 720°C), where CO_2–char gasification occurs, which increases char reactivity. Thus, the mass loss rate of coal pyrolysis in CO_2 was higher than that in N_2 owing to the

different properties of the bulk gases and char–CO_2 gasification, which also resulted in a higher total fuel weight loss in CO_2 than that in N_2.

Studies on the combustion behavior and reactivity of coal and its char in air and OF combustion conditions reveal that high concentrations of CO_2 cause a delay in volatile and char ignition and reduce the rate of their consumption [13, 20, 31, 33-37]. Once the concentration of O_2 in CO_2 is increased to around 30%, ignition behavior comparable to that in air was achieved. It was found that the lower diffusivity of O_2 in CO_2 reduces the O_2 flux in the combustion medium, thus decreasing the burning rate of volatiles and char particles. The higher heat capacity and density of CO_2 are the main reasons for the delay in fuel combustion. The reactivity and kinetic behavior of the different coal chars studied in Ref. [38, 39] showed that the chars obtained in CO_2 have slightly lower reactivity than those obtained in N_2 under a typical OF combustion atmosphere (30%O_2/70%CO_2). This difference was attributed to the chars obtained in CO_2 undergoing gasification by CO_2 during the char devolatilization process. According to the surface area analysis of high- and low-rank coals, the higher concentration of macro pores in low-rank coals leads to a higher reactivity compared with that of high-rank coals [39]. In a broader sense, coal, lignite, biomass, and their blend samples show slightly higher reactivities under air than under OF combustion conditions at the same O_2 level, as the higher specific heat of CO_2 in comparison with that of N_2 results in lower gas temperatures and therefore reduced fuel particle temperatures during OF combustion. The lower diffusivity of O_2 in CO_2 compared with that in N_2 was the main influence on the char–CO_2 gasification reaction, which becomes increasingly important in OF conditions. Therefore, whether a high concentration of CO_2 increases or decreases the overall rate of char consumption, it was concluded that the reactivity is fuel-dependent, as the oxidation rate of unburnt carbon decreases owing to gasification reactions (Boudouard (Eq. 2) and water-gas shift (Eq. 3)) at high temperatures. The combustion rate increases as the O_2 concentration and temperature increase and the particle size decreases [8, 40, 41].

$$C_{(s)} + CO_{2(g)} \rightarrow 2CO_{(g)} \text{ (boudouard reaction)} \qquad (2)$$

$$CO_{(g)} + H_2O_{(g)} \rightarrow CO_{2(g)} + H_{2(g)} \text{ (water-gas shift reaction)} \qquad (3)$$
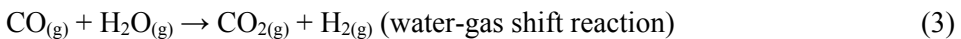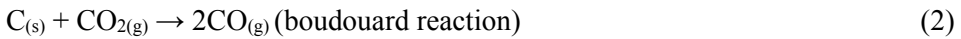
1.2.3 Modeling studies based on conventional fuels

Using the Aspen Plus simulation software (one of the comprehensive tools used to model combustion and gasification characteristics of coal and biomass and to predict the emissions of gaseous components), simulations [42-50] focusing on the modeling of the conversion process of solid fuels have been reported starting from drying followed by pyrolysis and char combustion. The combustion processes of solid fuels have been modeled with several reactors by considering

stoichiometric reactions (limited by reactant), chemical equilibrium (output described), and kinetic expressions, which consider the residence time in the calculation of the combustion products. In the case of combustion modeling in FB boilers, several assumptions have been considered for the gas and solid hydrodynamics in the bottom and dilute zones, as the reactor models do not treat the differences in bottom-zone and freeboard hydrodynamics. The most comprehensive model built in the Aspen interface by Sotudeh-Gharebaagh et al[42] for the combustion of coal in CFBs has become the basis for other studies. Although the model was built for air combustion, it successfully represented the important steps of coal combustion in CFB boilers and guided later works considering OF combustion (see for example Ref. [45]). Process simulation models for PC and FB boilers with kinetic free reaction models were also considered and the Gibbs free energy minimization method was used for simulations of coal and biomass combustion, as well as syngas production [43, 46-48, 50]. In the modeling work carried out by Hu et al. [44], different recycle options in an oxy-coal system were simulated. The various recycle options resulted in different requirements related parameters such as the gas loadings of the emission removal units and heat exchanger areas. However, it has also been shown that the various recycle options do not affect the FGR ratio and flue gas flow rate considerably, and there are only small differences in the boiler and electrical efficiencies when the air–coal combustion system is retrofitted with the oxy-coal combustion system. The recycle ratio, O_2 concentration, air ingress (increased mass flow of flue gases owing to the negative draft maintained in the boiler), SO_x removal method, and recycle position have been discussed for oxy-combustion of a coal system in comparison with air combustion in a simulation by Xiong et al. [50]. It was shown that the CO_2 concentration in the flue gas can be more than 80%, and without air ingress, can exceed 90%. The CO_2 concentration in the flue gas for a hot recycle case was around 60% and the SO_x fraction was higher than that for air combustion and for OF combustion with cold FGR. Considering corrosion protection and the sulfur dew point in the flue gas, the hot recycle option was found to be most suitable for OF combustion.

1.2.4. Experimental and modeling studies based on OS

OS is defined as a sedimentary rock and a kind of fossil fuel that contains combustible organic matter in a mineral matrix. The main difference between coal and OS is that the organic components of OS (kerogen) account for less than 35% of the total mass, whereas coal usually contains 75% organic matter. Thus, OS heating values are far lower than those of coal.

   EOS is a highly heterogeneous fuel with a complicated composition of organic and mineral matter. Among shales, EOS is considered a rich-grade (organic content) fuel. Moreover, it is characterized by high ash (45–50%), moisture (11–13%), and sulfur (1.4–1.8%) contents and a low net calorific value (8–12 MJ kg^{-1}). Detailed descriptions of EOS (composition, structure, formation, etc.) can be

found in Ref. [51, 52]. In general, more detailed information about OS as a non-conventional fuel and its utilization by different technologies can be found in Ref. [53] and the references cited therein.

In recent years, owing to the growing interest in alternative fuels, many studies have been performed on OS [53-61]. These studies on OS from different regions have mostly focused on direct conventional air-firing and OS conversion to shale oil (retorting) with investigations of the pyrolysis behavior and combustion characteristics. According to the studied pyrolysis and combustion mechanisms based on different OS sources, the thermal decomposition of OS in the absence of air or O_2 occurs in two stages. In the first stage, OS is heated and water is removed, while thermobitumen is formed; in the second stage, thermobitumen decomposes to form volatiles (shale oil and shale gas) and a solid residue (shale char and minerals). Furthermore, OS combustion also has two stages: volatile combustion followed by fixed carbon combustion. Additionally, it is understood that the different OS sources have different organic and mineral contents, and these contents differ, even in the same OS deposit. Thus, the formation of bitumen has a specific temperature range depending on the OS and its origin [53].

Although there have been numerous studies on OS pyrolysis and combustion, mainly targeting its conventional applications, it is difficult to utilize these studies for the development of OF combustion technology, as the pyrolysis behavior and oxidation characteristics of OS and its char, reaction kinetics, and mineral-related reactions strongly depend on the combustion atmosphere. Nevertheless, the effects of the pyrolysis environment and shale char–CO_2 gasification, which are relevant investigations for OF combustion, have been reported in several studies [58-60]. It was shown that CO_2 as a carrier gas leads to a slightly greater mass loss during the devolatilization stage compared with N_2, and the gasification reaction is more likely to occur at high temperatures. It was also reported that the heating rate has an important effect on the non-isothermal gasification reaction of residual carbon, and the gasification reaction follows first-order kinetics with respect to carbon [60]. There have been very few studies regarding OF combustion of OS, and the first experiments with OS under air and OF conditions ($27\%O_2/73\%CO_2$) were performed by Al-Makhadmeh et al. with Jordanian OS in a 20 kW electrically heated once-through furnace without consideration of the FGR [62]. The effect of OF conditions on SO_2 and NO emissions was investigated. The results showed that combustion of Jordanian OS under OF conditions is feasible and 100% OS burnout can be achieved. The CO profile during OF combustion was wider than that during air-firing, which could be explained by the gasification reactions in a CO_2-rich media, and a minimum 2% excess O_2 concentration in the flue gas was found to be optimum when considering the CO emissions. OS-N conversion to NO was significantly lower under OF conditions and lower SO_2 emissions were detected. As a continuation of this study, OF combustion of Jordanian OS was performed with NO injection to the furnace to model actual conditions [63]. It

was concluded that the simulated recycled NO was efficiently reduced during the tests, and OS combustion with lower SO_2 and NO emissions can be achieved under OF conditions.

There have been very few studies so far on the modeling of OS combustion and its retorting with Aspen Plus simulation software [64-66]. The complicated chemistry of OS fuel makes the definition of the fuel challenging in the Aspen Plus environment, as the simulation of OS processes requires several different types of model components, and OS must be defined as a non-conventional fuel under mixed sub-streams, including liquid, gas, and solid components. In the most comprehensive example, the composition of Green River OS was successfully defined and a steady-state process for retorting of the OS was modeled by Sherritt et al. [64]. It was reported that the Aspen Plus process simulator is a useful tool for the development of an OS conversion process and operations are sufficient for steady-state models.

1.3 Literature review conclusions and aims of the study

The works cited in the literature review give valuable insights into the differences between air and OF combustion processes. However, most of the available data is for coal and biomass combustion, which is not fully suitable for the possible implementation of OF combustion of OS, particularly for EOS, as the combustion specifics are strongly fuel-dependent. There are knowledge gaps in a wide range of research areas necessary for the realization of OF combustion of EOS, as the operating conditions found to be optimum for OF combustion of coal and biomass vary depending on the characteristic fuel properties.

Thus, the aim of the current study is to generate a fundamental knowledge base for OF combustion of EOS that can lead to its possible integration in large-scale electricity production systems.

Accordingly, experiments and process simulation models were conducted for OF combustion of EOS. The following objectives describe and constitute the specific topics in this work:

- Comparison of conventional (coal, anthracite) and non-conventional (EOS) fuels under modeled air and OF conditions by means of TA methods;
- Effect of CO_2 and various combustion atmospheres on the stages of EOS combustion, including both its organic and mineral parts;
- Oxidation characteristics and kinetic analysis of OS and its char under modeled air and OF combustion conditions;
- Process modeling of OF combustion of EOS with respect to specific CFB operating parameters;
  - o Applicability of FB reactor block of Aspen Plus Software for CFB OF combustion of EOS,
  - o Calculation of the flue gas composition for CFB OF combustion with different FGR methods.

2. EXPERIMENTAL AND MODELING

2.1 Materials and methods

Preparation and characterization of samples

Four different solid fuel samples were selected for the TA experiments: two oil shale samples (OS1, OS2) and two coal samples (C1, C2). The OS samples were obtained from Narva Power Stations. The OS1 sample is a common energetic OS and OS2 is an enriched sample–oil shale concentrate. The coal samples were obtained from Russia. The C1 sample is a Russian anthracite coal and C2 is a common volatile-rich coal sample that is widely used in boilers for heating.

   OS1 was considered as the main sample and was used for additional tests in certain experiments. In the appended papers, the abbreviations EOS and OS refer to the OS1 sample. The detailed characteristics of the samples are given in Table 2.

 Table 2. Characterization of samples

	OS1	OS2	C1	C2
HHV^d, MJ/kg	11.86	13.64	30.39	30.22
Content, % mass				
Ash^d	49.30	45.60	8.90	8.10
Moisture ^{ar}	-	-	14.80	19.20
Moisture ^{ms}	0.70	0.70	2.10	2.70
N^d	0.10	0.10	0.60	2.00
C^d	30.40	35.00	81.80	73.70
H^d	3.00	3.60	1.50	4.20
S^d	1.63	1.87	0.24	0.36
TC	31.50	36.40	87.00	75.80
TIC	4.55	4.35	0.00	0.00
CO_2^M from TIC	16.67	15.94	0.00	0.00

^{d} Per dry sample, ^{ar} as received, ^{M} mineral CO_2 ^{ms} moisture in the sample

Each sample was treated as follows. The obtained sample was crushed with a jaw crusher. A mean sample was taken from the crushed material and ground in a big ball mill. Then, the sample was dried at 105°C for 4 h and ground further in a Retsch PM 100 grinding machine in a four-ball planetary mill (20 min at 350 rpm, reverse 5 min), until the entire sample passed through a 200 µm sieve.

Experimental methods

A Setaram Setsys Evo 1750 thermoanalyzer coupled to a Nicolet 380 Fourier transform infrared (FTIR) spectrometer was used for the experiments. Non-isothermal and isothermal tests were performed to investigate the different stages of OF combustion for selected samples. Standard 100 µL Pt crucibles were used, and the mass of the sample was 20 ± 0.5 mg in most experiments and 30 ± 0.5 mg for the tests with gas analysis. Commonly, the non-isothermal tests were carried out at a 10 K min^{-1} heating rate up to 1000–1100°C with a 30 mL min^{-1} gas flow rate using different atmospheres (Ar, CO_2, O_2/Ar, and O_2/CO_2). In some particular experimental series, different gas concentrations and heating rates were used, depending on the calculation and analysis needs.

TA experiments are most often carried out in Ar instead of N_2, as N_2 is not completely inert at high temperatures and has a somewhat higher heat capacity than Ar, which enables heat effects to be measured more precisely in an Ar atmosphere. Here, Ar was used instead of N_2 in the experimental series modeling air combustion conditions (21%O_2/79%Ar). However, there could be slight differences in the experimental results, as the diffusivity of O_2 is higher in Ar than in N_2. To clarify these differences, comparative experiments were also carried out with N_2 as the inert gas (Fig. 4).
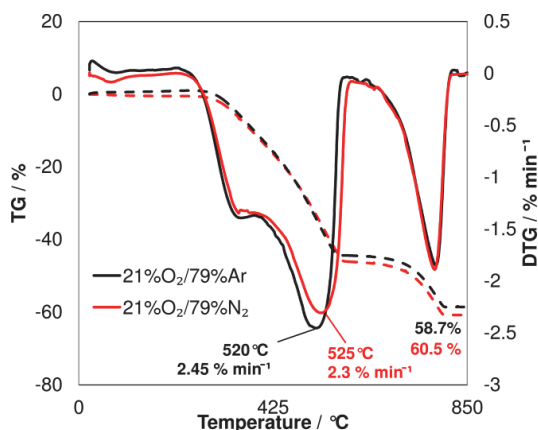
Figure 4. Comparison of 21%O_2/Ar and 21%O_2/N_2 conditions for OS1 (71…100µm)

As shown in Fig. 4, the difference is small, with somewhat more active oxidation in the case of 21%O_2/79%Ar, as the mass loss rates are slightly higher. This small difference can be accounted for when comparing the air combustion

and OF combustion conditions. In conclusion, replacing N_2 with Ar does not affect the experimental results and related discussions notably; however, if necessary, this small shift can be taken into account.

The controlled experimental conditions (gas concentrations, heating rates etc.) during the TA tests are given in Table 3.

Table 3. Controlled experimental conditions during the thermal analysis tests

Gas concentrations	Heating rates (K min^{-1})
21%O_2/79%Ar (model air)	10 (For most)
21%O_2/70%CO_2	2.5…15 (For kinetic calculations)
30%O_2/70%CO_2 (OF)	20 (For gas analysis)
21…35%O_2/CO_2	**Sample fractions**
100%CO_2, Ar, N_2, O_2	<200 μm (For most)
Gas flow rates mL min^{-1}	71…100 μm
30 (For most)	(For kinetic calculations)
50 (For gas analysis)	**Mass of samples (mg)**
Crucible type	20 ± 0.5 (For most)
100 μL Platinum (Pt)	30 ± 0.5 (For gas analysis)

For evolved gas analysis (EGA), the thermoanalyzer was coupled to a Nicolet 380 FTIR spectrometer using a heated transfer line (220°C). A higher heating rate (20 K min^{-1}) and higher gas flow rate (50 mL min^{-1}) were used, as well as a larger sample mass (30 ± 1 mg), to increase the sensitivity [67]. FTIR measurements were recorded in the range of 400–4000 cm^{-1} with a resolution of 4 cm^{-1} and each spectrum was the average of four scans. The evolved gaseous compounds and groups were identified using the Thermo-Scientific OMNICTM software and the HR Aldrich Vapor Phase Library [68]. The AKTS Advanced Thermokinetics software [69] was used to calculate the kinetic parameters for the oxidation stage of the OS1, C2, and OS1 char samples. To calculate the conversion-dependent activation energies, a model-free approach, based on differential isoconversional methods was applied. The changes in activation energy E (kJ mol^{-1}) and pre-exponential factor A depending on the reaction progress α were determined from non-isothermal experiments with 2.5, 5, 10, and 15 K min^{-1} heating rates under three different atmospheres (21%O_2/Ar, 21%O_2/CO_2, and 30%O_2/CO_2). For the calculation method, see the equations describing the reaction rate and isoconversional approach [70, 71] in Papers I and II.

To prepare the OS1 char sample, the OS1 sample was heated to 450°C in an Ar atmosphere and maintained at this temperature for 1 h until devolatilization ceased. This freshly obtained char sample was used in the following tests. The char preparation temperature was selected from preliminary pyrolysis

experiments according to the highest reaction rate. For isothermal tests, oxidation of the obtained OS1 char was performed at three different temperatures (450, 500, and 550°C). To perform series of non-isothermal tests and kinetic calculations, an additional OS1 char was prepared in an electric tube furnace under the same conditions to obtain a greater amount of char with uniform properties.

2.2 Modeling approaches and descriptions

In this section, some key aspects related to the simulated models are discussed in connection with the simulation tool and the considered modeling approaches. Detailed descriptions of the simulated models can also be found in Papers III and IV and in Ref. [72].

Simulation model for CFBC process (Paper III – Ref [72]*)*

Figure 5. Process flowsheet for kerogen combustion and CFB hot loop modeling

The circulating fluidized bed combustion (CFBC) model simulated in Aspen Plus is presented in Fig. 5 (process flowsheet) and 7 (scheme of the overall process layout).

Briefly, the simulated process focuses on the gas and solid hydrodynamics of the FB boiler to determine the required elutriated mass flows to maintain the heat balance for OF combustion. The air combustion experiments in the Chalmers CFB boiler were compared with the simulated air–OS combustion case, and later, the model was used to discuss the conversion of an experimental air–OS-fired CFB unit to OF–OS combustion.

The boiler geometry in the model is same as that of the Chalmers 12 MWth CFB boiler. The solid properties of the bed material used in the model in terms of particle size distribution (PSD) and density are similar to those applied in the CFB boiler case, which are used as a reference in the modeling. The input parameters of the FB reactor are given in Paper III (Table 3 therein). Silica

(SiO$_2$) sand was used as the bed material with the PSD given in Paper III (Fig. 2 therein). The Colakyan and Levenspiel (Paper III, Eq. 1) and Geldart et al. (Paper III, Eq. 2) correlations were tested separately for the elutriation models. For more detailed explanations on evaluating the elutriation models, see Ref. [72] and the references cited therein.

The majority of the experimental data was obtained from pressure measurements in the CFB boiler. The boiler has a furnace with dimensions of 13.5 × 1.7 × 1.4 m and is therefore smaller than commercial CFB boilers, but large enough to have most of the characteristics of such boilers. The main outline of the unit is shown in Fig. 6 [73].
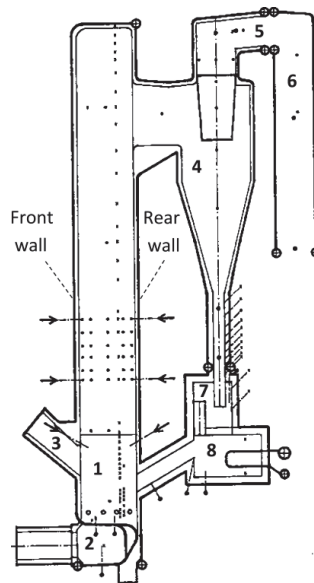
Figure 6. The main outline of the Chalmers 12 MWth CFB boiler: 1. Furnace, 2. Air plenum, 3. Fuel feed, 4. Cyclone, 5. Exit duct, 6. Convection pass, 7. Particle seal, 8. Particle cooler

The simulated model (Fig. 7) was divided into two main parts: addressing the combustion of kerogen (organic matter in EOS) and the hydrodynamics, including a description of the solids circulation rate.

Figure 7. Scheme of the overall process lay out of the CFBC model, circle (1) is the combustion model and (2) the CFB model

The combustion modeling considers moisture evaporation, the decomposition stage of kerogen, and the basic combustion reactions. The heat of combustion calculated from the combustion of kerogen was added as an input term for the FB reactor. Hot flue gases produced from the combustion of kerogen were used as a fluidization gas. The amount of oxidizer and the O_2 concentration in the flue gas (3.6%, excess O_2) were kept constant for all cases. The oxidation of decomposed kerogen was modeled with the equilibrium reactor at 850°C. The following four main reactions were considered: $C + O_2 = CO_2$, $H_2 + Cl_2 = 2HCl$, $S_2 + 2O_2 = 2SO_2$, and $H_2 + 1/2O_2 = H_2O$.

Key points of the simulation model based on Gibbs free energy minimization (Paper IV)

Figure 8. Process flowsheet for simulation model based on Gibbs free energy minimization

As a main modeling strategy, OF combustion cases have been simulated with dry and wet FGR strategies (Fig. 8) by controlling the O_2 percentage in the flue

gas to maintain temperatures (gas–solid mixture) at the outlet of the combustion reactor similar to those during air combustion. The considered modeling strategy has been used to estimate the composition of the product gas by calculating the mass–energy balance and chemical equilibrium of the process, rather than the gas and solid hydrodynamics in the FB reactors. The simulated model introduced here can be used to predict the flue gas composition for OF combustion of EOS and for fundamental comparisons regarding heat transfer in the boiler. The calculated temperatures are key parameters that allow possible adjustments that are necessary for retrofitting operations. The energy balance of the system is based on the heat generated from the exothermic reactions, which is partially consumed by the endothermic reactions, while the rest is converted to sensible heat that raises the temperature of the gas–solid mixture. Owing to the small amount of char, high amount of volatile matter in EOS, and complexity of EOS kinetics, the EOS combustion process has been simulated using the assumption that the combustion products form an equilibrium mixture. Based on the weight fraction of organic matter of EOS and oxidants (air, O_2/FGR), equilibrium compositions have been calculated using the Gibbs free energy minimization method.

To compare the obtained results for EOS combustion with the combustion of another carbonate-rich OS, Utah White River OS (UOS) was included, and OF combustion of UOS with two different FGR strategies has been modeled.

Considering the main characteristic reactions of the organic and mineral components in EOS and UOS (Paper IV, Table 2 and 3 therein), several compounds have specifically been taken into account during the simulations according to the simplified definition of non-conventional fuels. The defined components are presented in Table 4.

Table 4. Defined components as products in Gibbs reactor

Gases	Solids
O_2, CO_2, CO, H_2, H_2O, S, SO_2, SO_3, N_2, NO, NO_2, NO_3, Cl_2, HCl	FeS_2, $FeSO_4$, Fe_2O_3, SiO_2, $MgCO_3$, MgO, $CaCO_3$, CaO, $CaSO_4$, $MgSO_4$

3. RESULTS AND DISCUSSION

3.1 Thermal analysis (TG-DTG-DTA/FTIR) and kinetics

TG-DTG-DTA analysis

A comparison of the thermal behavior of each fuel sample in $30\%O_2/CO_2$ and $21\%O_2/Ar$ at a 10 K min^{-1} heating rate is presented by the TG (mass change, %), DTG (mass change rate, % min-1), and DTA (heat effect, µV) curves in Fig. 9.
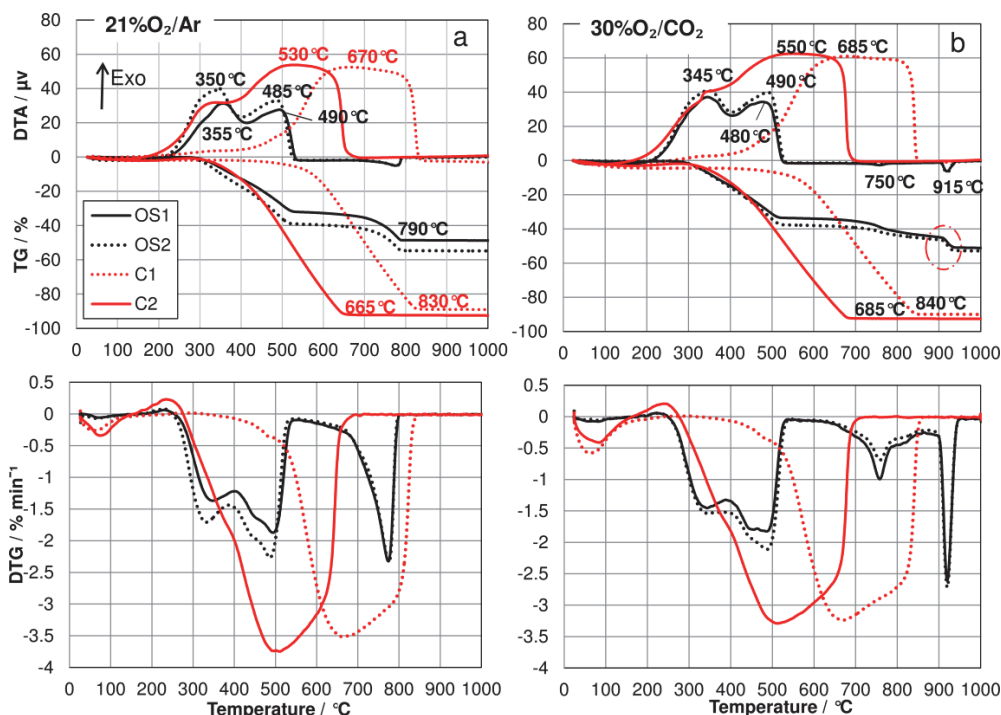
Figure 9. Comparison of all fuel samples in $21\%O_2/Ar$ (a) and $30\%O_2/CO_2$ (b), TG/DTA (above) and DTG (below)

The first very weak mass loss step between 0 and 150°C observed for each sample is considered as a residual and adsorbed moisture releasing step, which includes the beginning of the devolatilization stage. After moisture release, the process for each sample continues with devolatilization, volatile combustion, and char oxidation stages. Considering the mineral component of OS samples, thermal decomposition also occurs at the end of the process. The mass loss of the coal samples in the oxidation stage proceeds in one smooth step with a wide exotherm from 300°C to 665°C for C2 and 830°C for C1 in $21\%O_2/Ar$ (Fig. 9a). In the $30\%O_2/CO_2$ atmosphere, the characteristic peak temperatures of the coal samples are shifted towards higher temperatures compared with the $21\%O_2/Ar$

atmosphere. However, oxidation still takes place in one step, and there are no big differences in the total mass loss of the samples in either atmosphere.

The OS samples show two distinctive mass loss steps in $21\%O_2/Ar$ and three steps in $30\%O_2/CO_2$. These distinctive steps are related to the devolatilization and oxidation of the organic component, followed by decomposition of the mineral component. The third step in $30\%O_2/CO_2$ is related to the different behavior of carbonates in this atmosphere. In the $21\%O_2/Ar$ atmosphere, $MgCO_3$ and $CaCO_3$, which are the main carbonate compounds in EOS, decompose in the same temperature region (700–800°C). On the other hand, the decomposition temperatures of $MgCO_3$ and $CaCO_3$ become separated in $30\%O_2/CO_2$, proceeding with maximum rates at 750ºC (decomposition of $MgCO_3$) and 915ºC (decomposition of $CaCO_3$), as determined from the DTG curves (Fig. 9b). In both atmospheres, exothermic decomposition (organic component) occurs with two peaks, which likely correspond to the devolatilization and thermobitumen/char oxidation stages. However, the chemistry is more complex owing to the simultaneously occurring reactions and substages. In the $30\%O_2/CO_2$ atmosphere, the exotherms of the OS samples have somewhat lower peak temperatures compared with those in $21\%O_2/Ar$, which can be explained by the higher O_2 concentration (Fig. 9b). The peaks in the exotherm of the enriched sample (OS2) are more intense in both atmospheres, and a higher mass loss is observed during the oxidation stage compared with that observed for OS1, which is in accordance with the higher organics content in OS2.

The DTG peak maxima of the samples indicate that the reaction rate is slightly higher in $21\%O_2/Ar$ than in $30\%O_2/CO_2$, in spite of the lower O_2 concentration, and this phenomenon is clearly observed in the case of the OS2 sample. In $30\% O_2/CO_2$, the reaction rate decreases more slowly during char oxidation (final stage of oxidation) and the peak is slightly wider, indicating a slight lowering of the reaction rate for this stage of the process in the $30\%O_2/CO_2$ atmosphere. For general evaluations, the replacement of N_2 with Ar (for model air conditions) can be taken into account at this stage. In this case, the slight differences mentioned above can be disregarded, as similar differences exist between the characteristics of N_2 and Ar: peaks shifted by approximately 5–10°C towards lower temperatures and slightly higher reaction rates in the oxidation stage for $21\%O_2/Ar$ compared with $21\%O_2/N_2$ (Fig. 4).

Overall, the temperature profiles (offset, onset, and peak temperatures), reaction rates, and heat effect at oxidation of OS and coal samples in $21\%O_2/Ar$ and $30\%O_2/CO_2$ atmospheres do not differ much. There are no significant differences in the total mass loss of the samples in these different atmospheres.

Figure 10. TG/DTA (above) and DTG (below) curves of OS1 (a) and C2 (b) in different O_2 concentrations with CO_2

The possible impact of a higher O_2 concentration on the oxidation and thermal decomposition characteristics of OS1 and C2 has been analyzed, as presented in Fig. 10. The results show that the characteristic temperatures (offset, onset, and peak temperatures) of the TG-DTG-DTA curves for the OS1 and C2 samples move significantly towards lower temperatures as the O_2 fraction in the combustion atmosphere increases. Moreover, the maximum combustion rate $(d_w/d_t)_{max}$ for each sample increases with the increase in O_2 concentration. The elevated O_2 content increases the rates of devolatilization and oxidation, which causes an increase of the particle temperature. Therefore, by increasing the O_2 concentration, the combustion reactivity of solid fuels can be enhanced considerably.

Table 5. Characteristic values obtained from TG-DTG curves for OS1

Conditions	Peak 1 / °C	Peak 2 / °C	T_{onset} / °C	T_{offset} / °C	Mass loss / % oxidation / total
$21\%O_2/CO_2$	343	490	236	524	33 / 50
$30\%O_2/CO_2$	340	464	246	520	32 / 48
$35\%O_2/CO_2$	314	445	242	507	31 / 48
$21\%O_2/Ar$	360	491	242	530	32 / 48

The final mass losses are almost the same, with 21% O_2 giving a slightly higher mass loss for both samples (Table 5). However, it is difficult to associate this result with any reaction mechanism, as the heterogeneity of samples could also cause such differences. The increased role of gasification ($C_{(s)}$ + $CO_{2(g)}$ → $2CO_{(g)}$) could be one reason for this difference. The characteristic temperatures obtained for the decomposition of carbonates in the case of OS1 did not change remarkably in different O_2 levels. However, owing to the higher partial pressure of CO_2 in 21%O_2/CO_2, the decomposition of $CaCO_3$ shifts slightly to higher temperatures (Fig. 10a, lower).

Pyrolysis of OS1 and C2 in Ar and CO₂
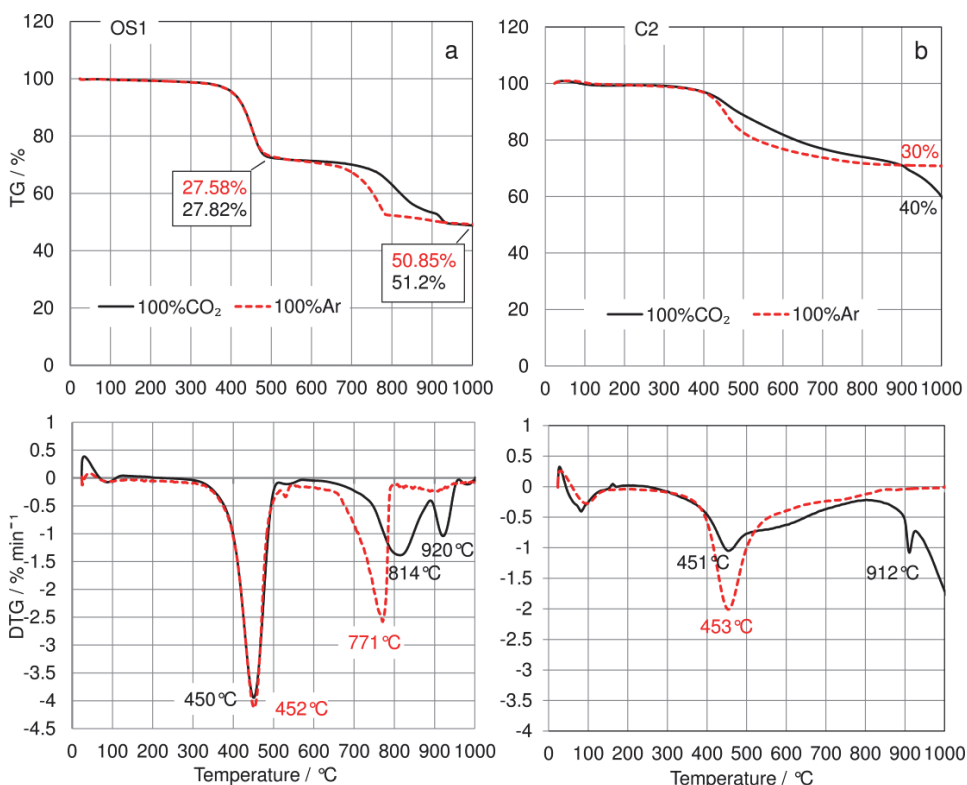
Figure 11. Pyrolysis TG (above) and DTG (below) curves of OS1 (a), and C2 (b)

In this section, the effect of CO_2 on the chemistry of the overall process and the specifics of pyrolysis are discussed, mainly based on the OS1 and C2 samples using Ar and CO_2. The pyrolysis TG and DTG curves of OS1 and C2 at a 10 K min^{-1} heating rate under 100% Ar and 100% CO_2 are shown in Fig. 11. In general, two stages can be differentiated for OS1: pyrolysis in the low temperature zone (300–520°C) for both CO_2 and Ar atmospheres and decomposition of mineral carbonates (magnesite, dolomite, calcite, and siderite)

at higher temperatures (above 650°C). The characteristic temperatures and mass loss of the OS1 sample in Ar and CO_2 are very similar, which indicates that CO_2 behaves like an inert gas and has the same influence as Ar on the organic component until the end of the devolatilization stage. The main difference for OS1 in the CO_2 atmosphere is separation of the decomposition temperatures of $MgCO_3$ and $CaCO_3$, which proceed with maximum rates at 814 and 920° C, respectively (Fig. 10a lower).

The difference between the Ar and CO_2 atmospheres for the pyrolysis of C2 is more obvious. Above 400°C, owing to the differences in heat capacities, diffusivities, and radiative properties of the gases, reactivity during the devolatilization stage is higher in the Ar atmosphere. Unlike OS1, the char gasification reaction under a CO_2 atmosphere for C2 is easily identified above 800°C, signifying that the reactivity and mass loss differ. Clearly, the gasification reaction becomes important in the case of coal combustion, but it is not as evident in the case of OS combustion because of the low carbon content.

The effect of the char gasification reaction (Paper II, Eq. 1) is not clearly distinguished in the TG-DTG curves of OS1 owing to the possible overlap of the thermal decomposition of carbonate minerals. According to the CO emission profile obtained from gas analysis (Paper II, Fig. 4) in a CO_2 atmosphere, the role of the gasification reaction increases at temperatures above 650°C, reaching its peak level at 800°C. For both the Ar and CO_2 atmospheres, it should also be mentioned that above 650°C, the thermal decomposition of carbonate minerals occurs, which produces large quantities of CO_2 (Paper II, Eq. 12 and 13). The increased concentration of CO_2 in the pores may also favor the gasification reaction during pyrolysis with Ar. Further, the reaction products from the mineral components, such as CaO and MgO, can participate in the char reactions as catalysts to promote further production of CO. However, the combination of various possible parallel reactions at higher temperatures and trapped char content in the mineral matrix after the devolatilization stage makes identification of the char reactions even more complex for low-grade fuels like OS1 compared with C2.

FTIR analysis

The FTIR spectra of the evolved gases and the emission profiles of some characteristic compounds and groups evolved during the oxidation of OS1 in a $30\%O_2/CO_2$ atmosphere are presented in Fig. 12–14. For more detailed results, see also Paper I (Fig. 3a–c therein) and Paper II (Fig. 4a–d therein) for relevant descriptions.
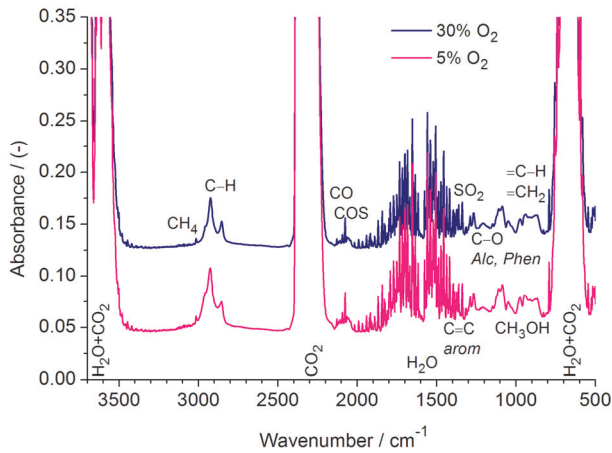
Figure 12. FTIR spectra of evolved gases for OS1 at 30% and 5%O_2 in CO_2 atmospheres taken at 20th min (440°C)

Analysis of the emission profiles shows that the main peaks in the selected emission profiles correspond to the temperature interval of the oxidation stage in $30\%O_2/CO_2$ atmosphere, which is from 250 to 500–600°C. The peaks show a steeper shoulder at lower temperatures (beginning of the process) and a smoother shoulder at higher temperatures, indicating that complex chemical processes occur during the devolatilization stage and initial oxidation.
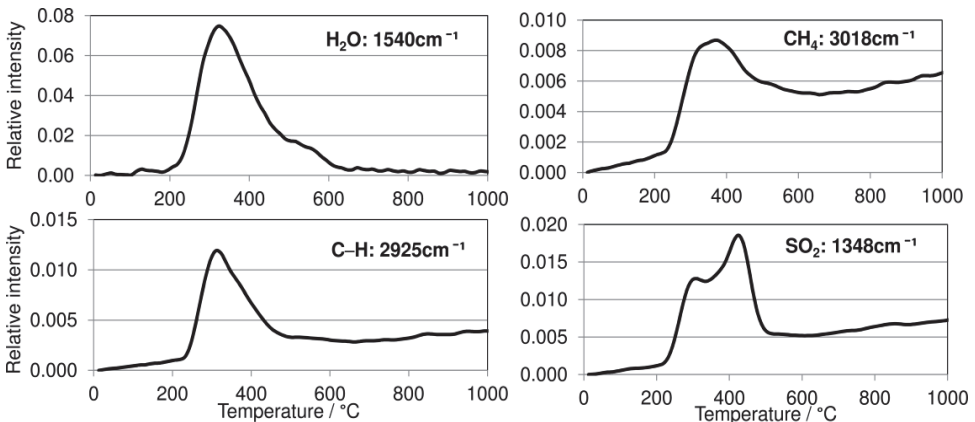
Figure 13. Emission profiles of some characteristic compounds and groups evolved during OS1 oxidation in $30\%O_2/CO_2$ atmosphere

In $30\%O_2/CO_2$, H_2O, as the main oxidation product, reaches its maximum intensity during the early stages of oxidation. Additionally, C–H bonds show a high intensity in the early stages of oxidation, which is related to the emission of volatiles during the first stage of oxidation. The presence of C–H bonds (saturated organic compounds) is observed until the end of oxidation. Compared

34

with H_2O, CH_4 reaches a maximum intensity at slightly higher temperatures. The emission profile of SO_2 shows two peaks, with the maximum intensity observed for the second peak. The first peak is related to organic sulfur in OS, whereas the second is related to the oxidation of pyrite.
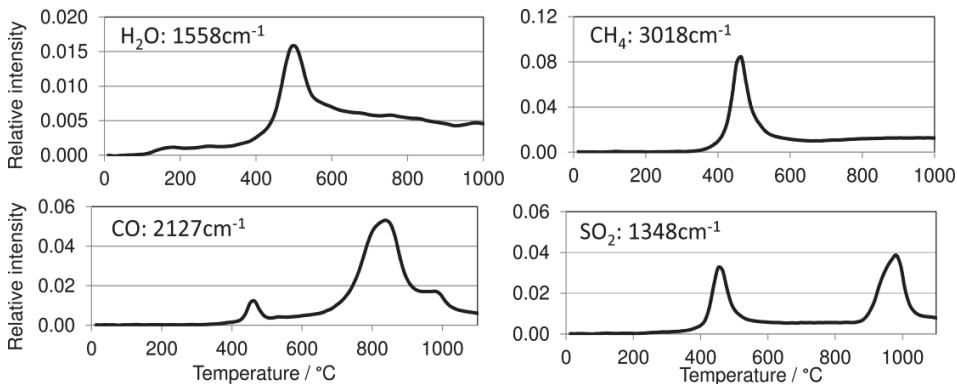
Figure 14. Emission profiles of some selected compounds in the evolved gases for OS1 in 100% CO_2

To observe the effect of CO_2 on the chemistry of the overall process, the emission profiles of some selected compounds were obtained in CO_2. In 100% CO_2 (Fig. 14), the peaks are narrower, shifted to higher temperatures, and more symmetrical over the decomposition temperature interval (400–550°C). Oxidation can also occur in this temperature range, driven by fuel O_2. The CO emission profile indicates that CO emissions are divided into two parts, with a small amount of CO emitted at lower temperatures during the decomposition of the organic component of OS at ~500°C and a notable increase in intensity at temperatures around 800°C. This increase is related to the gasification reaction, and it can be concluded that the role of the gasification reaction becomes important at temperatures above 750°C. The emission of SO_2 is also divided between two temperature regions: the main OS decomposition region and a high temperature region above 900°C. The first peak in the emission profile is related to organic sulfur, whereas the high temperature emission, which has to be studied in more detail, is related to the decomposition of sulfates or sulfides formed earlier.

Kinetic calculations

To calculate the conversion-dependent activation energies, the oxidation process was carried out for the samples under non-isothermal conditions at four different heating rates: 2.5, 5, 10, and 15 K min^{-1}. The normalized TG signals and respective DTG data were used in the calculations. The calculations were conducted using 21%O_2/Ar, 21%O_2/CO_2, and 30%O_2/CO_2 atmospheres for the

oxidation stage (the subsequent carbonate decomposition stages were not considered).
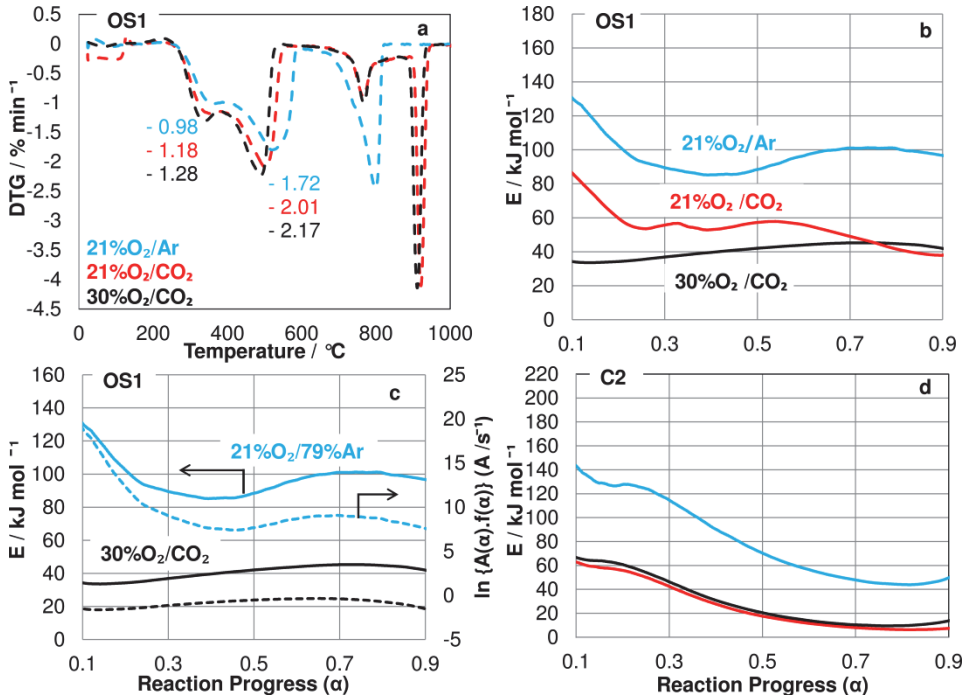
Figure 15. DTG curves of OS1 (a), conversion-dependent activation energy E of OS1 and C2 in three different atmospheres (b,d) and logarithm of pre-exponential factor A for the oxidation stage of OS1 in two different atmospheres (c)

The conversion α was calculated from the mass loss during oxidation stage:

$$\alpha = \frac{W_0 - W_t}{W_0 - W_f} \qquad (4)$$

Where W_0 is the initial weight of the sample, W_t is the weight of the sample instantaneously obtained and W_f is the final mass.

The apparent activation energy E for the oxidation stage of OS1 in the range of α = 0.2–0.9 was 80–100 kJ mol^{-1} in 21%O_2/Ar, 35–45 kJ mol^{-1} in 30%O_2/CO_2, and 40–55 kJ mol^{-1} in 21%O_2/CO_2. This parameter is higher at the beginning of oxidation, subsequently diminishes, and then increases slightly for the final stage (Fig. 15b). A comparison of the three different atmospheres shows that the reactivity during the oxidation stage is highest for the 30%O_2/CO_2 OF atmosphere (Fig. 15a) and lowest for 21%O_2/Ar. As CO_2 is a reactive gas and Ar is an inert gas, the calculated activation energy values for model air conditions are higher than those for OF conditions throughout the entire reaction. The increase of the O_2 concentration in the OF atmosphere

decreases the apparent activation energy for the OS1 sample. However, an opposite effect is observed in the case of the C2 sample (Fig. 15d). The activation energy calculated for C2 for $\alpha = 0.1–0.9$ is between 12 and 70 kJ mol^{-1} in $30\%O_2/CO_2$ and between 8 and 60 kJ mol^{-1} in $21\%O_2/CO_2$, which are quite similar but slightly lower values. One explanation for this phenomenon is the increased effect of the char gasification reaction (as the offset temperature of the oxidation stage reaches 840°C), which maintains similar E values in $21\%O_2/CO_2$ and $30\%O_2/CO_2$ atmospheres. This type of opposite effect has also been observed in the literature for other type of coals (see examples in Ref. [33]).

Conversion predictions

Based on the activation energies obtained, isothermal conversion predictions for the process duration were calculated, as given in Fig. 16.
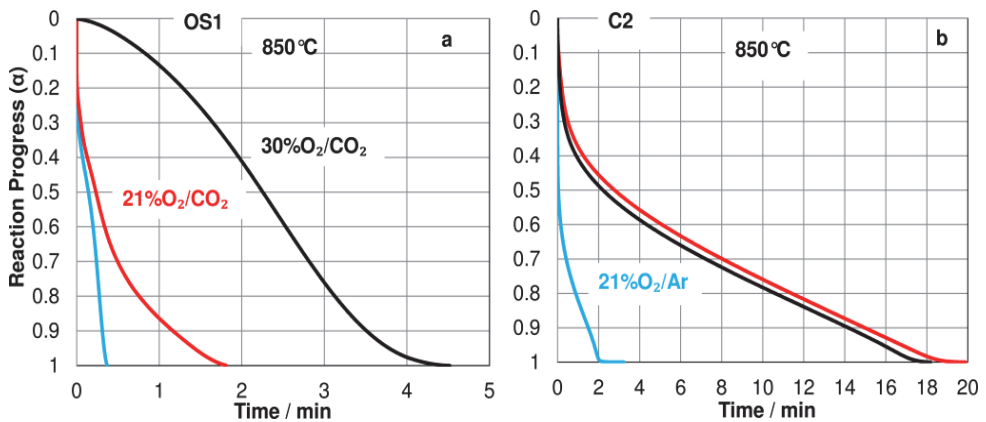
Figure 16. Conversion predictions of OS1(a) and C2(b) samples at 850°C

It can be seen that full oxidation of C2 takes much longer than that of the OS1 sample. The char combustion stage of coal should take longer because of the much higher carbon content. However, based on the values obtained from the DTG curves (Fig. 9), the difference in a real process can be somewhat less. For both samples, oxidation in $21\%O_2/Ar$ takes notably less time than oxidation in $21\%O_2/CO_2$ and $30\%O_2/CO_2$, and higher temperatures are needed to operate OF combustion with the same residence times as in air combustion. As the lower activation energies in OF atmospheres should favor the process, the differences here seem too drastic: almost 5 min is required for oxidation of OS1 in $30\%O_2/CO_2$ and only 0.5 min in $21\%O_2/Ar$.

Analysis of conversion predictions

From theory, it is known that the diffusivity of O_2 in CO_2 is ~17% lower than that in N_2 and Ar. This difference can result in longer process durations under

real combustion conditions. A comparison of the mass loss rates of the oxidation stage under dynamic heating conditions in the TA experiments also shows that differences exist (Fig. 15a), but the differences are small. The mass loss rate of OS1 corresponding to the two peaks in the DTG curves is almost the same, but slightly higher in $30\%O_2/CO_2$. Thus, a remarkable difference in residence times is not expected in the real process, as there are few differences observed in the TG-DTG-DTA curves of the samples tested in different atmospheres in terms of characteristic temperatures and mass losses.

It has been noted in the literature that in this kind of kinetic analysis based on an isoconversional approach, a specific factor, the kinetic compensation effect (KCE), can affect the prediction calculations [74, 75]. It can be seen that the plot of the pre-exponential factor function (Fig. 15c) follows the shape of the E plot. E and A have opposite effects on the value of the rate constant at some fixed temperature, with lower E values corresponding to higher rates and lower A values corresponding to lower the rates. In Fig. 15c, the A function is plotted on a logarithmic scale, while the values of E are plotted on a linear scale; therefore, the small changes in E correspond to changes in the magnitude of A. This can affect the results of conversion calculations based on non-isothermal TA experiments.

Based on our previous research experience and literature data on combustion kinetics [76], the *D3* reaction model (Eq. 5) was chosen as the most appropriate reaction model to calculate the values of the pre-exponential factor A. However, the simple first-order reaction model *F1* (Eq. 6) is also widely used and is included for calculations of the kinetic parameters and model gas–solid processes based on the Arrhenius equation.

Jander equation; three-dimensional diffusion:

$$\textbf{D3}: f(\alpha) = \frac{3}{2}\,(1-\alpha)^{\frac{2}{3}}(1-(1-\alpha)^{1/3})^{-1} \tag{5}$$

Avrami-Erofeev equation; random nucleation; first order reaction:

$$\textit{F1}: f(\alpha) = \,1-\alpha \tag{6}$$

As seen in Table 6, the average value of the pre-exponential factor A for the $21\%O_2/Ar$ atmosphere is ~25 000 (even if the first extremely high value in the table is excluded), but only 0.57 for $30\%O_2/CO_2$. The constant values of the activation energy calculated by the standardized method (based on Ozawa) are 145 kJ mol^{-1} for $21\%O_2/Ar$, 78 kJ mol^{-1} for $30\%O_2/CO_2$, and 81 kJ mol^{-1} for $21\%O_2/CO_2$.

Table 6. Average values for activation energy and pre-exponential coefficient

Conditions	E^{avg}	$\ln\{A(\alpha) \cdot f(\alpha)\}$	A^{avg}
	(kJ mol^{-1})	A(s^{-1})	(s^{-1})
30%O$_2$/CO$_2$	78	0.246	0.573
21%O$_2$/CO$_2$	81	1.67	2.16
21%O$_2$/Ar	145	10.525	24900

This information enabled us to conclude that the remarkable difference in residence times is related to the computerized methods in TA (KCE) and is probably not followed in a real process. However, there can be a slowdown in the oxidation process under OF conditions owing to differences in the diffusivities of O$_2$, and therefore, slightly higher temperatures or longer residence times are needed when compared with air combustion.

Pyrolysis kinetics

The calculated apparent activation energy E values in the range of the conversion extent for the devolatilization stage (the decomposition of carbonates is not included) for OS1 under 100%CO$_2$ and 100%Ar atmospheres are presented in Fig. 17.
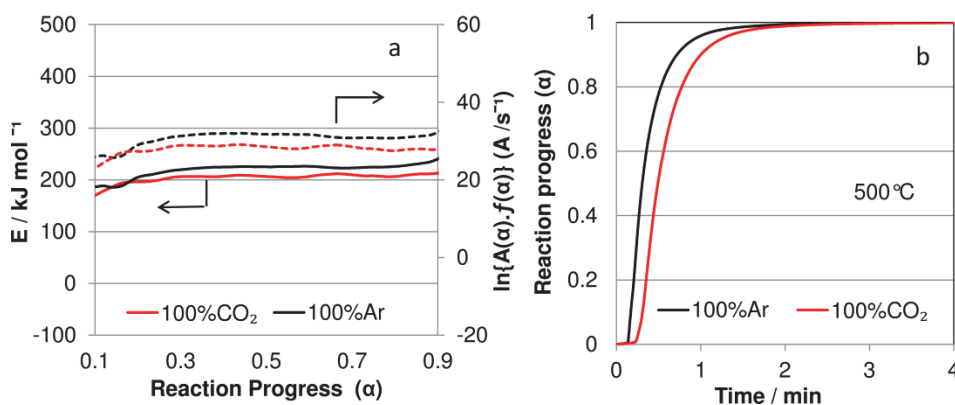
Figure 17. (OS1)Conversion-dependent activation energy E (a) and conversion prediction at 500°C (b) under 100%CO$_2$ and 100%Ar atmospheres

There are no notable changes in the E values (190–230 kJ mol^{-1}) throughout the devolatilization stage in both 100% CO$_2$ and 100% Ar, as the reaction rates were also quite similar in these atmospheres. This indicates that there is no considerable difference in reactivity at low temperatures (until 500°C) (Fig. 11a, lower).

As the E values are slightly lower in the 100% CO$_2$ atmosphere compared with those in 100% Ar, it can be concluded that the CO$_2$ char gasification reaction does not occur at these low temperatures. Nevertheless, as there are many

parallel reactions, it is difficult to characterize the specific reasons for these slight differences, as they could also be attributed to differences in the sample properties and experimental conditions. However, higher activation energy values are expected above 650°C owing to the delay in the decomposition of carbonates and the occurrence of the CO_2 char gasification reaction above 750°C. According to the conversion prediction calculations for the devolatilization stage of OS1 in 100% CO_2 and 100% Ar atmospheres, devolatilization takes slightly longer in 100% CO_2 owing to the different diffusivities of volatiles in these two media and the different thermal properties of these gases.

Char oxidation
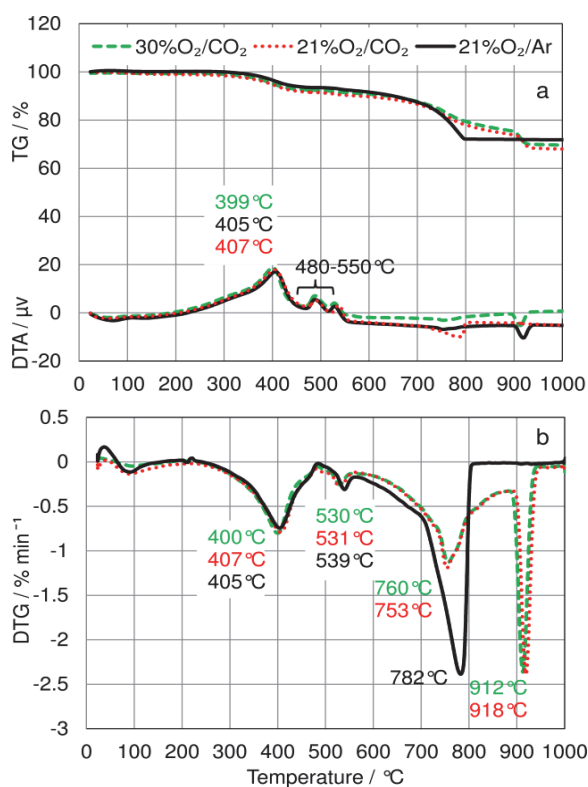
Figure 18. TG, DTA (a) and DTG (b) curves of OS1 char in 21%O₂/Ar, 21%O₂ /CO₂ and 30%O₂/CO₂ mixtures

The thermal behavior of OS1 char and its oxidation kinetics were studied in three different atmospheres with non-isothermal analysis methods (Fig. 18) and in two different atmospheres with isothermal analysis methods (Fig. 19). The first mass loss step in the TG curves (approximately 7%) is related to the oxidation of residual carbon and some residual heavier organic compounds

(thermobitumen). The DTA curves of OS char in the three different atmospheres (Fig. 18a) show a single distinctive exothermic maximum, which is lowest for $30\%O_2/CO_2$ and highest for $21\%O_2/CO_2$. The small peaks between 480 and 550°C are related to char oxidation and reactions with pyrite and organic sulfur, as EGA (Paper II, Fig. 4b therein) showed increased emission of SO_2 in this temperature interval. During direct combustion, the mass loss of sample OS1 typically has two exothermic peaks in the DTA curves (Paper III, Fig. 4a and b therein). The first peak corresponds to devolatilization and the release of lighter hydrocarbons and the second corresponds to oxidation of heavier hydrocarbons (thermobitumen) and char.

After char combustion, reactions with pyrite in the temperature range of 480–550°C are observed, which were not distinguishable in direct OS1 oxidation tests. This indicates that char combustion is followed by processes in the mineral component of the fuel that involve a complex set of competitive endothermic and exothermic reactions that depend on temperature, oxidative/reductive properties of the gas phase, and CO_2 partial pressure inside the char particles. For a detailed description of these reactions, see Paper II (Eq. 2–25).
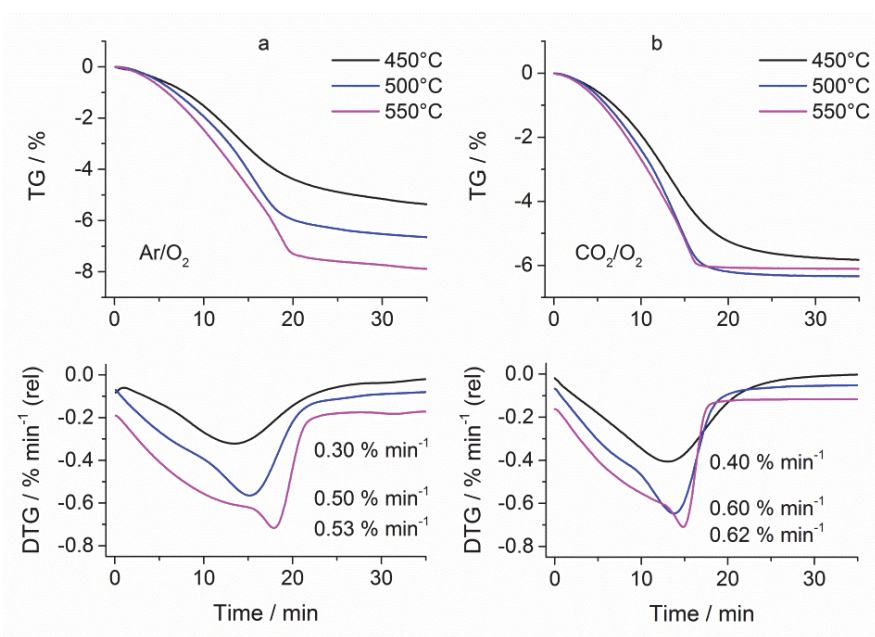
Figure 19. TG and DTG curves of isothermal oxidation of OS1 char in 21%O$_2$/Ar (a) and 30%O$_2$/CO$_2$ (b) at different temperatures

Experiments were carried out with OS1 char in two different atmospheres under isothermal conditions at three different temperatures (Fig. 19). The specific shape of the DTG curves illustrates that the char oxidation process is limited at

low temperatures. A possible explanation for the slow oxidation of char is the continued diffusion of heavier pyrolysis products during the isothermal tests.

Although the basic oxidation reactions (Eq. 7–10) for coal char (high carbon concentration) are as follows:

$$C(s) + \tfrac{1}{2} O_2 \rightarrow CO \tag{7}$$

$$C(s) + O_2 \rightarrow CO_2 \tag{8}$$

$$C(s) + CO_2 \rightarrow 2CO \tag{9}$$

$$CO + \tfrac{1}{2} O_2 \rightarrow CO_2 \tag{10}$$

In addition to the common features, the combustion rate of OS1 char (low carbon concentration) is affected by the chemical kinetics of these reactions, as well as internal gas diffusion (mainly O_2) in the voluminous mineral matter, external mass transfer, trapped volatiles that depend on the char preparation process, thermal decomposition reactions of carbonates, reactions of MgO and CaO with quartz and silicates, CO_2 and H_2O partial pressures, changes in sulfur compounds, and changes in porosity and other physical properties.

Char oxidation kinetics

To calculate the conversion-dependent activation energies, the oxidation process of OS1 char was carried out under non-isothermal conditions applying three different heating rates: 5, 10, and 15 K min^{-1} (Fig. 20).
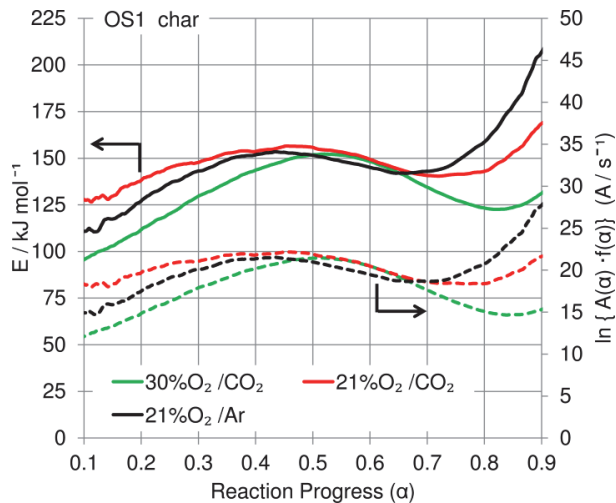
Figure 20. Conversion-dependent activation energy E and logarithm of pre-exponential factor A for OS1 char in three different atmospheres

Kinetic calculations showed that the conversion-dependent activation energy of OS char is 110–200 kJ mol^{-1} in 21%O_2/Ar, 90–125 kJ mol^{-1} in 30%O_2/CO_2, and

125–160 kJ mol^{-1} in 21%O_2/CO_2 in the range of $\alpha = 0.1$–0.9. In comparison, the activation energies for the oxidation of OS char are higher than those for OS itself, as they were in the range of 120–100 kJ mol^{-1} in 21%O_2/Ar and 35–45 kJ mol^{-1} in 30%O_2/CO_2. Moreover, the values were higher at the beginning, subsequently decreased, and then increased slightly during the final stage of oxidation. However, the activation energy of OS char is lower at the beginning of oxidation, indicating most likely related to diffusion limitation. Thereafter, the activation energy increases until a conversion of almost half is reached. Subsequently, a slight decrease and increase is observed in the final stages. The initial and final stage activation energies are lower in 30%O_2/CO_2 than in 21%O_2/Ar. For the final stage, the higher activation energies for oxidation in 21%O_2/Ar are related to the increased role of the reactions of the mineral component with increasing temperature.

Kinetic modeling of char oxidation was also carried out based on isothermal data. Several well-known mechanism models were tested to find the best fit, and the obtained results (rate constants) are presented in Paper II (Table 2 therein). However, char oxidation between 450 and 550°C was found to show non-Arrhenius behavior.

3.2 Modeling results

CFB hot loop modeling

Comparisons were carried out between the vertical distribution of the solids by analyzing the solids concentration profiles obtained from the simulation and real boiler pressure-drop measurements.
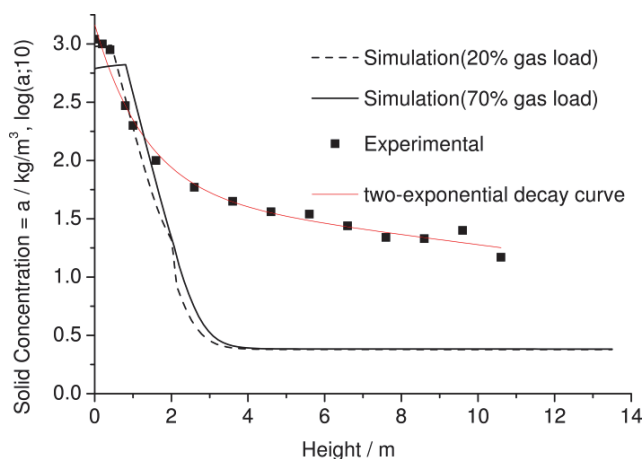
Figure 21. Solids concentration curves obtained from the simulation and the experimental measurements for conventional combustion. (Conditions: superficial gas velocity (4.7 m/s), fluidized bed pressure drop (7 kPa), particle size (0.32 mm), and bed material (SiO$_2$))

43

According to the results, the bottom bed of the modeled CFB boiler has the characteristics of a bubbling bed, like the 12 MWth CFB boiler. However, there are differences in the solids concentration levels of the bottom, splash, and transport zones.

Three different zones can be specified in the vertical distribution of solids by means of pressure-drop measurements in the 12 MWth CFB boiler [73]:

- A bottom zone with constant solid concentration (approximately 1000kg m^{-3}),
- A splash zone with an exponential decay in particle concentration with height,
- A transport zone also with lower exponential decay in solids concentration with solid back-mixing mainly at the furnace walls.

However, in the modeling results, there is an exponential decay (only for the splash zone), in which the solids concentration decreases with height until it becomes constant. In the upper dilute zone, there is no consideration of solids back-mixing (Fig. 21). Therefore, the concept of solids back-mixing cannot be explained by the flow and solids mixing behavior in a modeled CFB furnace. Thus, this is a drawback of Aspen simulations, which makes the upper dilute zone calculations problematic for CFB-related simulations. Principally, solids back-mixing is a process causes solids to remain for a certain time in the furnace, even though the superficial velocity exceeds the terminal (free fall) velocity of the individual particles. Thus, the process simulation model for the FB reactor does not include the full complexity of the behavior of CFB boilers. Considering the modeling strategy and the behavior of solids, to model CFB boilers in Aspen Plus, the solid particles entering the boiler have to be almost elutriated, with a very small discharge flow. For inspection of this behavior, it should be verified that elutriated and entering particles have similar PSDs. Essentially, such an approach is quite controversial, especially when higher gas velocities are required to recirculate the particles, as the superficial gas velocities are strongly dependent on the net solid flux (see Fig. 4 in Ref. [72] and Fig. 5b in Paper III). Nevertheless, to obtain a first insight into the overall heat and mass balances of the CFB furnace under different OF cases, the obtained modeling data is valuable. As expected, the bottom bed behaviors can be simulated with the FB reactor of Aspen Plus, which has the characteristics of a bubbling bed. Additionally, for specific thermodynamic boundaries of the CFB boiler, heat balance calculations can be performed to determine approximate values for heat losses and credits.

Modeling based on Gibbs free energy minimization

In this modeling approach, the composition of the product gas was estimated by calculating the mass–energy balance and chemical equilibrium of the process, rather than the gas and solid hydrodynamics in FB reactors. For OF combustion cases, two different FGR strategies were applied by controlling the O_2 percentage in the flue gas to maintain similar temperatures at the outlet of the combustion reactor to those obtained with air combustion.

The applied modeling approach demonstrated that it is possible to achieve similar temperatures in the simulated OF cases to those in air combustion case by increasing the O_2 concentration in the oxidant. After condensation and the FGR processes, ~87% less flue gas requires treatment in the wet and dry FGR cases of EOS for flue gas cleaning and CO_2 capture compared with the air combustion case, and ~80% for UOS (UOS for comparison) (Table 7). However, there is a notably higher ash flow rate in OF combustion cases, which changes the heat and mass balance of the system during the system transition from air to OF combustion.

Table 7. Selected simulation results for air and OF combustion of EOS

	Air EOS/UOS	OF EOS		OF UOS	
Fuel flow rate, kg/s	100	100	100	100	100
FGR option		Wet	Dry	Wet	Dry
Temperature, °C	1556/1384	1558	1560	1387	1383
FGR[1] ratio, %		67.3	64.1	66.5	65.6
O_2 concentration, %Vol	21%/N_2	26.7	28.2	28.8	30.6
Flue gas flow rate, kmol/s	14.9/10.8	11.6	10.7	7.5	7.3
Flue gas composition at 810°C, %Vol					
CO_2	14.4/14.6	65.6	77.8	67.6	80.1
H_2O	12.8/10.2	30.1	17.5	28.1	14.9
O_2	3.4/3.1	3.09	3.01	3.03	3.08
N_2	69.3/71.9	1.01	1.1	0.94	1.15
NO (ppmv)	2604/2875	355	381	345	393
NO_2 (ppmv)	26.9/34.5	4.1	4.3	3.95	4.2
SO_3 (ppmv)	0.01/0.01	0.02	0.024	0.021	0.016
SO_2 (ppmv)	0.12/0.1	0.16	0.195	0.156	0.19
CO (ppmv)	0.07/0.068	0.3	0.37	0.31	0.4
Ash flow rate, kg/s	47.9/65.5	61.7	61.7	76.9	76.9
Ash Composition, %mass					
$CaCO_3$	0/0	50.5	50.5	33.8	33.8
CaO	36.8/22.1	0	0	0	0
$CaSO_4$	11/8.1	8.5	8.5	6.9	6.9
$FeSO_4$	7.8/7.2	6.1	6.1	5.8	5.8
Recycled Flue gas composition, %Vol					
CO_2		74.6	94.57	76.1	95.1
H_2O		20.33	0	18.8	0
O_2		3.51	3.65	3.58	3.54
N_2		1.15	1.45	0.89	0.95
SO_2 (ppmv)		0.12	0.23	0.23	0.21

$$^1FGR = \frac{mol\ of\ recycled\ flue\ gas}{total\ mol\ of\ gas\ in\ boiler\ outlet}$$

Comparison of modeling results with experimental results

In both the OF combustion cases for EOS, ~88% of $CaCO_3$ is not decomposed in the ash. By increasing the boiler temperatures with sensitivity analysis, the decomposition temperatures are shifted to above 834°C for the wet FGR case and 855°C for the dry FGR case owing to the higher partial pressure of CO_2 in the dry FGR case compared with the wet FGR case. However, the decomposition temperatures were expected to be above 900°C according to the

TA results discussed throughout the thesis (Fig. 9, 10, and 18). In accordance with the TG tests in 21%O_2/Ar, although the amount of decomposed carbonates and ash values are similar for both fuels, there are considerable differences in the ash flow rates and ash composition between the air and OF cases, including different concentrations of $CaCO_3$, CaO, $CaSO_4$, and $FeSO_4$. The high level of $CaCO_3$ decomposition for the air combustion simulation arises from the assumed general reaction model in the RGibbs reactor and the simplified definition of mineral component of the fuel, which does not reflect the complete physical properties of the fuel. Thus, it should be remembered that the results are also strongly dependent on the kinetics and residence time of fuel particles in the CFB boiler. Additionally, in the case of solids (combustion of carbon and decomposition of carbonates), the obtained results should be taken into account carefully, with the awareness that carbon to CO_2 conversion, which is more limited than in the obtained results, also influences CO emissions. In this sense, for further studies including char combustion and detailed reactions in the mineral component of the EOS, the simulated model may be extended for specific solid processes by means of chemical kinetics, although possible difference would be small, as there is not much carbon-rich residue in OS1.

4. CONCLUSIONS

The main outcomes of this PhD work are listed below:

Experimental

- According to the amounts of oxidized organic matter and products formed during the combustion and pyrolysis tests, it is clear that there are no principle differences for the fuel samples at the devolatilization and oxidation stages until 500°C.
- Comparing $21\%O_2/Ar$ and $30\%O_2/CO_2$ atmospheres; the amounts of oxidized organic matter and the products formed do not differ significantly. Although the characteristic temperatures (onset, offset and peak temperatures) are shifted towards lower values due to the higher O_2 content in OF, there are no principle differences for the fuel samples in the oxidation stage. The combustion reactivity of OS and coal can be notably affected by changing the O_2 concentration.
- The pyrolysis behavior is very similar in Ar and CO_2 until 500°C and there is no visible char carbon and CO_2 reaction under OF conditions up to this temperature. However, the decomposition of carbonates in the mineral part of OS is notably influenced by the CO_2 partial pressure.
- Under OF combustion conditions, the decomposition of calcite takes place at higher temperatures (above 900°C), enabling a reduction of CO_2 emissions from the mineral part of OS and a decreased influence of the endothermic effect of $CaCO_3$ decomposition at lower combustion temperatures.
- Compared with $21\%O_2/Ar$ atmosphere, the oxidation processes of OS and coal proceed with lower activation energies in O_2/CO_2.
- Char oxidation under OF conditions occurs with lower activation energies than under $21\%O_2/Ar$, especially at higher conversion levels. Thus, applying OF combustion to OS should enhance the process when compared with air combustion.
- The gas analysis results show that the release of CO from OS in a 100% CO_2 atmosphere increases notably at temperatures above 650–700°C, indicating the occurrence of the char carbon–CO_2 reaction. However, the various possible reactions in this temperature region, which include reactions of the mineral component, makes identifying the role of the char carbon and CO_2 reaction complicated.
- Combined TG–FTIR analyses enable determination of a number of important (in regards to emissions) gaseous compounds produced in the process.
- Isothermal conversion predictions calculated from non-isothermal data showed that despite a lower activation energy, oxidation in O_2/CO_2 takes more time than that in an $21\%O_2/Ar$ atmosphere. One reason for this is

related to the KCE, which is specific to the isoconversional model used. Therefore, these predictions should be taken with some caution.

Modeling

- The FB model used in the OF CFBC simulation using Aspen Plus can predict the solids density of the bottom bed and splash zone. However, it does not allow the prediction of the solids concentration in the transport zone owing to the single entrainment correlation, which can be considered as a limitation of the current Aspen FB modeling block.
- To minimize NO_x and, especially, SO_x emissions from OF combustion of EOS, high temperatures (above 840°C) should be avoided.
- FGR options have no effect on the ash flow rates and ash composition owing to the simplified set of conditions for OF cases; however, for the air combustion case, there is a notably lower ash flow rate with higher CaO content because of the almost complete decomposition of carbonates.
- For operational adaptability (during system transitions or retrofitting applications), to compensate for the additional heat transfer area required in OF combustion, external heat exchangers could be a necessary technical upgrade.
- Compared with air combustion, the heat duty in the combustion reactor and heat capacity of the flue gases are higher for the OF combustion cases, which indicates that the amount of heat output and boiler efficiency can be increased when the system is converted to OF combustion.

Concluding remarks

The studies described in this thesis cover some of the fundamental aspects with respect to OF combustion of EOS with a focus on the oxidation characteristics, the effect of CO_2 on the chemistry of the overall processes, and the specifics of the different stages of OF combustion.

Together with the developed models, the obtained data in this PhD work constitute a well-documented first step and guide for the intermediate stages through to the operation of pilot- and demonstration-scale units, which are the next steps towards commercialization of OF combustion technology.

The developed models can easily be modified, if necessary, and can be used to evaluate the effect of the main operating parameters of OF combustion processes.

As a consequence, for further reduction of CO_2 emissions from the Estonian energy sector, the results of these first experiments and modeling studies indicate that despite several differences discussed in the current study, there should be no fundamental difficulties in applying OF combustion to EOS.

REFERENCES

1.   International Energy Agency. Carbon Capture and Storage: The solution for deep emissions reductions. **2015**, IEA, Paris. Available online: www.iea.org/publications/. *(12.03.2016)*

2.   IEA Clean Coal Centre, (Report) Developments in Oxyfuel Combustion of Coal. Lockwood, T. IEA Clean Coal Centre Park House 14 Northfields London SW18 1DD United Kingdom, **2014.** Available online: https://www.usea.org/sites/default/files/082014 _ Developments %20in%20oxyfuel%20combustion%20of%20coal_ccc240.pdf. *(15.04.2016)*

3.   Lyngfelt, A., Leckner, B. Technologies for CO_2 separation. – *Minisymposium on Carbon Dioxide Capture and Storage, School of Environmental Sciences Chalmers University of Technology, Göteborg University,* **1999**, 25-35. Available online: http://www.entek.chalmers. se/~anly/symp/sympco2.html. (15.06.2016)

4.   IPCC Special Report on Carbon Dioxide Capture and Storage. **2005**, Metz, B., Davidson, O., deConinck, H.C., Loos, M., Meyer, L.A. Editors., IPCC - Working Group III IPCC: Cambridge University Press, Cambridge, United Kingdom and New York. Available online: https://www.ipcc.ch/pdf/special – reports/srccs/srccs _ wholereport.pdf. (11.04.2016)

5.   Wall, T.F. Combustion processes for carbon capture. – *Proceedings of the Combustion Institute*. **2007**, 31(1), 31-47.

6.   Toftegaard, M. B., Brix, J., Jensen, P. A., Glarborg, P., Jensen, A. D. Oxy-fuel combustion of solid fuels. – *Progress in Energy and Combustion Science.* **2010**, 36(5), 581-625.

7.   Stanger, R. et. al. Oxyfuel combustion for CO_2 capture in power plants. - *International Journal of Greenhouse Gas Control*. **2015**, 40, 55-125.

8.   Buhre, B.J.P., Elliott, L. K., Sheng, C. D., Gupta, R. P., Wall, T. F. Oxy-fuel combustion technology for coal-fired power generation. - *Progress in Energy and Combustion Science.* **2005,** 31(4), 283-307.

9.   Yin, C., Yan, J. Oxy-fuel combustion of pulverized fuels: Combustion fundamentals and modeling. – *Applied Energy*. **2016**, 162, 742-762.

10.   Andersson, K., Johansson, R., Hjärtstam, S., Johnsson, F., Leckner, B. Radiation intensity of lignite-fired oxy-fuel flames. – *Experimental Thermal and Fluid Science*. **2008**, 33(1), 67-76.

11.   Croiset, E., Thambimuthu, K., Palmer, A. Coal Combustion in O_2/CO_2 mixtures compared with air. – The Canadian Journal of Chemical Engineering. 2000, 78, 403-407.13.

12.   Liu, H., Zailani, R., Gibbs, B. M. Comparisons of pulverized coal combustion in air and in mixtures of O_2/CO_2. – *Fuel*. **2005**, 84(7-8), 833-840.

13. Riaza, J., Alvarez, L., Gil, M. V., Pevida, C., Pis, J. J., Rubiera, F. Ignition and NO emissions of coal and biomass blends under different oxy-fuel atmospheres. – *Energy Procedia*. 2013, 37, 1405-1412.

14. Tan, Y., Croiset, E., Douglas, M. A., Thambimuthu, K. V. Combustion characteristics of coal in a mixture of oxygen and recycled flue gas. – *Fuel*. **2006**, 85(4), 507-512.

15. Lupion, M. et al. 30 MWth CIUDEN Oxy-cfb boiler - First experiences. - *Energy Procedia*. **2013,** 37**,** 6179-6188.

16. Duan, L., Sun, H., Zhao, C., Zhou, W., Chen, X. Coal combustion characteristics on an oxy-fuel circulating fluidized bed combustor with warm flue gas recycle. – *Fuel*. **2014**, 127, 47-51.

17. Li, H. et. al. Experimental results for oxy-fuel combustion with high oxygen concentration in a 1MWth pilot-scale circulating fluidized bed. – *Energy Procedia.* **2014,** 63, 362-371.

18. Kuivalainen, R. et. al. Characterization of 30MWth Circulating Fluidized Bed Boiler under Oxy-combustion Conditions. – *IEAGHG 3rd Oxyfuel Combustion Conference,* **2013**. Available at: http://www.ieaghg.org/docs/General_Docs/OCC3/Secured%20presentat ions/P1_2_Characterization_of_30_MWth_Circulating_Fluidized_Bed_ Boiler_under_OxyCombustion_Conditions.pdf (07.06.2016)

19. Normann, F., Andersson, K., Leckner, B., Johnsson, F. Emission control of nitrogen oxides in the oxy-fuel process. – *Progress in Energy and Combustion Science.* **2009**, 35(5), 385-397.

20. Khare, S.P., Wall, T. F., Farida, A. Z., Liu, Y., Moghtaderi, B., Gupta, R. P. Factors influencing the ignition of flames from air-fired swirl PF burners retrofitted to oxy-fuel. – *Fuel*. **2008**, 87(7), 1042-1049.

21. Croiset, E., Thambimuthu, K. V. NO_x and SO_2 emissions from O_2/CO_2 recycle coal combustion. – *Fuel*. **2001**, 80**,** 2117-2121.

22. Trikkel, A., Zevenhoven, R., Kuusik, R. Modelling SO_2 capture by Estonian limestones and dolomites. – *Proceedings of the Estonian Academy of Sciences Chemistry*. **2000,** 49, 1, 53-70.

23. Tan, Y., Jia, L., Wu, Y., Anthony, E. J. Experiences and results on a 0.8MWth oxy-fuel operation pilot-scale circulating fluidized bed. – *Applied Energy.* **2012**, 92, 343-347.

24. Pikkarainen, T., Saastamoinen, J., Saastamoinen, H., Leino, T., Tourunen, A. Development of 2nd generation oxyfuel CFB Technology – small scale combustion experiments and model development under high oxygen concentrations. - *Energy Procedia*. **2014,** 63, 372-385.

25. Gómez, M., Fernández, A., Llavona, I., Kuivalainen, R. Experiences in sulfur capture in a 30 MWth Circulating Fluidized Bed boiler under oxy-combustion conditions. – *Applied Thermal Engineering.* **2014**, 65(1-2), 617-622.

26. Hofbauer, G., Beisheim, T., Dieter, H., Scheffknecht, G. Experiences from oxy-fuel combustion of bituminous coal in a 150 kWth circulating fluidized bed pilot facility. – *Energy Procedia*. **2014,** 51, 24-30.

27. Andersson, K., Normann, F., Johnsson F., Leckner B. NO emission during oxy-fuel combustion of lignite. – *Industrial & Engineering Chemistry Research.* **2008**, 47, 1835-1845.

28. Hu, Y., Naito, S., Kobayashi, N., Hasatani, M. CO_2, NO_x and SO_2 emissions from the combustion of coal with high oxygen concentration gases. – *Fuel.* **2000**, 79, 1925- 1932.

29. Liu, H., Zailani, R., Gibbs, B. M. Pulverized coal combustion in air and in O_2/CO_2 mixtures with NO_x recycle. – *Fuel*. **2005**, 84(16), 2109-2115.

30. Guedea I., P.D., Díez L. I., Johnsson, F. Conversion of large coal particles under O_2/N_2 and O_2/CO_2 atmospheres - Experiments and modeling. – *Fuel Processing Technology*. **2013**, 112, 118–128.

31. Abbasi-Atibeh, E., Yozgatligil, A. A study on the effects of catalysts on pyrolysis and combustion characteristics of Turkish lignite in oxy-fuel conditions. – *Fuel*. **2014**, 115**,** 841-849.

32. Meng, F., Yu, J., Tahmasebi, A., Han, Y. Pyrolysis and combustion behavior of coal gangue in O_2/CO_2 and O_2/N_2 mixtures using thermogravimetric analysis and a drop tube furnace. – *Energy & Fuels*. **2013**, 27(6), 2923-2932.

33. Wang, C., Zhang, X., Liu, Y., Che, D. Pyrolysis and combustion characteristics of coals in oxyfuel combustion. – *Applied Energy.* **2012**, 97, 264-273.

34. Yuzbasi, N.S., Selçuk, N. Air and oxy-fuel combustion behaviour of petcoke/lignite blends. – *Fuel*. **2012**, 92(1), 137-144.

35. Li, X., Rantham, R. K., Yu, J., Meesri, J. Pyrolysis and combustion characteristics of an Indonesian low-rank coal under O_2/N_2 and O_2/CO_2 conditions. – *Energy & Fuels.* **2010**, 24(1), 160-164.

36. Molina, A., Shaddix, C. R. Ignition and devolatilization of pulverized bituminous coal particles during oxygen/carbon dioxide coal combustion. - *Proceedings of the Combustion Institute.* **2007,** 31(2), 1905-1912.

37. Man, C.K., Gibbins, J. R. Factors affecting coal particle ignition under oxyfuel combustion atmospheres. – *Fuel.* **2011**, 90(1), 294-304.

38. Gil, M.V., Riaza, J., Álvarez, L., Pevida, C., Pis, J. J., Rubiera, F. Oxy-fuel combustion kinetics and morphology of coal chars obtained in N_2 and CO_2 atmospheres in an entrained flow reactor. – *Applied Energy.* **2012**, 91(1), 67-74.

39. Gil, M.V., Riaza, J., Álvarez, L., Pevida, C., Pis, J. J., Rubiera, F. Kinetic models for the oxy-fuel combustion of coal and coal/biomass blend chars obtained in N_2 and CO_2 atmospheres. – *Energy*. **2012**, 48(1), 510-518.

40. Dhaneswar, S.R., Pisupati, S. V. Oxy-fuel combustion: The effect of coal rank and the role of char-CO_2 reaction. - *Fuel Processing Technology.* **2012**, 102, 156-165.

41. Rathnam, R.K., Elliott, L. K., Wall, T. F., Liu, Y., Moghtaderi, B. Differences in reactivity of pulverised coal in air (O_2/N_2) and oxy-fuel (O_2/CO_2) conditions. – *Fuel Processing Technology.* **2009**, 90(6), 797-802.

42. Sotudeh-Gharebaagh, R., Legros, R., Chaouki, J. Paris, J., Simulation of circulating fluidized bed reactors using Aspen Plus. – *Fuel.* **1998**, **77**, 327-337.

43. Begum, S., Rasul, M. G., Akbar, D., Ramzan, N. Performance analysis of an integrated fixed bed gasifier model for different biomass feedstocks. –- *Energies.* **2013**, 6(12), 6508-6524.

44. Hu, Y., Yan, J., Li, H. , Effects of flue gas recycle on oxy-coal power generation systems. – *Applied Energy.* **2012**, 97, 255-263.

45. Liu, B., Yang, X., Song, W. Lin, W. Process simulation of formation and emission of NO and N_2O during coal decoupling combustion in a circulating fluidized bed combustor using Aspen Plus. – *Chemical Engineering Science.* **2012**, 71, 375-391.

46. Nikoo, M.B., Mahinpey, N. Simulation of biomass gasification in fluidized bed reactor using Aspen Plus. – *Biomass and Bioenergy.* **2008**, 32(12), 1245-1254.

47. Pei, X., He, B., Yan, L., Wang, C., Song, W., Song, J. Process simulation of oxy-fuel combustion for a 300MW pulverized coal-fired power plant using Aspen Plus. – *Energy Conversion and Management.* **2013**, 76, 581-587.

48. Doherty, W., Reynolds, A., Kennedy, D. The effect of air preheating in a biomass CFB gasifier using Aspen Plus simulation. – *Biomass and Bioenergy.* **2009**, 33(9), 1158-1167.

49. Jurado, N., Darabkhani, H. G., Anthony, E. J. B., Oakey, J. Co-firing performance of a retrofitted oxy-combustor burning coal/biomass blends: experimental and simulation study. – *IEAGHG 3rd Oxyfuel Combustion Conference,* 2013. Available online: http://www.ieaghg.org/docs/General_Docs/OCC3/Secured%20presentations/4c_4_OCC3_NJ-V.1.pdf (09.05.2016)

50. Xiong, J., Zhao, H., Chen, M., Zheng, C. Simulation study of an 800 MWe oxycombustion pulverized-coal-fired power plant. – *Energy & Fuels.* **2011,** 25, 2405-2415.

51. Ots, A. Estonian oil shale properties and utilization in power plants. – *Energetika.* **2007**. 53(2), 8-18.

52. Arro, H., Prikk, A., Pihu, T. Calculation of qualitative and quantitative composition of Estonian oil shale and its combustion products. Part 1. Calculation on the basis of heating value. – *Fuel.* **2003**, 82(18), 2179-2195.

53. Qian, J., Yin, L., Oil Shale – Petroleum Alternative 2010: China Petrochemical Press; First Edition (May 18, 2010).

54. Williams, P.T., Ahmad, N. Investigation of oil-shale pyrolysis processing conditions using thermodynamic analysis. – *Applied Energy*. **2000**, 66, 113-133.

55. Tiwari, P., Deo, M. Detailed kinetic analysis of oil shale pyrolysis TGA data. – *AIChE Journal*. **2012**, 58(2), 505-515.

56. Kök, M.V., Pamir, M. R. Comparative pyrolysis and combustion kinetics of oil shales. - *Journal of Analytical and Applied Pyrolysis*. **2000**, 55, 185-194.

57. Li, S., Yue, C. Study of pyrolysis kinetics of oil shale. – *Fuel. 2003*, 82, 337-342.

58. Jaber, J.O., Probert, S. D. Pyrolysis and gasification kinetics of jordanian oil-shales. – *Applied Energy*. **1999**, 63, 269-286.

59. Fang-Fang, X., Ze, W., Wei-Gang, L., Wen-Li, S. Study on thermal conversion of huadian oil shale under N_2 and CO_2 atmospheres. – *Oil Shale*. **2010**, 27(4), 309.

60. Barkia, H., Belkbir, L., Jayaweera, S. A. A. Non-isothermal kinetics of gasification by CO_2 of residual carbon from timahdit and tarfaya oil shale kerogens. – *Journal of Thermal Analysis and Calorimetry*. **2004**, 76(2), 623-632.

61. Loo, L., Maaten, B., Siirde, A., Pihu, T., Konist, A. Experimental Analysis of the Combustion Characteristics of Estonian Oil Shale in Air and Oxy-fuel Atmospheres. – *Fuel Processing Technology*. **2015**, 134, 317−324.

62. Al-Makhadmeh, L., Maier, J., Al-Harahsheh, M., Scheffknecht, G. Oxy-fuel technology: An experimental investigations into oil shale combustion under oxy-fuel conditions. – *Fuel*. **2013**, 103, 421-429.

63. Al-Makhadmeh, L., Maier, J., Scheffknecht, G. Oxyfuel technology: NO reduction during oxy-oil shale combustion. – *Fuel*. **2014**, 128, 155-161.

64. Sherritt, R., Jia, J., Purnomo, M., Schmidt, J. Advances in steady-state process modeling of oil shale retorting. 29th Oil Shale Symposium, 2009.

65. Jing-Ru, B., Zhang, B., Qing, W., Shu-Yuan, L. Process simulation of oil shale comprehensive utilization system based on huadian-type retorting technique. – *Oil Shale*. **2015**, 32(1), 66-81.

66. Pambudi, N.A., Laukkanen, T., Fogelholm, C., Kohl, T., Jarvinen, M. Prediction of gas composition of Jatropha curcas Linn oil cake in entrained flow reactors using Aspen Plus simulation software. – *International Journal of Sustainable Engineering*. **2013**, 6(2), 142-150.

67. Meriste, T., Yörük, C.R., Trikkel, A., Kaljuvee T., Kuusik, R. TG–FTIR Analysis of Oxidation Kinetics of Some Solid Fuels Under Oxy-fuel Conditions. – *Journal of Thermal Analysis and Calorimetry*. **2013**, 114(2), 483-489.

68.   HR Aldrich Vapor Phase Library v3.2 (Serial No: 110412213)
69.   Advanced Kinetics and Technology Solutions. AKTS Thermokinetics. http://www.akts.com. AKTS AG. Switzerland.
70.   Roduit, B., Folly, P., Berger, B., Mathieu, J., Sarbach, A., Andres, H., et al. Evaluating sadt by advanced kinetics-based simulation approach. – *Journal of Thermal Analysis and Calorimetry*. **2008,** 93(1), 153-61
71.   Roduit, B., Xia, L., Folly, P., Berger, B., Mathieu, J., Sarbach, A., et al. The simulation of the thermal behavior of energetic materials based on DSC and HFC signals. – *Journal of Thermal Analysis and Calorimetry* **2008**, 93(1), 143-52.
72.   Yörük, C.R.; Normann, F.; Johnsson, F.; Trikkel, A.; Kuusik, R. Applicability of the FB reactor of Aspen Plus for CFB Oxy-fuel Combustion of Estonian Oil Shale: Gas and Solid Hydrodynamics. 22nd International conference on fluidized bed conversion 2015, Turku, Finland. Ed. D. Bankiewicz, M. Mäkinen, P. Yrjas. VTT, 150−159.
73.   Johnsson, F., Leckner, B. Vertical distribution of solids in a CFB-furnace. – *13th International Conference on Fluidized Bed Combustion*. 1995.
74.   Galwey, A.K. Is the science of thermal analysis kinetics based on solid foundations?: A literature appraisal. – *Thermochimica Acta*. **2004**, 413(1–2), 139-183.
75.   Brown, M.E., Galwey, A.K. The significance of "compensation effects" appearing in data published in "computational aspects of kinetic analysis": ICTAC project, 2000. – *Thermochimica Acta*. **2002**, 387(2), 173-183.
76.   Niu, S. et al. Thermogravimetric analysis of combustion characteristics and kinetic parameters of pulverized coals in oxy-fuel atmosphere. – *Journal of Thermal Analysis and Calorimetry*. **2009**, 98(1), 267-274.

ACKNOWLEDGEMENTS

ABSTRACT

Circulating fluidized bed combustion (CFBC), in operation since 2004, has been an impetus in the energy sector of Estonia by providing a reliable technology for combustion of Estonia oil shale (EOS) in terms of combustion efficiency, fuel flexibility, and reduced emissions, including SO_2 and CO_2. However, control of CO_2 emissions is still challenging, owing to international climate conventions and the continuously increasing demand for electricity. Therefore, future decreases require application of CO_2 capture because of the widespread usage of EOS in heat and power production.

CO_2 capture and storage (CCS) technologies have the potential for application to large sources of CO_2. Research on CCS, especially on oxy-fuel (OF) combustion technology, which is the topic of the current study, is still highly active. Notably, OF combustion has potential advantages compared with other CO_2 capture technologies, as laboratory studies and pilot-scale experiments on OF combustion of coal and biomass have shown that this method can be applied to pulverized combustion and CFBC technologies. The analysis of combustion processes for OF combustion technology including different solid fuels and their properties, devolatilization, char burn out, and gasification reactions have been key research areas, as this knowledge is important for the development of OF combustion systems. The earliest challenges for OF combustion technology have now successfully been met, and the first generation of full-chain OF combustion technology has already been demonstrated as a feasible technology in different countries. Currently, expectations are growing for commercial units.

For the implementations of OF combustion for unconventional fuels like EOS, the available data for coal and biomass combustion is not completely suitable, as the combustion specifics are strongly fuel-dependent. There are also knowledge gaps in a wide range of research areas required for the realization of OF combustion of EOS, as the optimal operating conditions for OF combustion of coal and biomass vary depending on the characteristic fuel properties.

The research in this thesis is aimed at generating a fundamental knowledge base using experimental investigations (focusing on the oxidation characteristics, effect of CO_2 on the overall process, and the specifics of the different stages of OF combustion) and process modeling (with respect to the specific CFB operating parameters) to understand and analyze the complex combustion behavior of EOS under OF combustion conditions, which could support the development of its possible integration.

The thermal analysis experimental results presented in this thesis showed that the emission of CO_2 from the mineral component of EOS can be decreased, as the decomposition of calcite occurs at higher temperatures in OF combustion. Additionally, CO_2 did not have a notable effect on the devolatilization stage of EOS. Although identification of the role of the char carbon–CO_2 reaction was complex owing to the various possible reactions, the emission profiles showed that the gasification reaction is accelerated above 750–800°C. The conversion-

dependent activation energies were calculated for different process stages. These values were notably lower for the oxidation of EOS and its char in O_2/CO_2 than those calculated for a model air (21%O_2/Ar) atmosphere. Therefore, compared with air combustion, the application of OF combustion to oil shale should enhance the process.

The OF cases simulated using the Aspen Plus software showed that it is possible to achieve temperatures similar to those in the air combustion case by increasing the O_2 concentration in the gaseous phase. Heat transfer profiles similar to those in the air combustion case can be maintained with the calculated O_2 concentrations; however, owing to the lower mass flow in the convective pass, a slightly higher O_2 concentration in the gaseous phase and a slightly higher flue gas recycle ratio would be more suitable for retrofitting applications. To decrease emissions of CO, SO_2, and mineral CO_2, high temperatures should be avoided (above 840°C) during OF combustion, especially in the zones with lower O_2 concentrations. There was a higher ash flow rate during the simulated OF combustion case with a higher $CaCO_3$ content because of the decreased decomposition of carbonates. For operational adaptability (during system transitions), to compensate for the additional heat transfer area required for OF combustion, external heat exchangers could be a necessary technical upgrade. The heat duty in the combustion reactor and heat capacity of the flue gases were higher for the OF combustion cases, indicating that the heat output and boiler efficiency can be increased.

The thesis concludes that despite several characteristic differences observed under O_2/CO_2 and 21%O_2/Ar atmospheres, there should be no fundamental difficulties in applying OF combustion to EOS. Additionally, the EOS combustion process can be enhanced in comparison with air combustion, and achieve the prerequisites for effective CCS.

KOKKUVÕTE

Tsirkuleerivas keevkihis põletamine, mida rakendatakse alates aastast 2004, on edendanud Eesti energiasektorit, kindlustades usaldusväärse tehnoloogia Eesti põlevkivi põletamiseks, mis väljendub kasvanud kasuteguris, kütuste varieeritavuses ja vähenenud emissioonides nii SO_2 kui CO_2 osas. CO_2 emissioonide edasine vähendamine on siiski väljakutset esitav, tulenedes rahvusvahelistest kliimat puudutavatest konventsioonidest ja kasvavast energiavajadusest. Seetõttu on põlevkivi jätkuva massiivse kasutuse korral elektri ja soojuse tootmisel vajalik rakendada CO_2 püüdmist.

Mitmed süsiniku püüdmis- ja ladustamistehnoloogiad (CCS) omavad rakenduspotentsiaali seal, kus tekivad suured CO_2 vood. Nende tehnoloogiate arendamine, eriti kütuste hapnikus-põletamise (täpsemalt hapnikuga rikastatud suitsugaasides põletamise) uurimine, mis on ka käesoleva töö teema, on jätkuvalt aktuaalne. Seejuures omab hapnikus-põletamine mitmeid potentsiaalseid eeliseid võrreldes teiste CCS tehnoloogiatega nagu näitavad ka mitmed laboratoorsed ja pilootseadmete tasemel tehtud uuringud söe ja biomassi põletamise osas, kinnitades selle rakendatavust nii tolm- kui keevkihtpõletuse puhul. Hapnikus-põletamise protsessi analüüs, mis hõlmab erinevaid tahkeid kütuseid ning nende omadusi, lendainete eraldumist, koksi väljapõlemist ja gaasistamisreaktsiooni mõju, on oluliseks uurimisvaldkonnaks, andes väärtuslikke alusteadmisi hapnikus-põletamise süsteemide arendamiseks. Teatud edu selle tehnoloogia osas on praeguseks saavutatud ja esimese generatsiooni pilootseadmed mitmetes riikides näidanud edukalt protsessi teostatavust. Nüüd kasvavad ootused hapnikus-põletamise tööstuslikuks realiseerimiseks.

Hapnikus-põletamise kasutuselevõtuks mittetraditsiooniliste kütuste puhul nagu seda on põlevkivi, pole olemasolevad andmed, mis on saadud peamiselt kivisöe ja biomassi põletamisel, sobivad, sest protsess sõltub oluliselt kütuse omadustest. Nii on teadmised, mis puudutavad Eesti põlevkivi võimalikku hapnikus-põletamist, suuresti puudulikud, kuna optimaalsed tingimused võivad põlevkivi spetsiifiliste omaduste tõttu oluliselt erineda võrreldes söe või biomassi põletamisega.

Sellest lähtuvalt on antud uurimistöö eesmärgiks tekitada alusteadmised, mis aitaksid arendada ja toetada Eesti põlevkivi hapnikus-põletamise protsessi kasutuselevõttu. Et mõista ja analüüsida Eesti põlevkivi põlemisel toimuvaid keerukaid protsesse hapnikus-põletamise tüüpilistes tingimustes, viidi läbi rida eksperimendiseeriaid fookusega oksüdatsiooni eripärale ning CO_2 mõjule nii tervikprotsessile kui selle üksikstaadiumidele. Lisaks rakendati modelleerimist, mis võimaldas uurida spetsiifiliste keevkihtprotsessi parameetrite varieerimise mõju.

Termilise analüüsi tulemused näitasid, et CO_2 emissioon põlevkivi mineraalosast väheneb, sest kaltsiidi lagunemine nihkub hapnikus-põletamise tingimustel kõrgemale temperatuurile. CO_2 ei omanud nähtavat mõju lendainete eraldumise staadiumile. Kuigi kütuse süsiniku ja CO_2 vahelise reaktsiooni

osakaalu kogu protsessis on raske hinnata paljude paralleelselt toimuvate reaktsioonide tõttu, saab CO emissiooniprofiilide põhjal väita, et selle gaasistamisreaktsiooni kiirus kasvab temperatuuridel üle 750 – 800°C. Erinevatele protsessi staadiumidele arvutati konversioonsõltuvate aktivatsioonienergiate väärtused. Need olid nii põlevkivi kui tema koksi oksüdatsioonile märgatavalt madalamad O_2/CO_2 keskkonnas võrreldes 21% O_2/Ar keskkonnaga, mida kasutati õhus põletamise mudelina. Seega peaks Eesti põlevkivi hapnikus-põletamine olema efektiivsem võrreldes õhus põletamisega.

Modelleerimine Aspen Plus keskkonnas näitas, et õhus põletamisega sarnastele temperatuuridele on võimalik jõuda suurendades gaasifaasis hapniku kontsentratsiooni. Samasugune soojusülekande profiil nagu õhus põletamisel saavutatakse selle töö arvutustes näidatud hapniku sisaldustel, samas oleks soovitav moderniseeritavate boilerite puhul suurendada mõnevõrra nii hapniku sisaldust oksüdeerivas gaasis kui tsirkuleerivate suitsugaaside suhtarvu vähenenud konvektiivsete massivoogude tõttu. Vähendamaks CO, SO_2 ja karbonaatse CO_2 emissioone, tuleks hapnikus-põletamisel vältida kõrgeid temperatuure (üle 840°C), seda eriti madalama hapniku sisaldusega tsoonide olemasolul boileris. Tuha massivoog hapnikus-põletamisel on suurem ja selle $CaCO_3$ sisaldus kõrgem karbonaatide madalama lagunemisastme tõttu. Süsteemide kohandamisel hapnikus-põletamisele võivad tehnilise poole pealt vajalikuks osutuda välised soojusvahetid, et tekitada lisasoojusvahetuspinda. Soojuskoormus põlemisreaktoris ning suitsugaaside soojusmahtuvus on hapnikus-põletamisel kõrgem, näidates eralduva soojuse ning boileri efektiivsuse kasvu.

Töös jõutakse järeldusele, et sõltumata mitmetest spetsiifilistest erinevustest, mis tehti kindlaks võrreldes protsesse O_2/CO_2 ja 21%O_2/Ar keskkonnas, ei tohiks olla fundamentaalseid takistusi hapnikus-põletamise kasutuselevõtuks Eesti põlevkivi põletamisel. Seejuures peaks protsess muutuma efektiivsemaks võrreldes õhus põletamisega ning luuakse eeldused nõutavaks CO_2 püüdmiseks.

APENDIX A. PUBLICATIONS

PAPER I

Meriste, T.; Yörük, C.R.; Trikkel, A.; Kaljuvee T.; Kuusik, R. TG–FTIR Analysis of Oxidation Kinetics of Some Solid Fuels Under Oxy-fuel Conditions. Journal of Thermal Analysis and Calorimetry 2013, 114(2), 483-489.

TG–FTIR analysis of oxidation kinetics of some solid fuels under oxy-fuel conditions

T. Meriste · C. R. Yörük · A. Trikkel ·
T. Kaljuvee · R. Kuusik

Abstract A possible technology that can contribute reduction of carbon dioxide emission is oxy-fuel combustion of fossil fuels enabling to increase CO_2 concentration in the exhaust gas by carrying out the combustion process with oxygen and replacing air nitrogen with recycling combustion products to obtain a capture-ready CO_2 stream. The laboratory studies and pilot-scale experiments discussed during the last years have indicated that oxy-fuel combustion is a favorable option in retrofitting conventional coal firing. Estonian oil shale (OS) with its specific properties has never been studied as a fuel in oxy-fuel combustion, so, the aim of the present research was to compare thermo-oxidation of OS and some coal samples under air and oxy-fuel combustion conditions by means of thermal analysis methods. Experiments were carried out in Ar/O_2 and CO_2/O_2 atmospheres with two oil shale and two coal samples under dynamic heating conditions. FTIR analysis was applied to characterize evolved gases and emission dynamics. Kinetic parameters of oxidation were calculated using a model-free kinetic analysis approach based on differential iso-conversional methods. Comparison of the oxidation characteristics of the samples was given in both atmospheres and it was shown that the oxidation process proceeds under oxy-fuel conditions by all studied fuels with lower activation energies, however, it can last longer as the same temperatures are compared.

Introduction

CO_2 is the most important anthropogenic greenhouse gas and its global concentration has increased from its pre-industrial value of about 280–379 ppm in the last decade [1, 2]. To stabilize atmospheric CO_2 concentration, several approaches can be distinguished: energy generation from non-fossil sources, reduction of fossil fuel consumption, and increase in energy efficiency, and also carbon capture and storage (CCS). CCS technologies consist generally of three steps: capture, transportation, and storage [3, 4]. Capture technologies can be more efficient if the concentration of CO_2 in the flue gases is increased. A possible technology for that can be oxy-fuel (OF) combustion of fuels.

Conventional coal-fired boilers use air for combustion in which N_2 dilutes CO_2 in the flue gas. Capture of CO_2 from such dilute mixtures using amines is expensive. In OF combustion, a mix of oxygen and recycled flue gas is used for combustion. By recycling the flue gas, a gas consisting mainly of CO_2 and H_2O is generated, which is after removal of H_2O by condensing ready for sequestration. The recycled flue gas is used to control the temperature in the boiler and to insure that there is enough gas volume for heat transfer.

Laboratory studies on OF combustion of coal and lignite have provided some understanding of the parameters of the process. Besides, limited number of pilot-scale facilities exist. The available data has been generalized in [5–10]. These studies have indicated that OF combustion is a favorable option in diminishing CO_2 emissions. However,

T. Meriste
Estonian Energy SC, Laki 24, 12915 Tallinn, Estonia

C. R. Yörük · A. Trikkel (✉) · T. Kaljuvee · R. Kuusik
Laboratory of Inorganic Materials, Tallinn University
of Technology, Ehitajate tee 5, 19086 Tallinn, Estonia
e-mail: andres.trikkel@ttu.ee

Estonian oil shale with its specific properties, strongly different from coal, has never been studied as a fuel in OF combustion.

The specific characteristics of OF combustion involve the following [5, 6, 11–15]:

- Concentration of oxygen in the combustion gases has to be about 30 vol % with about 60 % of the flue gas recycling. Percent excess of oxygen required is 3–5 %;
- High content of H_2O and CO_2 determines higher emissivity enabling to reduce the gas volume passing through the burner to about 30 % of the conventional;
- The volume of flue gases after recycling is reduced by 80 %;
- SO_x and NO_x may have higher ppm concentration in flue gases due to its reduced volume;
- Power is lost to flue gas compression and oxygen production.

In laboratory studies, atmospheric and pressurized thermal analysis methods have been widely employed. It has been found that the changed composition of gas atmosphere influence both heat transfer and combustion reaction kinetics [16–19]. Comparing the reactivity of 20 different rank coals it was noticed that in the 21 % O_2/79 % CO_2 atmosphere, the curves of mass loss rate shifted to higher temperatures in relation to those in the 21 % O_2/79 % N_2 conditions [19]. This implies that there was a delay in the burning process, which may have been due to the higher specific heat of CO_2 as compared to N_2, leading to lower gas temperatures and also the fuel particle temperatures during OF combustion in comparison to combustion in air [19]. Kinetic parameters and the effect of oxygen concentration on the oxidation process have been determined for several coal samples under OF conditions in [18]. The results showed that combustion got harder to progress as the coalification degree increased. Within the range of 10–40 %, the increase in O_2 concentration favored the combustion process, but beyond this zone, the effect leveled off. To evaluate the kinetic triplet ($f(\alpha)$, E, A), the Coats–Redfern method [20] was used. The calculations showed that $D3$-Jander was the proper reaction model. Activation energy values for the coals studied and in the range of 10–60 % oxygen concentration in the combustion gas varied from 111 to 317 kJ mol^{-1} [18].

Kinetic analysis of char combustion showed that reaction rates decrease with the increase in the ash content in char. The elevated CO_2 concentration surrounding the burning char particle can result in gasification reactions increasing mass loss of char. However, at lower temperatures up to 900 °C high concentration of CO_2 did not influence the char burnout kinetics notably, but it can become significant at practical combustion temperatures up to 1400 °C [5, 16]. Thermal analysis experiments have shown that char reactivity increases with increasing O_2 concentration in both air and OF combustion. The char oxidation reaction begins at around 400 °C and increases rapidly with the increase in temperature. After reaching a peak value, the reactivity starts to decrease due to the combustion of the less reactive portion of the char [5, 16]. The effect of coal rank during OF combustion and the role of the char-CO_2 reaction was explained in [21]. Char-O_2 and char-CO_2 reactivities showed an influence of rank with low-rank coals having higher reaction rates as compared to high-rank coals that can be explained by surface area analysis which showed a higher concentration of macropores in low-rank coals leading to higher reactivities. TG analysis showed that low-rank coals have both high gasification reactivity and high CO_2 effectiveness factors as compared to high-rank coals, so, their conversion is higher. The research highlighted the importance of the char-CO_2 reaction, especially, at high temperatures and high CO_2 partial pressures, and the necessity of its consideration in any OF combustion modeling [21].

First experiments with oil shale under OF conditions have been performed with Jordanian oil shale using air-firing as well as staged and unstaged combustion in 27 % O_2/73 % CO_2 gas mixture and a 20 kW electrically heated once through furnace [22]. These experiments showed that Jordanian El-Lajjun oil shale combustion under OF conditions can be feasible; 100 % oil shale burnout was achieved with 3 and 1 % oxygen excess. However, it was found that CO concentration in the burner zone was much higher under OF conditions as compared to air-firing, which can be explained by the gasification reactions in a CO_2-rich medium and indicates that controlling the level of CO is a problem if the oxygen excess decreases [22].

Experiments have shown that SO_2 content in ppm is directly proportional to the fuel sulfur content in both OF and air combustion, but it is greater in OF combustion [5, 22]. However, in some laboratory experiments it has been found that conversion of coal sulfur to SO_2 decreased up to 30 % as compared to the air case [12, 22, 23].

Pilot-scale tests have generally shown technical feasibility of CO_2 recycle technology without any major technical barriers. OF combustion reached efficiency and emissions similar to air operation and is applicable for PF boiler retrofitting [5]. Chalmers University has evaluated the retrofit of a 865 MWe lignite fired conventional power plant and concluded that the overall investment cost for the plant is similar as that will be for CCS-ready air fired case [24].

So, earlier investigations have shown that oxy-fuel process as compared to air firing is complex, but promising in creating prerequisites for CO_2 capture. However, its specifics are strongly dependent on the composition of the organic part of fuel, amount and composition of mineral part etc. Estonian oil shale has never been studied as a fuel

under oxy-fuel combustion conditions, so the aim of the present research was to obtain data and study the fundamentals of application of this technology to Estonian oil shale which is notably different from coal in its organic and mineral composition. A comparison with some common coal samples and air firing conditions is presented.

Experimental

Materials

Four solid fuel samples were under investigation—two OS samples (OS1; OS2), one anthracite coal (C1) and one conventional coal (C2). OS1 sample has been defined as a common energetic oil shale from Estonia, used in the boilers in Narva Power Stations. OS2 sample is an enriched sample—oil shale concentrate. C1 sample is a Russian anthracite coal obtained from JSC Siberian Anthracite (fraction 0–13 mm) and C2 is a common volatile-rich coal sample which is widely used in boilers for heating (imported from Novokuznetsk, Russia, grade ДГОМСШ, fraction 0–50 mm).

The samples used in the experiments were crushed with an alligator-type grinding machine. Mean sample was taken from the crushed material and ground in a big ball mill. The samples were then dried at 105 °C for several hours and ground additionally in a Retsch PM 100 grinding machine until all the sample passed the 200 μm sieve. Characterization of the samples is given in Table 1. For different experiments, specific size fractions were separated from this mean sample.

It can be seen from Table 1 that the higher heating values (HHV, MJ kg^{-1}) of the coal samples are similar and almost 2.5 times higher as compared to OS. Oil shale

Table 1 Characteristics of the fuel samples used

Characteristic	OS1	OS2	C1	C2
HHV^d/MJ kg^{-1}	11.86	13.64	30.39	30.22
Content/mass%				
Ash^d	49.3	45.6	8.9	8.1
Moisture W	0.7	0.7	2.1	2.7
Elements				
C^d	30.4	35.0	81.8	73.7
H^d	3.0	3.6	1.5	4.2
N^d	0.1	0.1	0.6	0.2
S^d	1.63	1.87	0.25	0.36
TC^a	31.5	36.4	87.0	75.8
TIC/CO$_2^M$ from TIC^a	4.55/16.7	4.35/16.0	0^{bd}	0^{bd}

d per dry sample, bd below detection limit, CO_2^M mineral CO_2

^{a} TC and TIC—total and inorganic carbon (ISO-9556; ISO-10694)

concentrate OS2 has about 15 % higher HHV value as compared to OS1 and its carbon content is also 15 % higher. C1 contains more carbon and notably less volatiles than C2, their mineral CO_2 content is almost zero. Diversely, mineral CO_2 (CO_2^M) content of OS samples is 16.0–16.7 %, so, these samples have high content of carbonates ($CaCO_3$, $MgCO_3$) and mineral matter (ash content 46–49 % as compared to 8–9 % for coal). The oil shale samples used contained approximately five times more sulfur than coal samples—from 1.6 to 1.9 %.

Methods

The experiments with a Setaram Setsys Evo 1750 thermoanalyzer coupled to a Nicolet 380 FTIR spectrometer were carried out under non-isothermal heating conditions up to 1000–1100 °C at 10 K min^{-1} heating rate in a stream of 79 % Ar/21 % O_2 (flow rate 30 mL min^{-1}) modeling air combustion and 70 % CO_2/30 % O_2 (OF conditions). Standard 100 μL Pt crucibles were used, the mass of samples was 20 ± 0.5 mg in most experiments and 30 ± 0.5 mg for tests with gas analysis. For kinetic analysis 2.5; 5 and 15 K min^{-1} heating rates were additionally applied and for gas analysis experiments also 20 K min^{-1}.

FTIR measurements were recorded in the 400–4000 cm^{-1} region with the resolution of 4 cm^{-1} and an average of four scans was taken. To discuss the evolved gaseous compounds the HR Aldrich Vapor Phase Library v3.2 (Serial No: 110412213) was used.

A model-free kinetic analysis approach based on the differential iso-conversional method [25, 26] and AKTS Advanced Thermokinetics software [28] was applied to calculate the kinetic parameters and conversion predictions of oxidation stage.

Results and discussion

TG–DTA analysis

Mass loss (TG, %) and differential thermal analysis (DTA, μV) curves of the samples in Ar/O_2 and CO_2/O_2 (OF conditions) at 10 K min^{-1} heating rate (Fig. 1a, b) show that temperature profiles of the oxidation process in different atmospheres do not differ much. Oxidation of OS1 in Ar/O_2 starts at 230 °C and proceeds with two peaks in exotherm at 370 and 525 °C up to 575 °C. Exotherms of OS concentrate OS2 are shifted slightly left—difference in peak temperatures is about 40 °C. Oxidation of coal samples is characterized by wide exotherms, being shifted notably toward higher characteristic peak temperatures, especially, for anthracite C1 (Fig. 1a).

Fig. 1 TG and DTA curves of fuel samples in Ar/O_2 (**a**) and CO_2/O_2 (**b**)

In CO_2/O_2 atmosphere the exotherms of OS samples reach the peak value at 350 and 480 °C and the offset temperature is about 550 °C (Fig. 1b). These somewhat lower temperatures can be explained by the higher oxygen concentration. Both coal samples oxidized almost in one step lasting in CO_2/O_2 from 150 to 700 °C with C2 and from 280 to 850 °C with C1. In Ar/O_2 these temperature intervals were similar.

There were no big differences in the total mass loss of the samples in different atmospheres. Mass loss of coal samples is expressed by one step, of OS samples by two steps in Ar/O_2 and even three steps in CO_2/O_2 that can be related to the behavior of carbonates in OS. It can be seen that in air the endothermic decomposition of OS carbonates proceeds in one step at 700–810 °C. In CO_2/O_2, the decomposition of $MgCO_3$ and $CaCO_3$ is shifted apart and proceeds with peak maximums at 750 and 915 °C, respectively. So, depending on the combustion temperature, endothermic decomposition of $CaCO_3$ could possibly be avoided under OF conditions diminishing CO_2 emissions from the mineral part of oil shale and reducing the negative effect of this endothermic reaction on the heat balance.

Evolved gas analysis

FTIR analysis of the evolved gases is complicated due to huge and partly overlapping H_2O and CO_2 peaks in the regions

below 800, 1400–1800, 2200–2400, and above 3500 cm^{-1} (Fig. 2). Here, increased heating rate (20 K min^{-1}), sample mass (30 mg), gas flow rate (50 mL min^{-1}), and varying CO_2/O_2 ratios (70/30–95/5) were used to discuss the composition and dynamics of evolved gases.

It can be seen from Fig. 2 that there are no big differences in the FTIR spectra of the gases from OS1 oxidation taken at 20 min (corresponds to 440 °C which is in the middle of the exotherm on DTA curve) at different oxygen concentrations. CO_2 and H_2O peaks cover a big part of the spectra. The emission of different organic compounds can be seen by the peaks of C–H bond of alkyl groups (2850 and 2925 cm^{-1}). Methane was clearly present in all spectra (3018 and 1306 cm^{-1}). In some spectra a weak HCl peak could be distinguished (region 2775–2822 cm^{-1}) before overlapping with methane peak and at higher oxygen concentrations also SO_2 (1348 and 1360 cm^{-1}). Examining the time-dependencies of peak intensities in different areas on spectra throughout the experiment, it can be assumed that alcohols and phenols are present in the gases evolved (C–O bonds in the region of 1150–1200 cm^{-1}) as well as carboxylic acids (region 1250–1300 cm^{-1}). Our previous analysis has shown that most often methanol is present (1018, 1033, 1058 cm^{-1}) and acetic acid (1182, 1775, 1796 cm^{-1}) [27]. The role of unsaturated hydrocarbons and aromatic compounds increased at low oxygen concentration—C=C bonds from aromatics (1450 cm^{-1}), C=CH_2, and C=CH groups (900 cm^{-1}). However, the obtained results indicated that FTIR analysis of evolved gaseous compounds from oxy-fuel experiments does not give adequate and full information about the composition of gas phase.

Emission profiles of some gaseous compounds or characteristic groups evolved during oxidation of OS1 at different O_2 concentrations in CO_2/O_2 atmosphere have been
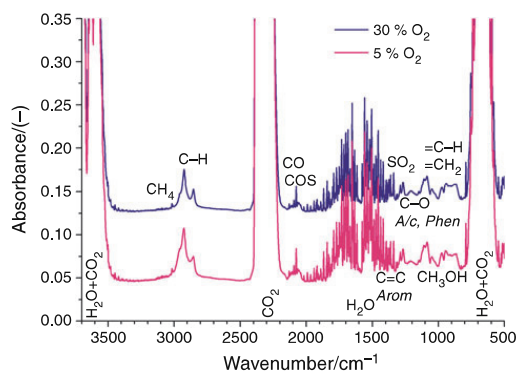
Fig. 2 FTIR spectra of the evolved gases for OS1 at 30 % and 5 % O_2 content in CO_2 taken at 20 min (440 °C)

given in Fig. 3. It can be seen that decreasing the oxygen concentration diminishes the exotherm area, shifts it toward higher temperatures and for 5 % O_2 it is already partly replaced by endotherm from 350 to 500 °C (Fig. 3a). Due to the increased heating rate, two peaks can no longer be separated on the exotherm for OS1 oxidation in CO_2/O_2 as in the case of 10 K min^{-1} heating rate. O_2 concentration does not affect notably the starting temperatures of oxidation, but the offset temperatures of the respective peaks on the DTA curves are for 30, 15, and 5 % O_2, respectively, 625, 775 and 925 °C. Final mass loss is the same for different oxygen concentrations.

Emission of H_2O is the most intensive during the initial period of oxidation. Decreasing the O_2 concentration from 30 to 5 % O_2 shifts the peak maximum of the profile from 360 to 450 °C and it corresponds to the tip of endotherm on the DTA curve. Emission of CH_4 is notably more intensive in 5 % O_2 and it reaches the maximum intensity at slightly higher temperature as compared to H_2O. The intensities of C–H and $=CH_2$ reach the maximum at the same temperature as CH_4. In 30 % O_2 emission of SO_2 starts above 200 °C and lasts up to 550 °C. Emission of alcohols and, possibly, also phenols (C–O; 1200 cm^{-1}) was fixed at higher O_2 concentrations and their emission profile is similar to that of H_2O.

Kinetic analysis

To obtain kinetic parameters for the oxidation stage of the fuels, series of non-isothermal experiments were carried out. The so called iso-conversional methods revert to the differential methods formerly proposed by Friedman [25].

The differential methods for the calculation of the kinetic parameters are based on the use of the well-known reaction rate equation:

$$\beta \frac{d\alpha}{dT} = A \ \exp \left(-\frac{E_A}{RT} \right) f(\alpha) \tag{1}$$

where β is the heating rate, T the temperature, A the pre-exponential factor in s^{-1}, and $f(\alpha)$ is the differential conversion function dependent on the reaction mechanism.

The equation describing the iso-conversional approach derived from the Friedman differential method can be expressed as follows:

$$\ln \left(\frac{d\alpha}{dt} \right) = \ln \left\{ A(\alpha) f(\alpha) \right\} - \frac{E(\alpha)}{RT} \tag{2}$$

The function dependent on the reaction model $f(\alpha)$ becomes a constant at each fixed conversion degree α in Eq. 2, and the relationship between the logarithm of the reaction rate $d\alpha/dt$ and $1/T$ is linear with the slope of E/R.

The changes in activation energy (E/kJ mol^{-1}) and pre-exponential factor A depending on the reaction progress α (Fig. 4) were determined from the experiments with 2.5, 5, 10, and 15 K min^{-1} heating rates. Conversion α was calculated from the mass loss during oxidation stage. After baseline correction the derivatives of the normalized TG signals were processed with the AKTS Advanced Thermokinetics software [27] enabling to obtain apparent conversion-dependent activation energies without assuming the form of $f(\alpha)$ function.

Kinetic calculations showed that activation energy of OS samples depending on the extent of oxidation was in the range of 80–100 kJ mol^{-1} in Ar/O_2 and 35–45 kJ mol^{-1} in CO_2/O_2 in the range of $\alpha = 0.2$–0.9, being higher at the beginning, then diminishing and increasing slightly for the final stage of oxidation. For the common coal sample C2,
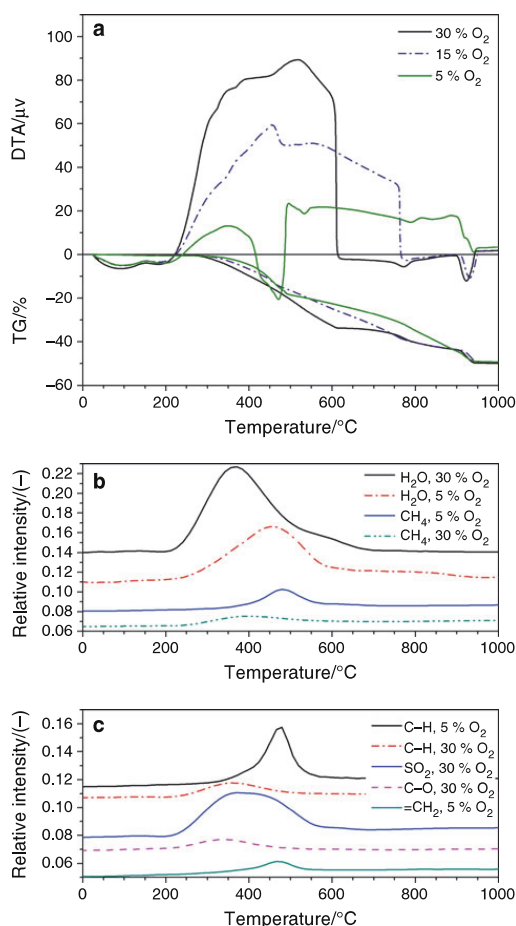
Fig. 3 TG and DTA curves (**a**) and emission profiles (**b**, **c**) of some characteristic compounds and groups evolved at OS1 oxidation in CO_2/O_2 atmosphere
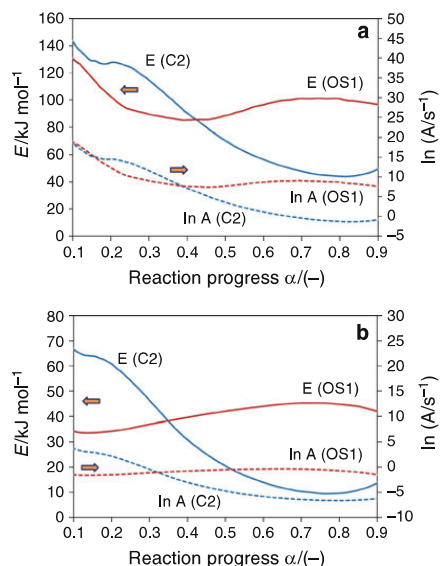
Fig. 4 Conversion-dependent activation energy E and logarithm of pre-exponential factor A for the oxidation stage of OS1 and C2 in Ar/O_2 (**a**) and CO_2/O_2 (**b**)

the activation energies in Ar/O_2 were in between 45–120 kJ mol^{-1} and in CO_2/O_2 10–80 kJ mol^{-1}. The E values were high for the initial stage of oxidation during which most chemical reactions take place ($\alpha = 0.1$–0.4) and notably low for the final, presumably, the char oxidation stage controlled by diffusion ($\alpha > 0.5$). As compared to coal, the activation energy for OS samples was much higher during the final stage of oxidation that can be explained by different diffusion situation due to high minerals content in OS and also continuing chemical reactions in the closely associated organic and mineral part in OS. Nevertheless, these phenomena needs a further detailed analysis.

Activation energies for both types of samples were higher in Ar/O_2 atmosphere as compared to OF conditions that is most likely the result of higher oxygen concentration (30 %) in oxy-fuel. So, carrying out the combustion under typical OF conditions, should favor the oxidation process. However, lower activation energy values mean also that the effect of temperature on reaction rate is less expressed, so, the process can take longer as the same temperatures are compared.

On the basis of the results of calculations and taking into account the differently changing values of activation energy, predictions about reaction rates and process duration were made also for constant-temperature conditions (Fig. 5).

It can be seen that despite lower activation energy in CO_2/O_2 as compared to Ar/O_2, longer residence times are necessary for oxidation for both types of fuel, or to keep
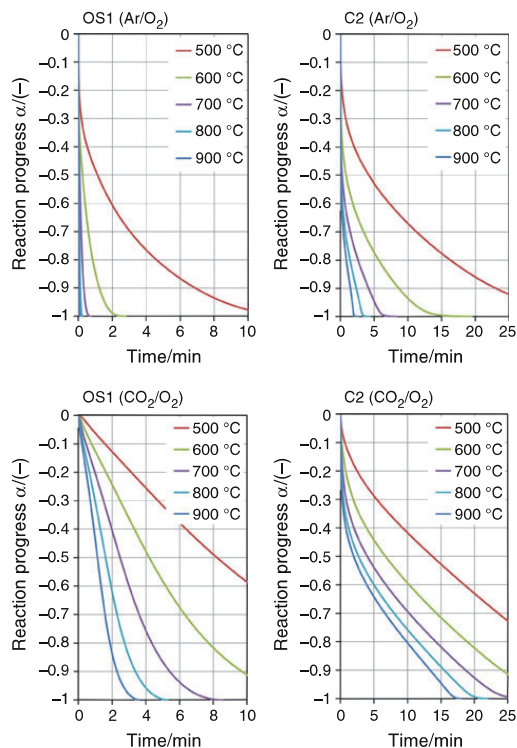
Fig. 5 Conversion predictions at constant temperatures for OS1 and C2 in Ar/O_2 (*above*) and CO_2/O_2 (*below*)

the same process duration, higher temperature is needed under OF conditions as compared to Ar/O_2 atmosphere, modeling conventional combustion in air. If at 800 °C and under OF conditions the OS1 sample is oxidized in 5 min, then in Ar/O_2 it is oxidized in only 0.5 min. Oxidation of coal sample C2 takes longer—at 800 °C about 20 min in CO_2/O_2 and 3 min in Ar/O_2.

So, the first calculations indicate that it might be necessary to carry out the oxy-fuel process at somewhat higher temperatures as compared to conventional air combustion or increase the residence times of fuel particles.

Conclusions

There were no remarkable differences in the characteristic temperatures at oxidation of the fuel samples studied in Ar/O_2 (modelling air) and oxy-fuel (CO_2/O_2) atmospheres as well as in the amounts of oxidized matter and the amounts of products formed enabling to assume that there should be no fundamental difficulties in applying oxy-fuel combustion to Estonian oil shale.

Another important finding is that in CO_2/O_2 atmosphere with the CO_2 content typical for oxy-fuel combustion, the decomposition of $CaCO_3$ is shifted to over 900 °C levels as compared to 700–810 °C in air, enabling to reduce CO_2 emissions from the mineral part of OS and diminish the role of endothermic effect of $CaCO_3$ decomposition on the heat balance at oxy-fuel combustion.

Combined TG–FTIR analysis enables to determine a number of compounds evolved and the profiles of their evolution during oxidation, however, it is sophisticated due to huge and overlapping CO_2 and H_2O peaks.

It was shown that the oxidation process proceeds under oxy-fuel conditions by all studied fuels with lower activation energies, however, the conversion predictions calculated on the basis of conversion-dependent activation energies showed that it might be necessary to carry out the oxy-fuel process at somewhat higher temperatures or increased residence times of fuel particles.

References

1. Climate Change 2007: The physical science basis. Summary for policymakers. IPCC Fourth Assessment Report of the intergovernmental panel on climate change. Approved at the 10th session of working group I of the IPCC, Paris, Feb 2007.
2. IPCC expert meeting on detection and attribution related to anthropogenic climate change. The world meteorological organization. Geneva, Switzerland, 14–16 Sep 2009.
3. Davison J, Thambimuthu K, Rubin ES, Keith DW, Gilboy CF, Wilson M, et al. Technologies for capture of carbon dioxide. Greenhouse gas control technologies 7. Oxford: Elsevier; 2005. p. 3–13.
4. Lyngfelt A, Leckner B, editors. Technologies for CO_2 sequestration. Minisymposium on carbon dioxide capture and storage, School of Environmental Sciences, October 22, 1999. Gothenburg: Chalmers University of Technology; 1999.
5. Wall T, Liu Y, Spero C, Elliott L, Khare S, Rathnam R, et al. An overview on oxyfuel coal combustion–State of the art research and technology development. Chem Eng Res Des. 2009; 87(8):1003–16.
6. Buhre BJP, Elliott LK, Sheng CD, Gupta RP, Wall TF. Oxy-fuel combustion technology for coal-fired power generation. Prog Energy Combust Sci. 2005;31(4):283–307.
7. Anheden M, Burchhardt U, Ecke H, Faber R, Jidinger O, Giering R, et al. Overview of operational experience and results from test activities in Vattenfall's 30 MWth oxyfuel pilot plant in schwarze pumpe. Energy Procedia. 2011;4(0):941–50. doi:10.1016/j.egypro.2011.01.140.
8. Kluger F, Prodhomme B, Mönckert P, Levasseur A, Leandri J-F. CO_2 capture system—confirmation of oxy-combustion promises through pilot operation. Energy Procedia. 2011;4(0):917–24.
9. Lupion M, Diego R, Loubeau L, Navarrete B. CIUDEN CCS project: status of the CO_2 capture technology development plant in power generation. Energy Procedia. 2011;4(0):5639–46. doi:10.1016/j.egypro.2011.02.555.
10. Lupion M, Navarrete B, Otero P, Cortés VJ. Experimental programme in CIUDEN's CO_2 capture technology development plant for power generation. Chem Eng Res Des. 2011;89(9):1494–500.
11. Stadler H, Christ D, Habermehl M, Heil P, Kellermann A, Ohliger A, et al. Experimental investigation of NO_x emissions in oxycoal combustion. Fuel. 2011;90(4):1604–11.
12. Krzywanski J, Czakiert T, Muskala W, Nowak W. Modelling of CO_2, CO, SO_2, O_2 and NO_x emissions from the oxy-fuel combustion in a circulating fluidized bed. Fuel Process Technol. 2011;92(3):590–6.
13. Liszka M, Ziebik A. Coal-fired oxy-fuel power unit–process and system analysis. Energy. 2010;35(2):943–51.
14. Seepana S, Jayanti S. Optimized enriched CO_2 recycle oxy-fuel combustion for high ash coals. Fuel. 2012;102(2012):32–40. doi:10.1016/j.fuel.2009.04.029.
15. Toftegaard MB, Brix J, Jensen PA, Glarborg P, Jensen AD. Oxy-fuel combustion of solid fuels. Prog Energy Combust Sci. 2010;36(5):581–625. doi:10.1016/j.pecs.2010.02.001.
16. Varheyi G, Till F. Comparison of temperature-programmed char combustion in CO_2–O_2 and Ar–O_2 mixtures at elevated pressure. Energy Fuels. 1999;13:539–40.
17. Heil P, Toporov D, Förster M, Kneer R. Experimental investigation on the effect of O_2 and CO_2 on burning rates during oxyfuel combustion of methane. Proc Combust Inst. 2011;33(2):3407–13.
18. Niu S, Lu C, Han K, Zhao J. Thermogravimetric analysis of combustion characteristics and kinetic parameters of pulverized coals in oxy-fuel atmosphere. J Therm Anal Cal. 2009;98(1):267–74. doi:10.1007/s10973-009-0133-1.
19. Gil M, Riaza J, Álvarez L, Pevida C, Pis J, Rubiera F. A study of oxy-coal combustion with steam addition and biomass blending by thermogravimetric analysis. J Therm Anal Cal. 2012;109(1):49–55. doi:10.1007/s10973-011-1342-y.
20. Coats AW, Redfern JP. Kinetic parameters from thermogravimetric data. Nature. 1964;201(4914):68–9.
21. Dhaneswar SR, Pisupati SV. Oxy-fuel combustion: the effect of coal rank and the role of char-CO_2 reaction. Fuel Process Technol. 2012;102:156–65. doi:10.1016/j.fuproc.2012.04.029.
22. Al-Makhadmeh L, Maier J, Al-Harahsheh M, Scheffknecht G. Oxy-fuel technology: an experimental investigations into oil shale combustion under oxy-fuel conditions. Fuel. 2013;103(2013):421–9. doi:10.1016/j.fuel.2012.05.054.
23. Croiset E, Thambimuthu KV. NO_x and SO_2 emissions from O_2/CO_2 recycle coal combustion. Fuel. 2001;80(14):2117–21. doi:10.1016/s0016-2361(00)00197-6.
24. Andersson K, Johnsson F. Process evaluation of an 865 MWe lignite fired O_2/CO_2 power plant. Energy Convers Manag. 2006;47(18–19):3487–98. doi:10.1016/j.enconman.2005.10.017.
25. Friedman H. Kinetics of thermal degradation of char-forming plastics from thermogravimetry. Application to a phenolic plastic. J Polym Sci. 1964;6:183–95.
26. Roduit B. Methodology for lifetime prediction and determination of TMRad and thermal runaway of energetic materials using DSC or C-80 data. Application of thermokinetic concept using DSC, DTA, TG, MS and FTIR signals. Advanced kinetics and technology solutions. Switzerland: AKTS AG; 2006. p. 45.
27. Kaljuvee T, Keelmann M, Trikkel A, Kuusik R. Thermooxidative decomposition of oil shales. J Therm Anal Cal. 2011;105(2):395–403. doi:10.1007/s10973-010-1033-0.
28. Advanced Kinetics and Technology Solutions: AKTS thermokinetics. AKTS AG, Switzerland. http://www.akts.com. Accessed 11 Mar 2011.

PAPER II

Yörük, C.R.; Meriste, T.; Trikkel, A.; Kuusik, R. Thermo-oxidation Characteristics of Oil Shale and Oil Shale Char Under Oxy-fuel Combustion Conditions. Journal of Thermal Analysis and Calorimetry 2015, 121(1), 509-516.

Thermo-oxidation characteristics of oil shale and oil shale char under oxy-fuel combustion conditions

Can Rüstü Yörük · Tõnis Meriste · Andres Trikkel · Rein Kuusik

Abstract The current research involves characteristics of pyrolysis and thermo-oxidation of Estonian oil shale (OS) and its char. Non-isothermal and isothermal thermal analysis methods were used to characterise and compare the specifics of these processes under air and oxy-combustion conditions using Ar, CO_2, O_2 and their mixtures. The study of reaction kinetics including pyrolysis and oxidation characteristics is crucial to understand the complex mechanism of OS oxy-fuel combustion. The experimental results showed that the pyrolysis behaviour is highly similar in Ar and CO_2 until the end of decomposition of organic part. There is no visible char carbon and CO_2 reaction during the char oxidation stage under oxy-fuel conditions. The release of CO related to the char carbon and CO_2 reaction in 100 % CO_2 atmosphere increases notably at temperatures above 650–700 °C. The role of inorganic minerals in the oxidation and gasification of char was described as well as the effect of oxy-fuel conditions on gaseous emissions. It was found that the rate constants for char oxidation in CO_2/O_2 are approximately 1.2–1.3 times higher as compared to Ar/O_2 atmosphere and that char oxidation under oxy-fuel conditions takes place with lower activation energies as compared to Ar/O_2.

Keywords Oil shale · Oil shale char · Oxy-fuel combustion · TG–DTA–EGA

C. R. Yörük (✉) · A. Trikkel · R. Kuusik
Laboratory of Inorganic Materials, Tallinn University of Technology, Ehitajate tee 5, 19086 Tallinn, Estonia
e-mail: can.yoruk@student.ttu.ee

T. Meriste
Estonian Energy SC, Laki 24, 12915 Tallinn, Estonia

Introduction

One of the largest contributors amongst greenhouse gas emissions is CO_2, and the major source of the CO_2 is the combustion of fossil fuels to supply energy. Carbon capture and storage technologies rely on the idea of CO_2 sequestration from fossil fuel-based power plants and transportation of this captured CO_2 to the storage sites. Amongst carbon capture and storage technologies, oxy-fuel combustion is one of the proven technologies which have less chemically complicated treatments. This technique is performed by using mixture of pure oxygen and a part of recycled flue gas instead of air as a combustion oxidiser. Nitrogen-free and oxygen-enriched atmosphere of oxy-fuel combustion increases the content of CO_2 in the flue gas comparing the conventional combustion. For this reason, CO_2 capturing and sequestration processes are easier and cost effective with the oxy-fuel combustion. The detailed description of oxy-fuel combustion technology can be found elsewhere [1, 2] and also in the previous research of oxy-combustion of Estonian oil shale [3].

Estonian energy sector is dominated by oil shale (OS) [4]. OS is a fine-grade sedimentary rock containing relatively large amounts of combustible organic matter (kerogen), which is well distributed in its mineral matrix [5]. Estonian oil shale is defined as highly heterogeneous fuel with complicated composition of organic and mineral matter. Its dry matter mainly consists of organic part, sandy-clay (terrigenous) minerals and carbonates [6]. During thermal decomposition of OS, a complex set of parallel reactions occurs in both organic and mineral parts of the fuel. Besides, mass and heat transfer in oxy-fuel combustion differs significantly from air firing because of the high CO_2 partial pressure. The knowledge of the effect of CO_2 atmosphere on the reactivity of OS and OS char is

needed for evaluating application of oxy-combustion to OS. The study of reaction kinetics including pyrolysis and oxidation characteristics is crucial to understand the complex mechanism of OS oxy-fuel combustion.

There are a few studies on pyrolysis and kinetics of oxidation of OS and its char. Pyrolysis of OS using thermogravimetric analysis (TG) has been discussed in the literature from different regions: Colorado (Green River) [7], China [8], Jordan [9], Morocco [10], Turkey [11], etc. In general, kinetic calculations are based on non-isothermal and isothermal thermal analysis methods. Pyrolysis is regarded as occurring in two stages. In the first stage, OS is heated to form pyrobitumen; in the second stage, pyrobitumen decomposes to form shale oil, shale gas and shale char. Researchers have established that pyrobitumen is formed as an intermediate product when OS is heated [12]. According to the studies mentioned above, it was shown that formation of bitumen has specific temperature range depending on the OS. It was also reported that the heating rate has an important effect on pyrolysis. Effect of pyrolysis environment was also reported in several studies. Jaber and Probert [13] showed that CO_2 as carrier gas led to a slightly greater mass loss during the devolatilisation stage of two Jordanian OS samples than N_2. It was also reported that the carbon-dioxide/char reaction is more likely to occur at high temperatures. Fang-Fang et al. [14] studied Chinese Huadian OS under N_2 and CO_2 atmospheres. Much greater mass loss was reported at temperatures above 760 °C under CO_2 due to the residual carbon reaction with CO_2 forming CO. Residual carbon preparation in different heating rates by TG and its reactivity under isothermal conditions was carried out by Barkia et al. [15] with OS from Morocco. It was reported that the heating rate has an important effect on the amount of residual carbon obtained. Regarding OS residual carbon oxidation, there are a very limited number of studies in the literature. In [16], it was reported that the presence of minerals in OS can drastically alter the reactivity of residual char. It was also reported that removal of mineral matter with acid washing decreases the reactivity of residual carbon and the reactivity of residual carbon depends on the heating rate used for pyrolysis [17–19]. The effect of partial pressure of CO_2 had very small impact on the reactivity of residual carbon [18]. However, the residual carbon prepared under fast heating rates was more reactive [17–19]. The effect of prior pyrolysis and heating rate on the combustion of OS semi-cokes was studied by Miao et al. [20]. The Coats–Redfern [21] method was employed to find the combustion-reaction kinetic parameters for OS semi-coke. It was reported that the activation energy and the frequency factor were much larger at high temperatures than they are at low temperatures.

So, TG has been widely used to study pyrolysis and oxidation kinetics of different OSs and their chars.

However, there is very limited research conducted with Estonian oil shale. The knowledge about reaction kinetics including pyrolysis and oxidation characteristics of OS char is inadequate, and there is almost no research related to oxy-fuel conditions. So, more information is needed to understand the complex mechanism of Estonian oil shale oxy-fuel combustion.

In this study, non-isothermal and isothermal thermal analysis (TA) methods combined with FTIR spectroscopy have been applied to investigate pyrolysis of Estonian oil shale and combustion characteristics of its char. Kinetics of OS char oxidation has been analysed in different combustion atmospheres, and conversion-dependent apparent activation energies have been presented. The kinetic data reported here together with our previous research [3] are important for the future modelling of the complete conversion process of Estonian oil shale under oxy-fuel conditions.

Experimental

Materials

The OS sample used in the experiments is a common energetic OS from Estonia, and it was obtained from Narva Power Stations. The obtained OS sample was crushed with an alligator-type grinding machine. Mean sample was taken from the crushed material and ground in a big ball mill. Then, the sample was dried at 105 °C for several hours and ground additionally in a Retsch PM 100 grinding machine until the entire sample passed the 200-μm sieve. Characterisation of the OS sample is given in Table 1.

Methods

The Setaram Setsys Evo 1750 thermoanalyser coupled to a Nicolet 380 FTIR spectrometer was used in the experiments. Non-isothermal TG tests were performed at 10 K min^{-1} heating rate up to 1,000 °C with gas flow rate 30 mL min^{-1} using different atmospheres (Ar, CO_2, Ar/O_2 and CO_2/O_2). Standard 100-μL Pt crucibles were used, and the mass of samples was 20 ± 0.5 mg in most experiments and 30 ± 0.5 mg for the tests with gas analysis. To prepare residual carbon of OS, the sample was heated up to 450 °C in argon atmosphere. When the temperature was reached, the sample was maintained at 450 °C for 1 h. The temperature of the highest reaction rate from preliminary pyrolysis experiments was selected as 450 °C, and approximately in 1 h, the mass loss due to devolatilisation ceased.

Isothermal oxidation of the obtained residual carbon was performed at three different temperatures (450, 500 and 550 °C). For this, the samples were heated up to the

Table 1 Characterisation of the OS

HHV[d]/MJ kg^{-1}	Content/mass%		Elements[d]					
	Ash[d]	Moisture W	C	H	N	S	TC	TIC/CO$_2^M$ from TIC
11.86	49.3	0.7	30.4	3.0	0.1	1.63	31.5	4.55/16.7

[d] Per dry sample

[M] mineral CO_2

selected temperature in argon, and after reaching to the desired temperature, Ar/21 % O_2 mixture, CO_2/30 % O_2 or CO_2/21 % O_2 was introduced into the system.

5, 10 and 15 K min^{-1} heating rates were applied, and the AKTS Advanced Thermokinetics software [22] was used to calculate kinetic parameters of oxidation stage of OS char. For these experiments, the OS char was prepared in electric tube furnace under the same conditions to obtain bigger amount of char having uniform properties. FTIR measurements were recorded in the 400–4,000 cm^{-1} region with the resolution of 4 cm^{-1} taking an average of four scans.

Results and discussion

Pyrolysis in Ar and CO_2

The main stages of combustion of solid fuel particles are drying, pyrolysis (devolatilisation) and char combustion. Pyrolysis of OS in Ar and CO_2 and the OS char combustion stage were studied comparatively in Ar/O_2 or CO_2/O_2 atmospheres, respectively, using non-isothermal and iso-thermal methods.

The pyrolysis behaviour (characteristic temperatures and mass loss) of the OS sample in Ar and CO_2 was very similar up to 500 °C, which indicates that CO_2 behaves like an inert gas and has the same influence as Ar on the organic part until the end of devolatilisation stage. The same nature of TG curves and the very close peak temperatures in Ar and CO_2 atmospheres can be seen from Fig. 1a, b.

The pyrolysis peak rate occurs at around 450 °C in both Ar and CO_2 atmospheres. The pyrolysis reactivity is slightly higher in Ar atmosphere. This small difference can be explained by differences in heat capacity, diffusivities and radiative properties of the gas atmosphere. The effect of char gasification reaction[1]

$$C + CO_2 \rightarrow 2CO \quad \Delta H_r^0 = +172.4 \text{ kJ} \tag{1}$$
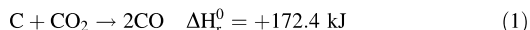
is not visible in this temperature range, and gas analysis has also shown that the role of gasification reaction increases at

[1] Standard reaction enthalpies were calculated with the HSC Chemistry 7.11 software and its database [23].
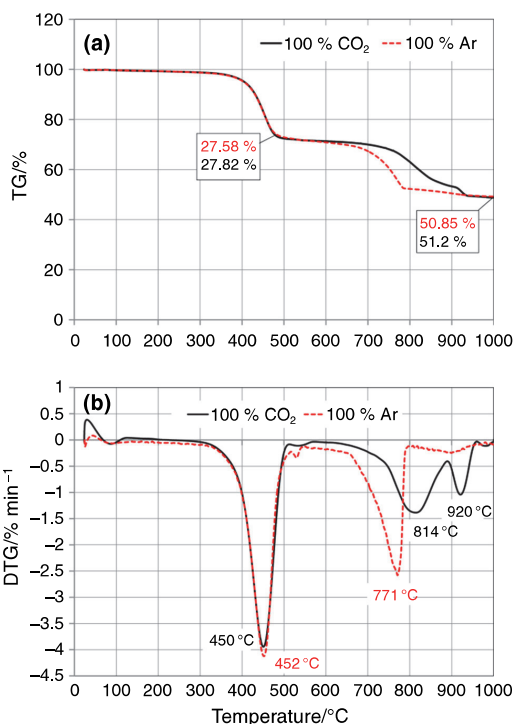
Fig. 1 Mass loss (TG) and differential mass loss (DTG) *curves* of initial OS sample in pure CO_2 and Ar

higher temperatures—above 650 °C. There is no significant mass loss difference until the end of devolatilisation of organic part; furthermore, TG curves of OS sample are almost superposing in Ar and CO_2 atmospheres. According to the steps of TG curves, two stages can be differentiated in general: pyrolysis in low temperature zone (300–520 °C) for both CO_2 and Ar atmospheres and decomposition of mineral carbonates (magnesite, dolomite, calcite, siderite) at higher temperatures (above 650 °C). Decomposition of $MgCO_3$ and $CaCO_3$ is shifted apart in CO_2 and proceeds with maximum rate at 814 and 920 °C (Fig. 1b), respectively.

Almost 27 % of the initial sample mass has been lost during thermal decomposition of organic part between 308

and 516 °C in Ar and between 328 and 513 °C in CO_2 atmospheres. Following the decomposition of organic matter, mineral part decomposition occurs in one step and mass loss reaches almost 57 % level giving peak temperature at 771 °C for Ar atmosphere. For the decomposition of mineral part in CO_2, there are two distinguishable mass loss steps. First step lies on a wide temperature region (650–890 °C) and results in almost the same amount of mass loss (30 %) like in Ar atmosphere. The final step has about 3 % additional mass loss in the temperature region of 889–956 °C.

The mass loss difference and slightly increased reaction rate in Ar in between 550 and 650 °C can be related to the processes in mineral part of OS. The effect of residual carbon and CO_2 reaction in CO_2 atmosphere (Eq. 1) can be assumed from the very small difference in the final mass loss and also from evolved gas analysis tests, which have shown increasing release of CO above 650 °C. However, the combination of different possible parallel reactions at higher temperatures is complex for such clear identification. Besides, the presence of carbonates can support CO_2-related self-gasification of residual carbon in fuel particles at their decomposition temperatures even under 100 % Ar atmosphere. In addition, higher partial pressure of CO_2 brings along more intensive decomposition at higher temperatures and can affect the pore structure, enhancing in-particle diffusion.

Char combustion in Ar/O_2 and CO_2/O_2

Thermal behaviour of OS char was studied in CO_2/O_2 and Ar/O_2 atmospheres using both non-isothermal and isothermal analysis methods.

It can be seen from non-isothermal data (Fig. 2) that higher O_2 content shifts the characteristic temperatures of oxidation of OS char slightly towards lower values. There are no big differences in the total mass loss of the samples in three different atmospheres. Solely, $CO_2/21$ % O_2 has slightly higher mass loss as compared to $CO_2/30$ % O_2 and $Ar/21$ % O_2. The presence of CO_2 can affect the equilibrium in carbonates/sulphates system and have some small effect also on the reactions with kerogen and impurities. Reactions with pyrite, its intermediates and pyritic or sulphide sulphur can be associated with the peaks at around 500 °C.

Slow reaction rate in the beginning of process during isothermal heating (Fig. 3a, b) can be explained by continuing diffusion of heavier pyrolysis products and slow oxidation of char. High CO_2 partial pressure in the char particles and possible blockage of pores by pyrolysis products restrict diffusion of oxygen into the particle. After the char carbon is consumed, oxygen concentration in the particle is increased and reactions with pyrite and related
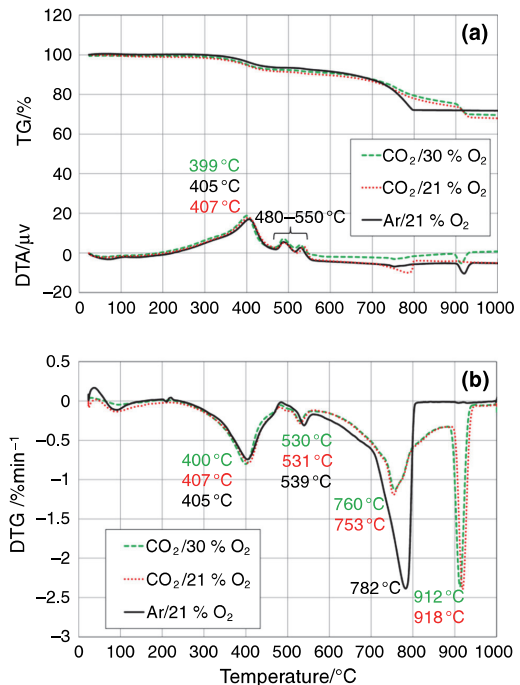
Fig. 2 TG, DTA (**a**) and DTG (**b**) curves of OS char in Ar/O_2 and CO_2/O_2 mixtures

intermediates increase the reaction rate. Char carbon can be oxidised also by CO_2 (Eq. 1). As the process is endothermic, char particle temperature can decrease. However, the results of gas analysis from non-isothermal experiments with OS have shown that release of CO in 100 % CO_2 atmosphere increases notably at temperatures above 650 °C (Fig. 4a). So, the char gasification reaction does not have significant role at 450–550 °C in the case of OS.

In the reactions with pyrite, in the given temperature range, the first reaction is the formation of iron sulphide proceeds partly already during the pyrolysis at 450 °C, and then, oxidation of iron sulphide and pyrite takes place in the gas mixtures with oxygen. Thermodynamic calculations showed also relatively high probability of formation of iron sulphate in the excess of oxygen in this system.[2]

$$FeS_2 \rightarrow FeS + S_{pyritic} \quad +78.2 \text{ kJ} \tag{2}$$

$$FeS_2 + 3O_2 \rightarrow FeSO_4 + SO_2 \quad -1047.4 \text{ kJ} \tag{3}$$

$$FeS + 2O_2 \rightarrow FeSO_4 \quad -828.9 \text{ kJ} \tag{4}$$
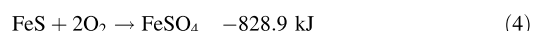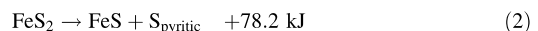
Formation of iron oxides (mainly Fe_2O_3, but also Fe_3O_4 and FeO) is also possible in the following reactions:

---

[2] ΔH_r^0 values, kJ.

Fig. 3 TG and DTG curves of isothermal oxidation of OS char in 79 %Ar/21 % O_2 (**a**) and 70 % CO_2/30 % O_2 (**b**) at different temperatures
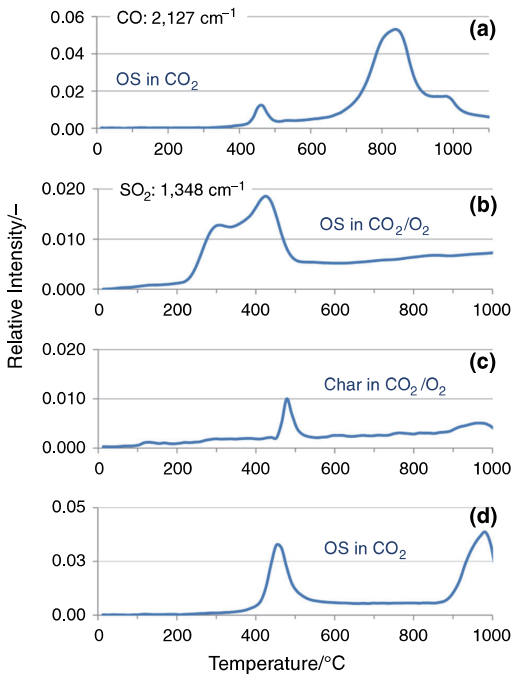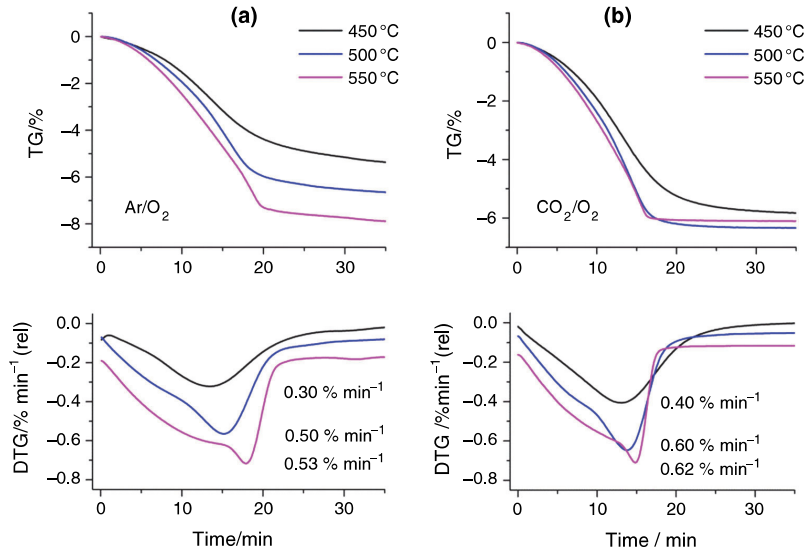
Fig. 4 CO emission profile of OS in CO_2 (**a**) and SO_2 emission profiles (**b–d**) of OS in CO_2/O_2 mixture (**b**), OS char in CO_2/O_2 mixture (**c**) and OS in CO_2 (**d**)

$$2FeS_2 + 5.5O_2 \rightarrow Fe_2O_3 + 4SO_2 \quad -1657.0 \text{ kJ} \quad (5)$$

$$2FeS + 3.5O_2 \rightarrow Fe_2O_3 + 2SO_2 \quad -1219.8 \text{ kJ} \quad (6)$$

$$2FeSO_4 + CO \rightarrow Fe_2O_3 + 2SO_2 + CO_2 \quad +154.9 \text{ kJ} \quad (7)$$

The last reaction becomes thermodynamically possible at quite low temperatures already, and it is affected by CO_2 partial pressure. These reactions are related to the release of SO_2, and gas analysis has shown intensive emission of SO_2 at these temperatures (Fig. 4). The first peak in emission profile (Fig. 4b) can be related to the oxidation of organic sulphur and the second to pyritic sulphur as it is repeated also on the emission profile of OS char (Fig. 4c) and corresponding to the peaks at around 500 °C in Fig. 2.

Siderite decomposes to give iron oxides, or in the presence of SO_2 also $FeSO_4$

$$FeCO_3 \rightarrow FeO + CO_2 \quad +74.9 \text{ kJ} \quad (8)$$

$$FeO + SO_2 + 1/2O_2 \rightarrow FeSO_4 \quad -359.9 \text{ kJ} \quad (9)$$
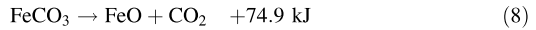
Different forms of sulphur left in the particle after pyrolysis stage and decomposition of pyrite (organic, sulphide, pyritic) can oxidise to give SO_2. Besides, gas analysis of the products has shown the presence of traces of COS in several spectra [3, 24].

$$S + O_2 \rightarrow SO_2 \quad -296.8 \text{ kJ} \quad (10)$$

$$S + CO \rightarrow COS \quad -31.5 \text{ kJ} \quad (11)$$

As in the Ar/O_2, mass losses are visibly different at different temperatures (Fig. 3a), and it can be assumed that half-decomposition of dolomite (part of $MgCO_3$) has also a definite role in the process of char oxidation.

$$MgCO_3 \cdot CaCO_3(\text{dolomite}) \rightarrow MgO + CaCO_3 + CO_2 \\ +124.6 \text{ kJ} \quad (12)$$
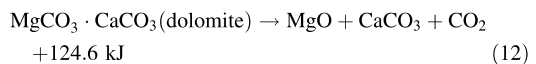
In CO_2/O_2 at high partial pressure of CO_2, the role of this reaction is minor and the mass loss at temperatures from 450 to 550 °C is almost the same (Fig. 3b). From non-isothermal data (Fig. 2), it can be seen that in CO_2/O_2, the maximum rate of $MgCO_3$ decomposition is shifted by 30–35 °C towards higher temperatures as compared to Ar/O_2 atmosphere.

Decomposition of $CaCO_3$ takes place at higher temperatures and is notably dependent on CO_2 partial pressure.

$$CaCO_3 \rightarrow CaO + CO_2 \quad +178.2 \text{ kJ} \tag{13}$$
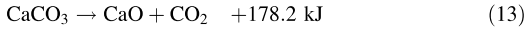
In Ar/O_2 decomposition of dolomite, calcite and magnesite proceed in one step with maximum rate at about 782 °C (offset of DTG peak at 640 °C), but in CO_2/O_2 decomposition of $CaCO_3$ takes place with maximum rate at 912–918 °C (Fig. 2).

During pyrolysis stage and at low partial pressures of O_2, CaS can form

$$4CaSO_3 \rightarrow CaS + 3CaSO_4 \quad -147.2 \text{ kJ} \tag{14}$$

$$CaSO_4 + 4CO \rightarrow CaS + 4CO_2 \quad -180.2 \text{ kJ} \tag{15}$$

$$2CaO + 3S \rightarrow 2CaS + SO_2 \quad +8.2 \text{ kJ} \tag{16}$$
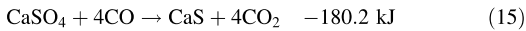
As the partial pressure of oxygen increases, CaS is oxidised

$$CaS + 2O_2 \rightarrow CaSO_4 \quad -951.7 \text{ kJ} \tag{17}$$
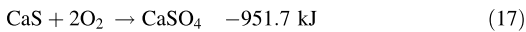
SO_2 formed in several reactions is bound by CaO (and partly also by MgO) or by direct sulphation of calcite.

$$CaO + SO_2 + 1/2O_2 \rightarrow CaSO_4 \quad -502.4 \text{ kJ} \tag{18}$$

$$CaO + SO_2 \rightarrow CaSO_3 \quad -227.7 \text{ kJ} \tag{19}$$

$$4CaO + 4SO_2 \rightarrow CaS + 3CaSO_4 \quad -1057.8 \text{ kJ} \tag{20}$$

$$CaCO_3 + SO_2 + 1/2O_2 \rightarrow CaSO_4 + CO_2 \quad -324.2 \text{ kJ} \tag{21}$$
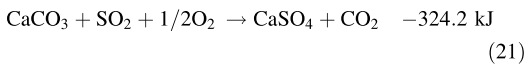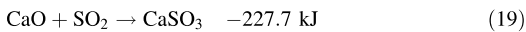
However, the last reaction is enhanced at higher pressures [25]. Formation of mixed Ca, Mg sulphate is also possible [26].[3]

$$CaO + 3MgO + 4SO_2 + 2O_2 \rightarrow CaMg_3(SO_4)_4 \tag{22}$$
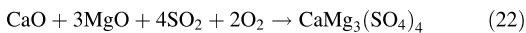
Part of free CaO reacts with SiO_2 (and other sandy-clay components like Al_2O_3) forming different silicates (belite, $CaO \cdot Al_2O_3$, etc.) [27]

$$2CaO + SiO_2 \rightarrow 2CaO \cdot SiO_2(\beta - Ca_2SiO_4) \quad -125.4 \text{ kJ} \tag{23}$$
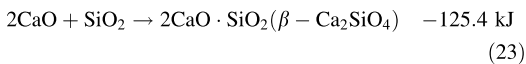
In the presence of CO, decomposition of sulphates can proceed well below 1,000 °C giving rise to additional emissions of SO_2

$$4FeSO_4 \rightarrow 2Fe_2O_3 + 4SO_2 + O_2 \quad +875.7 \text{ kJ} \tag{24}$$

$$CaSO_4 + CO \rightarrow CaO + SO_2 + CO_2 \quad +219.4 \text{ kJ} \tag{25}$$

---
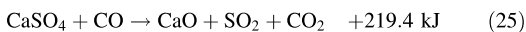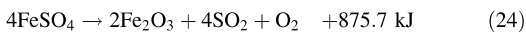
[3] Thermodynamic data for Ca, Mg sulphate are missing.

The increased intensity in SO_2 emission profile of OS in 100 % CO_2 at temperatures above 900 °C can be related to these reactions (Fig. 4d).

So, the process of char oxidation followed by mineral decomposition involves a complex set of competitive endo- and exothermic reactions depending on temperature, oxidative/reductive properties of the gas phase and CO_2 partial pressure inside the char particles resulting in the specific shape of DTG curves (Fig. 3a, b) as well as of SO_2 emission profiles (Fig. 4).

Oxidation kinetics

The changes in activation energy (E/kJ mol^{-1}) depending on the reaction progress α were determined from the experiments with 5, 10 and 15 K min^{-1} heating rates. Conversion α was calculated from the mass loss during oxidation stage. After the baseline correction, derivatives of the normalised TG signals were processed with the AKTS Advanced Thermokinetics software [22] enabling to obtain apparent conversion-dependent activation energies without assuming the form of $f(\alpha)$ function.

The equation describing the iso-conversional approach [28, 29] used in the software derived from the Friedman differential method [30] can be expressed as follows:

$$\ln \left(\frac{d\alpha}{dt} \right) = \ln \{A(\alpha) f(\alpha)\} - \frac{E(\alpha)}{RT} \tag{26}$$

The function dependent on the reaction model $f(\alpha)$ becomes a constant at each fixed conversion degree α in Eq. 26, and the relationship between the logarithm of the reaction rate $d\alpha/dt$ and $1/T$ is linear with the slope of E/R.

The relationship between the conversion-dependent activation energy and reaction progress for OS char in O_2/Ar and O_2/CO_2 mixtures is shown in Fig. 5.

Kinetic calculations showed that the conversion-dependent activation energy of OS char was 110–200 kJ mol^{-1} in Ar/21 % O_2, 90–125 kJ mol^{-1} in $CO_2/30$ % O_2 and 125–160 kJ mol^{-1} in $CO_2/21$ % O_2 in the range of $\alpha = 0.1$–0.9. In comparison, activation energies for OS itself in these atmospheres were in the range of 120–100 kJ mol^{-1} in Ar/O_2 and 35–45 kJ mol^{-1} in CO_2/O_2 in the range of $a = 0.1$–0.9, being higher at the beginning, then diminishing and increasing slightly for the final stage of oxidation. Kinetics of OS oxidation was discussed more in detail in [3]. The activation energies for the oxidation of OS residual carbon are lower at the beginning of oxidation, indicating more likely to diffusion limitation. Thereafter, there is an increase almost until 50 % of conversion. Following to this, a slight decrease and increase for the final stage can be seen. The initial and final stage activation energies were lower in $CO_2/30$ % O_2 as compared to Ar/O_2. For the final stage, oxidation in Ar/
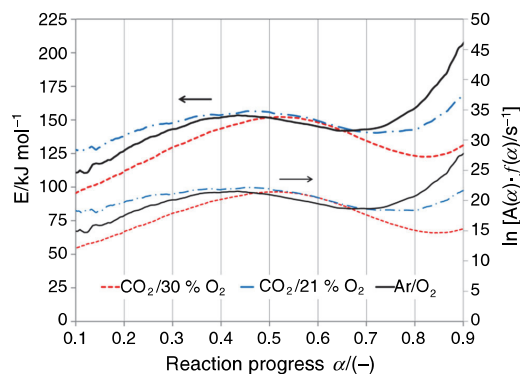
Fig. 5 Activation energy (E, kJ mol^{-1}) and pre-exponential factor ln $\{A(\alpha)*f(\alpha)/s^{-1}\}$ values for OS char oxidation in Ar/O$_2$ and CO$_2$/O$_2$ atmospheres

21 % O$_2$ shows higher activation energies than CO$_2$/21 % O$_2$ that can be related to the increased role of reactions in mineral part with the increase in temperature.

Simple kinetic modelling of char oxidation was carried out also on the basis of isothermal data. Several mechanism models, well organised lately in [31], were tested to find the best fit into

$$g(\alpha) = k\tau \tag{27}$$

where $g(\alpha)$ is the integral form of mechanism function, k—rate constant and τ—reaction duration. Conversion α was calculated as mass loss from the maximum mass loss at the respective temperature.

It was found that the highest regression coefficients ($R^2 = 0.993{-}0.932$) amongst all the models tested for Eq. 27 belonged to Avrami–Erofeev equation

$$\mathbf{A2} : g(\alpha) = [-\ln(1-\alpha)]^{1/2} \tag{28}$$

The calculated values of the rate constant at different temperatures for the model A2 are presented in Table 2. It can be seen that the rate constants for char oxidation in CO$_2$/O$_2$ are approximately 1.2–1.3 times higher as

Table 2 Rate constant values for char oxidation in CO$_2$/O$_2$ and Ar/O$_2$

Atmosphere	Temperature/°C	R^2	k/min^{-1}
CO$_2$/30 % O$_2$	450	0.9915	0.0696
	500	0.9319	0.0850
	550	0.9435	0.0854
Ar/21 % O$_2$	450	0.9930	0.0581
	500	0.9796	0.0664
	550	0.9777	0.0654

compared to Ar/O$_2$ atmosphere. So, OS char combustion under oxy-fuel conditions should proceed with higher rate as compared to air combustion.

However, apparent activation energy could not be calculated in the temperature region studied due to non-Arrhenius behaviour ($R^2 < 0.7$) as can be assumed also from the shape of DTG curves (Figs. 3, 4).

Conclusions

Isothermal and non-isothermal TA methods were used to characterise OS pyrolysis and OS char oxidation in different atmospheres related to OS oxy-fuel combustion. The following conclusions can be drawn by analysing the experiment data and emission profiles of gaseous products from OS and OS char:

- At OS pyrolysis, the influence of CO$_2$ on the organic part during devolatilisation stage is highly similar to Ar. mass loss and characteristic peak temperatures do not differ in Ar or CO$_2$. However, decomposition of carbonates in the mineral part of OS is notably influenced by CO$_2$ partial pressure.
- There is no notable effect of char carbon and CO$_2$ reaction on the char oxidation stage. The results of gas analysis have shown that the release of CO from OS in 100 % CO$_2$ atmosphere increases notably not until temperatures above 650–700 °C. Besides this, the combination of different possible reactions in this temperature region makes it complex to identify the role of char carbon and CO$_2$ reaction.
- The presence of inorganic minerals, such as pyrite, sulphides and sulphates, increases SO$_2$ emissions, especially, at higher temperatures and low O$_2$ concentrations. The presence of carbonates can support CO$_2$-related self-gasification of residual carbon in fuel particles and increase CO formation at their decomposition temperatures, but high partial pressure of CO$_2$ shifts the carbonate decomposition towards higher temperatures enabling to assume decreased CO$_2$ emissions under oxy-fuel conditions.
- The values of rate constants calculated for different temperatures from 450 to 550 °C indicate that OS char combustion should proceed under oxy-fuel conditions with higher rate as compared to air combustion.
- Oxidation of OS char takes place with higher activation energies as compared to the initial OS sample. Char oxidation under oxy-fuel conditions (CO$_2$/O$_2$) occurs with lower activation energies as compared to Ar/O$_2$, especially, at higher conversion levels. So, applying oxy-fuel combustion to OS should enhance the process as compared to air combustion.

References

1. Buhre BJP, Elliot LK, Sheng CD, Gupta RP, Wall TF. Oxy-fuel combustion technology for coal-fired power generation. Prog Energy Combust Sci. 2005;31(4):283–307. doi:10.1016/j.pecs.2005.07.001.

2. Anheden M, Burchhardt U, Ecke H, Faber R, Jidinger O, Giering R, et al. Overview of operational experience and results from test activities in Vattenfall's 30 MWth oxyfuel pilot plant in Schwarze Pumpe. Energy Procedia. 2011;4:941–50. doi:10.1016/j.egypro.2011.01.140.

3. Meriste T, Yörük CR, Trikkel A, Kaljuvee T, Kuusik R. TG–FTIR analysis of oxidation kinetics of some solid fuels under oxy-fuel conditions. J Therm Anal Calorim. 2013;114(2):483–9. doi:10.1007/s10973-013-3063-x.

4. Estonia 2013 Energy Policies Beyond IEA Countries, OECD/IEA 2013, Executive summary and key recommendations. [database on the Internet]2013. Available from: http://www.iea.org/Textbase/npsum/estonia2013SUM.pdf. Accessed: 01.09.2014.

5. Kaljuvee T, Keelmann M, Trikkel A, Kuusik R. Thermooxidative decomposition of oil shales. J Therm Anal Calorim. 2010;105(2):395–403. doi:10.1007/s10973-010-1033-0.

6. Ots A. Estonian oil shale properties and utilization in power plants. Energetika. 2007:8-18.

7. Tiwari P, Deo M. Detailed kinetic analysis of oil shale pyrolysis TGA data. AIChE J. 2012;58(2):505–15. doi:10.1002/aic.12589.

8. Li S, Yue C. Study of pyrolysis kinetics of oil shale. Fuel. 2003;82(3):337–42. doi:10.1016/S0016-2361(02)00268-5.

9. Nazzal JM. Influence of heating rate on the pyrolysis of Jordan oil shale. J Anal Appl Pyrolysis. 2002;62(2):225–38. doi:10.1016/S0165-2370(01)00119-X.

10. Thakur DS, Nuttall HEJ. Kinetics of pyrolysis of Moroccan oil shale by thermogravimetry. Ind Eng Chem Res. 1987;26(7):1351–6. doi:10.1021/ie00067a015.

11. Kök MV, Pamir RM. Comparative pyrolysis and combustion kinetics of oil shales. J Anal Appl Pyrolysis. 2000;55(2):185–94. doi:10.1016/S0165-2370(99)00096-0.

12. Qian J, Yin L. Oil shale: petroleum alternative. 1st ed. Hubei: China Petrochemical Press; 2010.

13. Jaber JO, Probert SD. Pyrolysis and gasification kinetics of Jordanian oil-shales. Appl Energy. 1999;63(4):269–86. doi:10.1016/S0306-2619(99)00033-1.

14. Fang-Fang X, Ze W, Wei-Gang L, Weng-Li S. Study on thermal conversion of Huadian oil shale under N2 and CO2 atmospheres. Oil Shale. 2010;27(4):309–20. doi:10.3176/oil.2010.4.04.

15. Barkia H, Belkbir L, Jayaweera SAA. Thermal analysis studies of oil shale residual carbon. J Therm Anal Calorim. 2004;. doi:10.1023/B:JTAN.0000028040.16844.40.

16. Cavalieri RP, Thomson WJ. The effect of mineral species on oil shale char combustion. Symposium on geochemistry and chemistry of oil shale presented before the divisions of fuel chemistry, geochemistry, and petroleum chemistry; American Chemical Society, Seattle. 1983.

17. Burnham AK. Reaction kinetics between CO2 and oil-shale residual carbon 1. Effect of heating rate on reactivity. Fuel. 1978;58(4):285–92. doi:10.1016/0016-2361(79)90138-8.

18. Burnham AK. Reaction kinetics between CO2 and oil-shale residual carbon 2. Partial pressure and catalytic- mineral effects. Fuel. 1979;58(10):713–8. doi:10.1016/0016-2361(79)90067-X.

19. Burnham AK. Reaction kinetics between steam and oil-shale residual carbon. Fuel. 1979;58(10):719–23. doi:10.1016/0016-2361(79)90068-1.

20. Miao Z, Wu G, Li P, Zhao N, Wang P, Meng X. Combustion characteristics of Daqing oil shale and oil shale semi-cokes. Min Sci Technol. 2009;19(3):380–4. doi:10.1016/S1674-5264(09)60071-5.

21. Coats AW, Redfern JP. Kinetic parameters from thermogravimetric data. Nature. 1964;201:68–9. doi:10.1038/201068a0.

22. Advanced Kinetics and Technology Solutions. AKTS Thermokinetics. http://www.akts.com. AKTS AG. Switzerland.

23. HSC Chemistry 7.11. Chemical reaction and equilibrium software with extensive thermochemical database and flowsheet simulation. License No. 70780. Antti Roine 09006-ORC-J. Outotec Research Center, 1974–2011. 2011.

24. Kaljuvee T, Radin M, Astahhov D, Pelovski Y. Evolved gas analysis at thermal treatment of some solid fossil fuels. J Therm Anal Calorim. 2006;84(1):59–66. doi:10.1007/s10973-005-7205-7.

25. Trikkel A, Zevenhoven R, Kuusik R. Modelling SO2 capture by Estonian limestones and dolomites. Proc Est Acad Sci Chem. 2000;49(1):53–70.

26. Kaljuvee T, Trikkel A, Kuusik R, Bender V. The role of MgO in the binding of SO2 by lime-containing materials. J Therm Anal Calorim. 2005;80(3):591–7. doi:10.1007/s10973-005-0699-1.

27. Trikkel A, Keelmann M, Kaljuvee T, Kuusik R. CO2 and SO2 uptake by oil shale ashes: effect of pre-treatment on kinetics. J Therm Anal Calorim. 2010;99(3):763–9. doi:10.1007/s10973-009-0423-7.

28. Roduit B, Folly P, Berger B, Mathieu J, Sarbach A, Andres H, et al. Evaluating sadt by advanced kinetics-based simulation approach. J Therm Anal Calorim. 2008;93(1):153–61. doi:10.1007/s10973-007-8865-2.

29. Roduit B, Xia L, Folly P, Berger B, Mathieu J, Sarbach A, et al. The simulation of the thermal behavior of energetic materials based on DSC and HFC signals. J Therm Anal Calorim. 2008;93(1):143–52. doi:10.1007/s10973-007-8864-3.

30. Friedman HL. Kinetics of thermal degradation of char-forming plastics from thermogravimetry. Application to a phenolic plastic. J Polym Sci Part C. 1964;6:183–95. doi:10.1002/polc.5070060121.

31. Tian L, Chen H, Chen Z, Wang X, Zhang S. A study of non-isothermal kinetics of limestone decomposition in air (O2/N2) and oxy-fuel (O2/CO2) atmospheres. J Therm Anal Calorim. 2014;115(1):45–53. doi:10.1007/s10973-013-3316-8.

PAPER III

Yörük, C.R.; Trikkel, A.; Kuusik, R. Oxy-fuel Combustion of Estonian Oil Shale: Kinetics and Modeling. Energy Procedia 2016, 86, 124–33.

The 8th Trondheim Conference on Capture, Transport and Storage

Oxy-fuel Combustion of Estonian Oil Shale: Kinetics and Modeling

Can Rüstü Yörük[a*], Tõnis Meriste[b], Andres Trikkel[a], Rein Kuusik[a]

aLaboratory of Inorganic Materials, Tallinn University of Technology, Ehitajate tee 5, 19086 Tallinn, Estonia
bEstonian Energy SC, Laki 24, 12915 Tallinn, Estonia

Abstract

In this work, non-isothermal thermal analysis (TA) methods combined with Fourier transform infrared (FTIR) spectroscopy were applied to investigate specifics of different stages of oxy-fuel (OF) combustion of Estonian oil shale (EOS) and its char. Kinetics of EOS and its char oxidation were analyzed in different atmospheres in order to understand the complex mechanism of oil shale (OS) OF combustion. Additionally, the OF combustion of OS in circulating fluidized bed (CFB) was simulated with the recently released Aspen Plus fluidized bed (FB) reactor which treats bottom zone and freeboard hydrodynamics. Particular attention was given to the determination of the required elutriated mass flows to maintain the heat balance of the system for OF combustion cases. Four case studies were simulated including: Case 1: Air combustion, Case 2: 21%O_2/flue gas, Case 3: 23%O_2/flue gas and Case 4: 30%O_2/flue gas. The results of TA experiments show that the pyrolysis behavior is very similar in Ar and CO_2 until 500°C and there is no visible char carbon and CO_2 reaction under OF conditions. The emissions of CO_2 from mineral part of OS can be diminished as decomposition of calcite takes place at higher temperatures in OF combustion. Activation energies calculated for oxidation of OS and its char in CO_2/O_2 are notably less than activation energies calculated for Ar/O_2 atmosphere. Modeling results show that higher fuel mass flow rate and higher O_2 concentration in the oxidizer have to be considered in the set of conditions for OF in order to extract the same amount of heat as in air combustion. The Case 3 with 23% inlet O_2 concentration has a similar behavior as compared to air combustion in terms of temperature of the boiler and recirculation rate of the particles. The data obtained from experimental measurements and models is valuable for the possible implementation of OF combustion of EOS in CFB boilers.

Keywords: oxy-fuel combustion; oil shale; thermal analysis; modeling

* Can Rüstü Yörük. Tel.: +372 6202872; fax: +372 6202801.
 E-mail address: can.yoruk@ttu.ee

1. Introduction

Estonian Oil Shale (EOS) is the main fuel used in power stations in Estonia hence CO_2 emissions have been a serious problem in the energy sector which produces over 90% of electricity from oil shale (OS). For this reason, oxy-fuel (OF) circulating fluidized bed combustion (CFBC) can play a significant role in the near future for possible CO_2 capture ready applications since OF combustion with Carbon Capture and Storage (CCS) provides the potential for an almost 100% reduction of CO_2. Furthermore, OF combustion has already been proven by bench scale applications [1-3] as reliable, CO_2 free, safe and feasible technology that has also a demonstration scale (30 MW CIUDEN) under operation since 2011 [4]. Detailed information about OF combustion and CCS is given for example in [5]. The process of OF combustion with CCS is a new technology and for EOS there is no experience. EOS is defined as highly heterogeneous fuel with complicated composition of organic and mineral matter [6] that increases the importance of its investigation under different operating conditions. During its thermal decomposition under conventional combustion conditions, complex set of parallel reactions occurs in both organic and mineral parts of the fuel [7]. All these reactions and the gas-solid hydrodynamics in circulating fluidized bed (CFB) boiler can be influenced by composition and physical properties (high CO_2 partial pressure, density, viscosity, thermal capacity and conductivity) of the fluidization gas at OF combustion. That is why experimentation and modeling are vital for the successful design and scale-up of OF combustion of EOS in CFB boilers. The knowledge of the effect of CO_2 atmosphere on the reactivity of OS and OS char is needed for evaluating the application of OS OF combustion. The study of reaction kinetics including pyrolysis and oxidation characteristics is also crucial to understand the complex mechanism of OS OF combustion. There have been a few studies on pyrolysis and kinetics of oxidation of OS and its char from Estonia and different countries [7-12]. However, there is still little knowledge related to the OF combustion of EOS and there is no study conducted with oil shale in fluidized bed (FB) and in particular, under oxy-fuel conditions. In this respect, having a special interest on OF combustion of EOS, non-isothermal thermal analysis (TA) methods combined with Fourier transform infrared (FTIR) spectroscopy have been applied to investigate pyrolysis stage of OS as well as combustion characteristics of OS and its char. Kinetics of OS and its char oxidation have been analyzed in different atmospheres. Additionally, CFBC model in Aspen Plus has been built using the FB reactor of Aspen in one set of operating regime similar to air combustion. CFBC model investigates characteristics of the air OS and OF OS combustion with respect to the specific CFB operating parameters (boiler temperature, recirculation rate, external heat exchanger duty etc.). Particular attention has been given to the determination of the required elutriated mass flows to maintain the heat balance of the system for OF combustion cases since it is known from the experience of coal firing CFB boilers, that the mass flow of elutriated particles from the boiler is important, as the recirculation rate of the particles controls the heat balance of the boiler both with respect to the heat transfer in the freeboard (furnace walls) and in the external heat exchanger [13].

2. Experimental and modeling

2.1. Materials and Methods

The common EOS sample used in energy production was crushed with an alligator-type grinding machine. Mean sample was taken from the crushed material and ground in a big ball mill. Then, the sample was dried at 105°C for 4 hours and ground additionally in a Retsch PM 100 grinding machine until the entire sample passed the 200 μm sieve. Characterization of the OS sample is given in Table 1.

Table 1.Characterization of OS

Content, %mass								Elements[d]	
HHV[d], MJ kg^{-1}	Ash[d]	Moisture	C	H	N	S	TC	TIC/CO_2[M] from TIC	
11.86	49.3	0.7	30.4	3.0	0.1	1.63	31.5	4.55/16.7	

[d] Per dry sample, TC/TIC total carbon/total inorganic carbon, [M] mineral CO_2

The Setaram Setsys Evo 1750 thermoanalyzer coupled to a Nicolet 380 FTIR spectrometer for evolved gas analysis was used in the experiments. Non-isothermal TG tests were performed at 10 K min^{-1} heating rate up to 1,000°C with gas flow rate 30 mL min^{-1} using different atmospheres (Ar, CO_2, Ar/O_2 and CO_2/O_2). Standard 100 μL

Pt crucibles were used, and the mass of samples was 20 ± 0.5 mg in most experiments and 30 ± 0.5 mg for the tests with gas analysis. To prepare residual carbon of OS, the sample was heated up to 450°C in argon atmosphere and maintained at this temperature for 1 h until devolatilization ceased. The temperature was selected from preliminary pyrolysis experiments according to the highest reaction rate. AKTS Advanced Thermokinetics software [14] was used to calculate kinetic parameters of oxidation stage of OS and its char. FTIR measurements were recorded in the 400–4,000 cm^{-1} region with the resolution of 4 cm^{-1} taking an average of four scans.

2.2. Model Description and Modeling Approach

The boiler in CFB model has been designed with the same geometry of 12 MW$_{th}$ CFB boiler at Chalmers University of Technology. Firstly, the applicability of the FB reactor has been tested by comparing the simulation results with CFB Chalmers boiler in the case of conventional combustion. Secondly, the model is used to discuss the conversion of an air-OS fired CFB unit to oxy-OS combustion. Detailed description of the real CFB unit can be found in [15]. The model presented in Fig. 1 is divided into two main parts described below; combustion of OS kerogen and the CFB model including the description of how the required elutriated mass flows are calculated in the model.
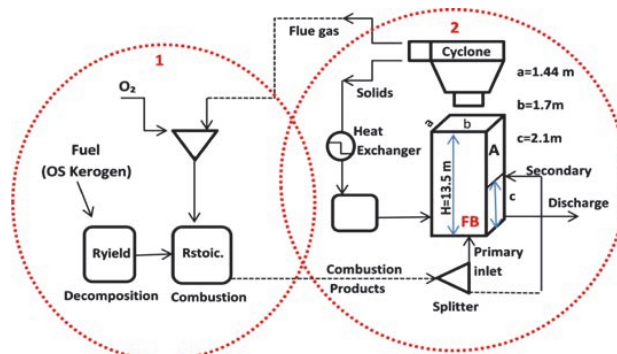
Fig. 1. Overall process lay-out of the CFBC model. *The circle (1) is the combustion part and (2) the CFB model.*

Air combustion and three OF cases have been simulated including: Case 1: Air combustion, Case 2: 21%O$_2$/flue gas, Case 3: 23%O$_2$/flue gas and Case 4: 30%O$_2$/flue gas. The fuel, EOS, consists of kerogen (27%), moisture (11%), and minerals (62%). The analysis of fuel kerogen used in the simulation is presented in Table 2.

Table 2. Properties of the organic matter (kerogen) of EOS [6].

Calorific Values, MJ kg^{-1}		Elemental Composition, (%)					
HHV	LHV	C	H	O	N	S	Cl
36.6	34.5	77.45	9.7	10.01	0.33	1.76	0.75

The combustion modeling of EOS considers moisture evaporation, decomposition stage of the kerogen and its combustion reactions. The OS kerogen was decomposed to C, H$_2$, S$_2$, Cl$_2$, O$_2$, and N$_2$ using the Ryield[1] reactor in the combustion model. The oxidation of the decomposed kerogen was modeled in the equilibrium reactor Rstoic[2] at 850°C by following four main reactions considered: C+O$_2$=CO$_2$, H$_2$+Cl$_2$=2HCl, S$_2$+2O$_2$=2SO$_2$, and H$_2$+1/2O$_2$=H$_2$O. All the components used in the simulations were defined as pure components (i.e. 100% pure O$_2$). The heat of combustion calculated from the combustion of OS kerogen was added as a source term in the FB reactor. The heat transferred in the internal heat exchanger was considered as a fixed heat loss (1.47MW) from the furnace for each simulation case and it was subtracted from the heat of combustion (Table 3). The amount of oxidizer and the oxygen concentration of 3.6% in the flue gas were kept constant for all cases. Case 2 has the same oxidizer oxygen

---

[1] Ryield block decomposes the fuel into its elemental constituents.
[2] Rstoic block enables to model combustion with known reaction stoichiometry.

concentration and the same fuel input as air combustion (Case 1). The O_2 concentration and fuel input was chosen particularly in Case 3 in order to extract same amount of heat from external heat exchanger and to maintain the similar operating regime as in the air combustion case. Case 4 is modeled for oxygen-enriched case with 30% of O_2 in the oxidizer.

FB reactor of Aspen requires several input parameters including particle size distribution (PSD), bed inventory (Geldart group for the bed material, bed pressure drop), geometry of the boiler, additional gas supply, and impact of heat exchangers on bed temperature [16]. FB reactor is given as bubbling FB thus cyclone and solid recycle streams have to be included in order to model circulating conditions. The bottom zone of FB is modeled as bubbling bed according to Werther&Wein [17] and the freeboard (upper dilute zone) is modelled according to Kuni and Levenspiel [18]. The modeling in this study considers cyclone (no loss of fines) and also external heat exchanger on solid recycle streams. The solid discharge stream was kept small by matching the gas feed to the required solid recirculation. The mass flow of elutriated particles was determined to maintain the temperature of the furnace at 900°C then the fixed heat loss (1.47 MW) from the in-furnace heat exchanger was subtracted from the heat duty of the combustion. This calculation approach was also tested if the same mass flow of the elutriated particles with the lowest solid discharge value can be achieved with lower gas velocities by controlling the primary gas stream with an additional bypass[3] stream. Table 3 presents the input parameters of the modeling for FB reactor.

Table 3. Input specifications considered for the FB reactor

Reactor Specifications	Values
Fluidized bed pressure drop, ΔP_{fb} (kPa)	7
Distributor pressure drop, ΔP_{dist} (kPa)	4
Voidage at minimum fluidization, ε_{mf}	0.47
Heat duty, (MW) Case 1	6.01-1.47=4.54
Solid density, ρ_s (kg m^{-3})	2648
Boiler cross section, A (m^2)	1.44 x 1.7
Boiler Height, H (m)	13.5

Hot flue gasses were used as a fluidization gas. Silica sand (SiO_2) was used as bed material with the PSD given in Fig. 2.
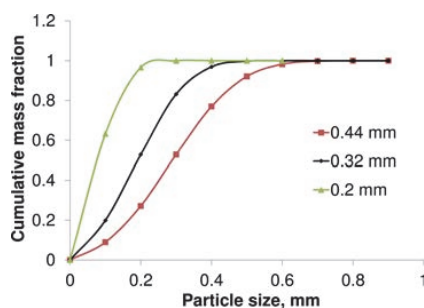
Fig. 2. PSD of the SiO_2 for three different mean particle diameters

PSD were determined according to the Rosin-Rammler-Sperling (RRSB) distribution function with Aspen Plus to obtain cumulative mass fractions as close as possible to the real bed materials by defining the average particle diameter for each 3 particle size fractions.

Both the Geldart et al. [19] and Colakyan&Levenspiel [20] correlations were tested separately for the elutriation models. The Geldart et al. and Colakyan&Levenspiel correlations for the determination of the elutriation coefficient:

---

[3] The "bypass" is referred to a flow subtracted from the primary gas flow in order to ensure the lowest superficial gas velocity and the possible lowest overall pressure drop, if the same mass flow of the elutriated particles with the lowest solid discharge value can be achieved by controlling the primary gas stream with the bypass stream.

Colakyan & Levenspiel: $k = A \cdot \rho_s \cdot \left(1 - \frac{u_t}{u}\right)^B$ A= 0.011   B= 2   (1)

Geldart et al.: $k = A \cdot \exp\left(B \cdot \frac{u_t}{u}\right) \cdot \rho_g \cdot u$ A= 23.7   B= -5.4   (2)

Herein, k is the particle related elutriation coefficient, u_t is the terminal velocity (m s^{-1}), ρ_g is the gas density (kg m^{-3}), u is the superficial gas velocity at the top of the bed (m s^{-1}) and ρ_s is the particle density (kg m^{-3}).

3. Results and discussion

3.1. *Pyrolysis of OS in Ar and CO$_2$*

The main stages of combustion of solid fuel particles after drying are pyrolysis (devolatilization) and char oxidation. Thermal analysis experiments with OS in 100% Ar and CO$_2$ (Fig.3a) showed that the characteristic temperatures and mass loss of the OS sample in Ar and CO$_2$ were very similar during devolatilization up to 500°C which indicates that CO$_2$ behaves similarly to an inert gas and has the same influence on the organic part as Ar.
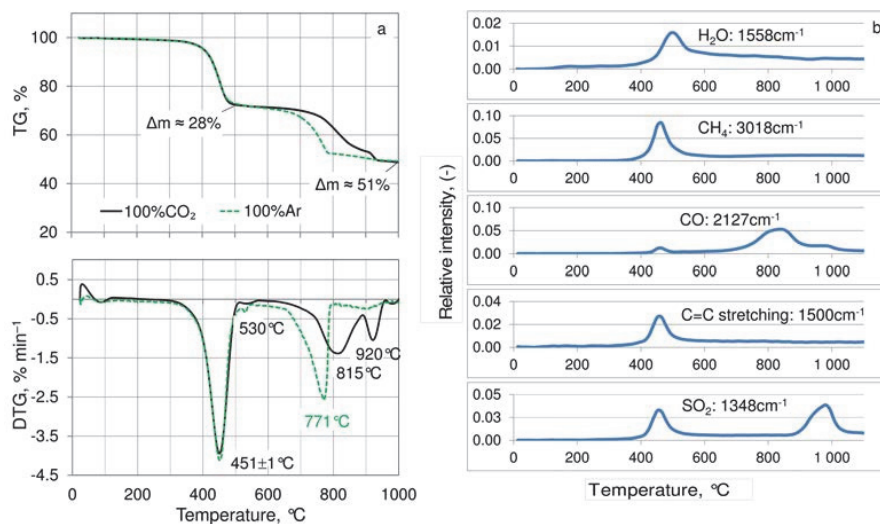
Fig. 3. (a) Mass loss (TG) and mass loss rate (DTG) curves of OS in CO$_2$ and Ar; (b) selected emission profiles from OS in 100% CO$_2$

At higher temperatures and in 100% CO$_2$ atmosphere decomposition of mineral carbonates contained in OS (dolomite and calcite) is shifted apart and proceeds with maximum rate at 815°C (MgCO$_3$) and 920°C (CaCO$_3$), respectively, while in 100% Ar both carbonates decompose in one step starting from 650°C. The small step on DTG curves at about 530°C can be related to the reactions with pyrite. At higher CO$_2$ partial pressures, the char – CO$_2$ reaction can become important, adding to the overall reaction rate and increasing CO emissions.

$C(s) + CO_2(g) \rightarrow 2CO(g)$ $\Delta H^0 = +172.4 \text{ kJ mol}^{-1}$ (3)

The experiments show that in the case of OS, the char gasification reaction does not have significant role at 450–550°C that can be assumed from the very small differences in the mass loss values in Ar and CO$_2$.

Analyzing the spectra of evolved gasses from OF combustion is complicated due to wide peaks of CO$_2$ and H$_2$O overlapping with peaks of other compounds and groups at different wave number regions. Emission profiles of some selected compounds or groups are presented on Fig. 3b. In 100% CO$_2$ atmosphere, in between 400–600°C CH$_4$ is always present. Peaks characteristic to C=C bond stretching from aromatics (1400–1500 cm^{-1}) appear also in this

temperature interval together with H_2O and CH_4. SO_2 has two maximums in the emission profiles. One can be related to organic sulfur, the other at higher temperatures to decomposition of sulphates in the presence of CO. The release of CO in 100% CO_2 increases notably at temperatures above 650°C. So, the impact of char – CO_2 reaction can increase at temperatures above 650–700°C taking into account that high content of carbonates can support also CO_2-related self-gasification of OS char at higher temperatures. To diminish SO_2 emissions, high temperatures and reducing conditions should be avoided.

3.2. Oxidation of OS char and OS in Ar/O₂ and CO₂/O₂

Thermal behavior of OS and its char was studied in $CO_2/30\%O_2$, $CO_2/21\%O_2$ and $Ar/21\%O_2$ (modeling air combustion) atmospheres. It can be seen from TA curves (Fig. 4ab) that mass loss of OS char up to 550°C in Ar/O_2 and CO_2/O_2 is similar – approximately 8%. This mass loss can be related to oxidation of residual carbon and some left-behind heavier organic compounds. Mass loss of OS in $CO_2/30\%O_2$ is 34%. OS samples have typically two exothermic peaks in DTA curves – under these experiment conditions at 345°C and 480°C. The first peak characterizes devolatilization and release of lighter hydrocarbons, the second oxidation of heavier hydrocarbons (thermobitumen) and char. DTA curve of OS char has one exothermic maximum in the DTA curve at 405°C and a smaller one at 490°C. The last one and the small peak at 530°C can be related to char oxidation and/or reactions with pyrite and organic sulfur as evolved gas analysis (Fig. 3b) showed increased emission of SO_2 in this temperature interval. DTG curves indicate that in $CO_2/30\%O_2$ decomposition of $CaCO_3$ takes place at 918–920°C, so, FB OF combustion of calcite rich fuels like some types of oil shale should decrease CO_2 emissions from the mineral part if temperatures are below 900°C.

$$\ln\left(\frac{d\alpha}{dt}\right) = \ln\{A(\alpha)\,f(\alpha)\} - \frac{E(\alpha)}{RT} \qquad (4)$$
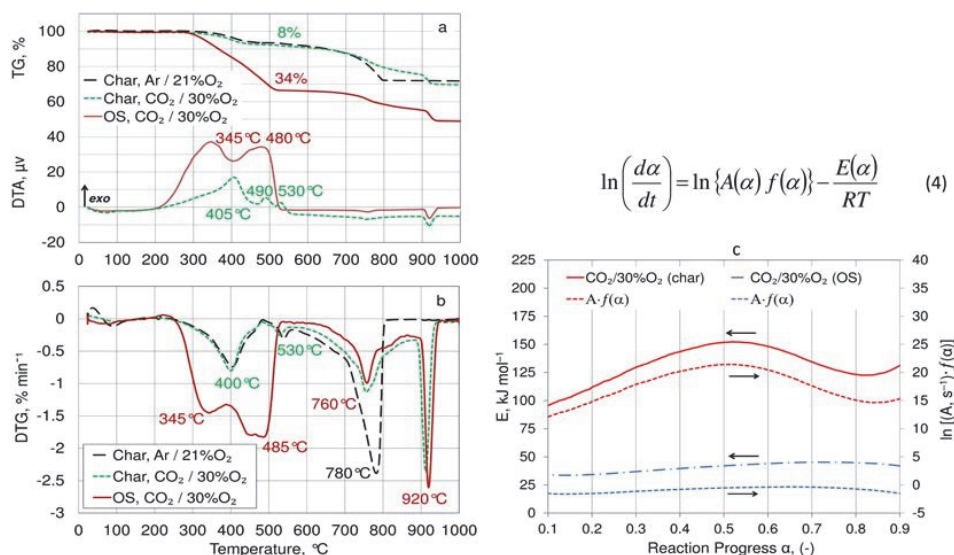
Fig. 4. (a,b) Thermal analysis curves of OS and its char in different atmospheres; (c) Conversion-dependent activation energy E and pre-exponential factor A·$f(\alpha)$ for OS and its char oxidation stage in CO_2 / 30% O_2 atmosphere

3.3. Oxidation kinetics

The changes in activation energy (E, kJ mol^{-1}) were determined from the experiments with different heating rates and conversion level α was calculated from the mass loss during the oxidation stage. This iso-conversional approach enables to obtain apparent conversion-dependent activation energies without assuming the form of the mechanism function f(α). The method used in the software [21, 22] is derived from the Friedman differential method [23].

According to this approach the reaction mechanism function $f(\alpha)$ becomes a constant at each fixed conversion degree α (Eq. 4), and the relationship between the logarithm of the reaction rate $d\alpha/dt$ and $1/T$ is linear with the slope of E/R. The relationship between the conversion-dependent activation energy and reaction progress for OS and its char in $CO_2/30\%O_2$ atmosphere is shown in Fig. 4c and the interval of activation energy values in the range of $\alpha = 0.1–0.9$ is listed in Table 4.

Table 4. Activation energy values for oxidation of OS and its char

OS in	E, kJ mol^{-1}	ln $[A \cdot f(\alpha)]$ A, s^{-1}	OS char in	E, kJ mol^{-1}	ln $[A \cdot f(\alpha)]$ A, s^{-1}
$CO_2 / 30\% \ O_2$	$35 - 45$	$-1.6 - -1.4$	$CO_2 / 30\% \ O_2$	$90 - 125$	$10 - 15$
$CO_2 / 21\% \ O_2$	$85 - 40$	$-1.5 - 10$	$CO_2 / 21\% \ O_2$	$125 - 160$	$17 - 22$
$Ar / 21\% \ O_2$	$120 - 100$	$7 - 18$	$Ar / 21\% \ O_2$	$110 - 200$	$15 - 27$

Kinetic calculations showed that activation energies are lower for OS and higher for its char that can be related to the shift of oxidation temperatures towards higher values in the case of OS char. As compared to Ar/O_2 atmosphere, the E values are notably lower for CO_2/O_2 atmosphere, especially, in the case of OS sample. Generally, the activation energies for the oxidation of OS char were lower at the beginning of oxidation, where diffusion limitation can control the oxidation rate. Thereafter, there is an increase up to 50% conversion. Another increase can be seen for the final stage above 70% conversion indicating to the increasing role of different reactions in mineral part. For OS, the activation energies were changed less with conversion. Their values were higher in the beginning of process, indicating that complex chemical reactions in the organic part can control the oxidation rate. Above 50% of conversion, there was a slight decrease in E values up to the end of oxidation stage.

3.4. Modeling Results

Simulations with the recently released FB reactor of Aspen for OF combustion of EOS to model overall heat and mass balances of the CFB furnace under air and different OF cases have been investigated and the results are discussed in this part focusing on the determination of required elutriated mass flows to maintain the heat balance of the system for OF combustion cases.

Results from the simulation cases with respect to the combustion products and characteristics are given in Table 5. By replacing air with O_2-flue gas mixture in Case 2 with the same oxidizer oxygen concentration and the same fuel input as in air combustion reduces the heat that can be extracted from the combustion of OS that is also used for source term in FB reactor. As a result of this, the heat extraction in the external particle cooler is lower by comparing Case 2 (21% O_2) with Case 1 (air). For the lowest gas velocities and the possible lowest overall pressure drop, required bypass values are presented and Case 2 requires almost 30% bypass from the primary gas stream as the recirculation rate of the particles was kept lower in order to maintain the thermal balance of the system according the modeling approach in this study that results with lower superficial gas velocity at the top of the bed comparing to other cases. Case 3 (23%O_2) with increased fuel input compared to an air combustion enables to extract same heat per definition and the same external solid recirculation stream which yields a same external heat exchanger duty with slightly higher furnace temperature. Simulation of Case 4 yields the highest heat extraction due to the highest fuel input which results in the highest boiler temperature and recirculation rate.

Table 5. Characteristic parameters of the air and OF combustion cases

Characteristic values	Case 1	Case 2	Case 3	Case 4
O_2, Volume (%)	3.55	3.52	3.72	3.7
CO_2, Volume (%)	11.8	83.4	80.9	77.1
H_2O, Volume (%)	12.7	12.83	15.1	18.89
SO_2, Volume (%)	0.012	0.161	0.176	0.19
N_2, Volume (%)	71.9	0.03	0.038	0.042
HCl, Volume (%)	0.038	0.059	0.066	0.07
Superficial gas velocity,(m s^{-1})	8.1	6.4	8.05	8.9
Oxidizer, (kmol s^{-1})/(kg s^{-1})	0.19/7.8	0.19/7.8	0.19/7.8	0.19/7.8
Heat extracted, (MW)	6.01	4.98	6.09	10.89
Fuel input/kerogen,(kg s^{-1})	0.38/1.4	0.38/1.4	0.42/1.55	0.57/2.1
Boiler temperature,(°C)	853	852	856	875
Recirculation rate,(kg m^{-2}s^{-1})	6.14	4.71	6.02	11.05
Heat exchanger,(MW)	4.53	3.37	4.54	9.07
Required bypass	10%	28%	12%	5%
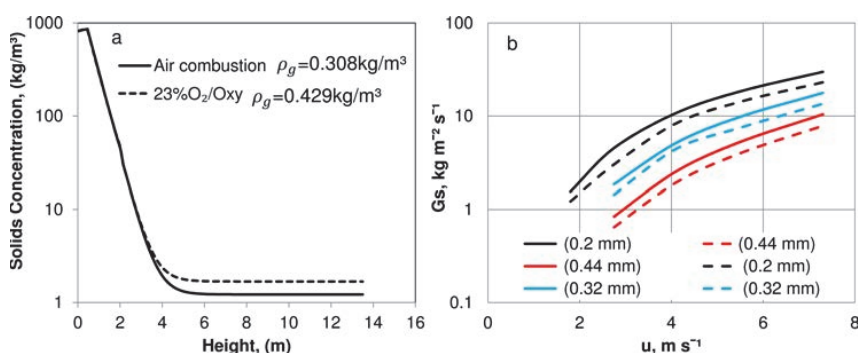
Fig. 5. (a) Solids hold up profiles for two different combustion atmospheres; (b) The net solid flux values at different velocities and particle sizes (—lines 23%O_2/Oxy, --- dashed lines air combustion)

Solids hold up profiles were obtained for two combustion atmospheres (Air case and 23%O_2/Oxy) at the same operating conditions (e.g. superficial gas velocity, bed material, PSD). Solids concentration curves folow only one exponential decay which corresponds to a splash zone (Fig. 5a). As it can be expected due to the one decay elutriation models (Eq. 1-2) in Aspen, there is no back mixing effect in the transport zone (the zone from the splash zone to the cyclone entrance). The solid concentrations in the bottom zone are very similar in both atmospheres below 1000 kg m^{-3} and splash zones have also very similar solid concentrations. However, lower solid volume concentration values were obtained in the case of air combustion for the upper dilute zone. This may be explained by the difference on the carrying capacity of the gasses between the air and OF cases. The higher gas density in OF combustion increases the particle related elutriation coefficient (Eq. 2) as well as the elutriated mass flow, resulting in a higher solid concentration in the upper part of the furnace. In this respect, the net solid flux (flow of solids) values (G_s) were obtained from the simulations in order to investigate the possible increase in G_s values in relation to superficial gas velocity (u) as it is an important design parameter, when comparing OF combustion conditions to air combustion. The simulated values were calculated (Fig. 5b) from the measured solids concentration at the boiler exit as:

$$G_s = \rho_{exit} \cdot (u - u_t) \qquad (5)$$

where ρ_{exit} is the solids concentration at the top of the boiler, u is superficial velocity and u_t is the terminal velocity.

G_s values were obtained from simulations for three different PSD applied with an average solids diameter of 0.2 mm, 0.32 mm and 0.44 mm. The increased gas velocity increases the net solids fluxes, in the case there is a reduction in average particle size. As it can be seen, there is a significant increase in G_s values ($\approx$ 24%) for each particle size in the case of OF combustion as the solids concentration values were higher at the top of the boiler compared to air combustion.

4. Conclusions

Using non-isothermal analysis methods, it was shown that characteristic temperatures and mass loss during pyrolysis stage of OS in Ar and CO_2 were very similar up to 500°C indicating that the char gasification reaction does not have significant role at 450–550°C in OS combustion. Impact of char gasification reaction can increase at temperatures above 650–700°C. Under OF combustion conditions, decomposition of calcite takes place at higher temperatures as compared to conventional combustion. Hence, emissions of CO_2 from mineral part of OS can be diminished in OF CFBC. To minimize SO_2 emissions, high temperatures and reducing conditions should be avoided. Activation energies for OS and its char are notably less for oxy-combustion conditions.

The FB model used in OF CFBC simulation can predict the solids density of the bottom bed and splash zone whereas it neglects the prediction of solids concentration in the transport zone due to the only one entrainment correlation. As the heat capacity of the flue gas is increased in oxy-fuel combustion, higher fuel mass flow rate and higher O_2 concentration in the oxidizer has to be considered for set of conditions in order to extract the same amount of heat as in air combustion. The Case 3 with 23% inlet O_2 concentration has a similar behavior as compared to air combustion in terms of temperature of the boiler and recirculation rate of the particles. The results show that the amount of heat output from a unit could be increased if converted to OF operation. To get first insight into the overall heat and mass balances of the CFB furnace under different OF cases, the obtained modeling data has a future in developing the models for the possible implementation of OF CFBC of OS.

Acknowledgements

References

[1] Jia L, Wu Y, Anthony EJ. Oxy-fuel tests and results using a pilot-scale circulating fluidized bed. in 2nd IEAGHG Oxyfuel Commbustion Conference. 2011.
[2] Liljedahl GN, Turek DG, Nsakala N, Mohn NC, Fout TE. Alstom's oxygen-fired CFB technology development status for CO2 mitigation in 31st International Technical Conference on Coal Utilization & Fuel Systems. 2006. Clearwater, Florida, USA.
[3] Czakiert T, Sztekler K, Karski S, Markiewicz D, Novak W. Oxy-fuel circulating fluidized bed combustion in a small pilot-scale test rig. Fuel Processing Technology, 2010. 91(11): p. 1617-1623.
[4] Lupion M, Alvarez I, Otero P, Kuivalainen R, Lantto J, Hotta A, Hack H. 30 MWth CIUDEN Oxy-cfb Boiler - First Experiences. Energy Procedia, 2013. 37: p. 6179-6188.
[5] Toftegaard MB, Jacob B, Jensen PA, Glarborg P, Jensen AD. Oxy-fuel combustion of solid fuels. Progress in Energy and Combustion Science, 2010. 36(5): p. 581-625.
[6] Ots A. Estonian oil shale properties and utilization in power plants. Energetika, 2007. 53(2): p. 8-18.
[7] Yörük CR, Meriste T, Trikkel A, Kuusik R. Thermo-oxidation characteristics of oil shale and oil shale char under oxy-fuel combustion conditions. Journal of Thermal Analysis and Calorimetry, 2015. (published first online) http://dx.doi.org/10.1007/s10973-015-4484-5
[8] Barkia H, Belkbir L, Jayaweera SAA. Thermal analysis studies of oil shale residual carbon Journal of Thermal Analysis and Calorimetry, 2004. 76: p. 615-622.
[9] Yan J, Jiang X, Han X, Liu J. A TG–FTIR investigation to the catalytic effect of mineral matrix in oil shale on the pyrolysis and combustion of kerogen. Fuel, 2013. 104: p. 307-317.
[10] Tiwari P, Deo M. Detailed Kinetic Analysis of Oil Shale Pyrolysis TGA Data. American Institute of Chemical Engineers AIChE, 2012. 58: p. 505-515.
[11] Kaljuvee T, Keelmann M, Trikkel A, Kuusik R. Thermooxidative decomposition of oil shales. Journal of Thermal Analysis and Calorimetry, 2010. 105(2): p. 395-403.

[12] Meriste T, Yörük CR, Trikkel A, Kaljuvee T, Kuusik R. TG–FTIR analysis of oxidation kinetics of some solid fuels under oxy-fuel conditions. Journal of Thermal Analysis and Calorimetry, 2013. 114(2): p. 483-489.
[13] Scala F. Fluidized Bed Technologies for Near-Zero Emission Combustion and Gasification. September 2013: Woodhead Publishing. ISBN: 978-0-85709-541-1
[14] Advanced Kinetics and Technology Solutions. AKTS Thermokinetics. http://www.akts.com. AKTS AG. Switzerland.
[15] Johnsson F, Leckner B. Vertical distribution of solids in a CFB-furnace. in 13th International Conference on Fluidized Bed Combustion, . 1995. Orlando
[16] Aspen Technology, Fluidization in Aspen Plus, Circulating Fluidized Bed Demo Guide. [database on the Internet] 2013.
[17] Werther J, Wein J. Expansion behavior of gas fluidized beds in the turbulent regime. A.I.Ch.E. Symp. , 1994: p. 31-44.
[18] Kunii D, Levenspiel O. Fluidization Engineering. 1991, Boston Butterworth-Heinemann.
[19] Geldart D, Cullinan J, Georghiades S, Gilvray S, Pope DJ. The effect of fines on entrainment from gas fluidized beds. Trans Inst Chem Eng, 1979: p. 269-275.
[20] Colakyan M, Levenspiel O. Elutriation from fluidized beds. Powder Technology, 1984 38(1): p. 223-32.
[21] Roduit B, Folly P, Berger B, Mathiue J, Sarbach A, Andres H, Ramin M, Vogelsanger B. Evaluating sadt by advanced kinetics-based simulation approach. Journal of Thermal Analysis and Calorimetry, 2008. 93(1): p. 153-161.
[22] Roduit B, Xia L, Folly P, Berger B, Mathiue J, Sarbach A, Andres H, Ramin M, Vogelsanger B, Spitzer D, Moulard H, Dilhan D. The simulation of the thermal behavior of energetic materials based on DSC and HFC signals. Journal of Thermal Analysis and Calorimetry, 2008. 93(1): p. 143-152.
[23] Friedman HL. Kinetics of thermal degradation of char-forming plastics from thermogravimetry. Application to a phenolic plastic. Journal of Polymer Science Part C, 1964. 6: p. 183-195.

PAPER IV

Yörük, C.R.; Trikkel, A.; Kuusik, R. Prediction of Flue Gas Composition and Comparative Overall Process Evaluation for Air and Oxy-fuel Combustion of Estonian Oil Shale using Aspen Plus Process Simulation. Energy&Fuels 2016. (available online)

Prediction of Flue Gas Composition and Comparative Overall Process Evaluation for Air and Oxyfuel Combustion of Estonian Oil Shale, Using Aspen Plus Process Simulation

Can R. Yörük,* Andres Trikkel, and Rein Kuusik

Laboratory of Inorganic Materials, Tallinn University of Technology, Ehitajate tee 5, 19086, Tallinn, Estonia

ABSTRACT: A set of conditions was simulated with ASPEN PLUS software, including air and oxyfuel (OF) combustion of carbonate-rich unconventional fuels: Estonian oil shale (EOS) and Utah White River oil shale (UOS). For OF combustion cases, two different flue gas recycle (FGR) strategies were applied by controlling the O_2 percentage in the flue gas on the basis of maintaining similar temperatures at the outlet of combustion reactor with those of air combustion. Differences between the fuels and simulated cases have been identified, focusing on the flue gas volumetric flow rates, heat capacities, flue gas compositions, and boiler efficiencies. The results show that it is possible to reach similar temperature levels in OF cases, as it was in air combustion by increasing the O_2 concentration in the recycled flue gas (RFG) mixture for both fuels. When the O_2 concentration is increased to almost 26% for wet recycle and 28% for dry recycle in the case of EOS combustion, the calculated temperatures are similar to the temperature in air combustion. The heat capacity of flue gases and heat duties in combustion reactors are higher for OF combustion cases, compared to the air combustion case, showing that the amount of heat output and boiler efficiency can be increased if conventional combustion of EOS is changed to an OF combustion process.

1. INTRODUCTION

Oil shale (OS) as an alternative energy source, and its utilization by different technologies has gained growing interest worldwide; many studies on OS from different regions have been performed in recent years.[1−5] The main attention has been given to the OS conversion to shale oil (retorting) and direct conventional air-firing of OS. Therefore, the study of OS pyrolysis, OS combustion behavior, and gasification characteristics of its char is crucial for understanding its complex conversion mechanism and the evolution of different gaseous combustion products, which is fully related to the chemical composition of OS. According to the pyrolysis and combustion mechanisms studied by thermal analysis methods and based on different OS sources,[1,6] the thermal decomposition of OS in the absence of air or O_2 is regarded as occurring in two stages. In the first stage, OS is heated to form pyrobitumen; in the second stage, pyrobitumen decomposes to form shale oil, shale gas, and shale char. Furthermore, the OS combustion has also two stages: volatile combustion, followed by fixed carbon combustion. It has also been understood that the specifics of OS combustion and retorting are strongly fuel-dependent, because the different sources of OS have different organic and mineral content and the content differs, even in the same OS deposit. Thus, intermediate stages during the OS conversion such as formation of bitumen can have a specific temperature range, depending on the OS and its origin. Kök[7] studied three OS samples taken from vicinal regions in Turkey, and it was concluded that the organic matter of different shales transforms at different temperatures due to differences in their type and maturity. In addition, the share of organic matter involved in the combustion reaction varied over a range of 7.5%−80%. Therefore, depending on the type of OS, some oxidation difficulties can occur, because the organic part of OS can be closely bound with mineral matrix, which strongly influences

the combustion characteristics of OS. In this sense, for more profitable energy production, OS, as an alternative energy source, offers opportunities to countries that have high-quality OS reserves, such as the United States, Estonia, China, Jordan, Morocco, and Brazil.[1,2]

Considering the operational experiences of the Estonian energy sector since 2004, conventional combustion of Estonian oil shale (EOS) in circulating fluidized bed (CFB) units has shown great success and solved the problems of OS pulverized firing. However, CO_2 emissions are still a serious problem and the reduction in CO_2 emission is a great challenge for the present power plants.[8] For further advantages on EOS firing in CFB, oxyfuel (OF) combustion can be introduced to contribute to the reduction of CO_2 emissions. In addition, OF combustion technology is a proven technology as the first generation of CFB boiler with OF combustion having already been demonstrated (CIUDEN, 30 MW_{th}) as a reliable and feasible technology and the full-scale commercialization is expected from several projects, such as Compostilla 300 MW_e air/oxy flexible and UK White Rose 426 MW_e by 2020.[9−11]

In OF combustion process, a mixture of partially recycled flue gas and oxygen is used during the combustion. The recycled flue gas is used to control the temperature of the boiler, as the combustion environment can cause higher flame temperatures, compared to air combustion. In order to keep operating conditions similar to those observed in air firing, the OF combustion system with flue gas recycle (FGR) must be optimized by ensuring that there is sufficient gas volume and efficient boiler temperatures for heat transfer. Many studies on coal and biomass have been carried out to understand the

differences between OF and air combustion.[9,12−14] Among the studies specifically focusing on flame and gas-phase temperatures during OF combustion, Croiset et al.[12] reported that changing of combustion environment from O_2/N_2 to O_2/CO_2 results in considerably lower temperature in the flame zone, caused by the higher specific heat capacity of CO_2, compared to N_2. Liu et al.[13] reported that replacing air combustion with 21% $O_2/79\%$ CO_2 causes a significant decrease in gas temperature and a delayed ignition of coal particles. Tan et al.[14] compared different O_2 concentrations in a combustion medium and reported that the heat flux and temperature profiles in 28% $O_2/$ recycled flue gas (RFG) are slightly lower than at air firing. As a result, researchers have established that, by increasing the oxygen concentration (to ∼30%), it is possible to obtain flame and gas-phase temperature profiles similar to air combustion.

Accordingly, in order to operate OF combustion of EOS at the temperature regimes similar to air combustion, the O_2 levels in OF combustion mode must be chosen to match the thermal design of air combustion mode; yet, there is lack of information. Previous studies with EOS cover experimental investigations using nonisothermal thermal analysis (TA) methods combined with Fourier transform infrared (FTIR) spectroscopy to investigate the pyrolysis and combustion characteristics of EOS and its char under air and OF combustion conditions with different concentrations of $O_2/$ CO_2.[15−17] According to the experimental investigations with EOS, it has been understood that high partial pressure of CO_2 has an effect on the mineral part of the fuel that can diminish mineral CO_2 emissions, depending on the combustion temperatures. So, it is important to clarify exact combustion conditions and consider the specific properties of OS in order to utilize the new combustion technologies. Furthermore, knowledge about the required O_2 concentration and the FGR ratio for OF combustion of EOS is a key parameter, because it has a significant effect on the flame temperatures and thermal capacity of the flue gases. In order to design and optimize possible OF combustion of EOS with FGR, models must be built under well-defined conditions. ASPEN PLUS is one of the comprehensive process simulation software programs that can be used for this purpose and can successfully apply steady-state process simulation for nonconventional fuels (coal, biomass, OS). It has been used for different cases[18−21] to study combustion and gasification characteristics of fuels, gas−solid hydrodynamics of boilers, and emissions of gaseous components. However, so far, there are no available studies related to OF combustion of OS and particularly for EOS, considering gas-phase temperatures and gaseous species. For this reason, the main objective of this study is to build a simulation model to reach desirable operation conditions by matching similar temperature regimes for OF combustion of EOS, compared to its air combustion. With this aim, the proposed work predicts the flue gas composition for OF combustion cases with two different FGR strategies by controlling the excess O_2 level in the flue gas and evaluates the overall process in order to underline the main differences of OF combustion of EOS, compared to its air combustion. In addition, in order to compare the obtained results of EOS combustion with the combustion of another carbonate-rich fuel, Utah White River OS (UOS) is also included and OF combustion of UOS with two different FGR strategies has been modeled. Detailed composition of flue gas at different temperature regimes and FGR strategies has been estimated by Gibbs free-energy minimization method and boiler efficiencies have been

evaluated for OF combustion of the EOS case, according to the results.

2. MODEL DESCRIPTION

2.1. Assumptions and Methodology. Air and OF combustion of EOS and UOS with FGR were simulated using the ASPEN PLUS V8.6 (APV86) software tool. Simulations are based on material balance, energy balance, and chemical equilibrium reactions. Simulated processes are steady state and isothermal. Because of the complexity of OS combustion kinetics, the process has been simulated here by the assumption that combustion products form an equilibrium mixture. Based on the weight fraction of the kerogen (organic part of OS) and oxidants (air, O_2/RFG), equilibrium compositions have been calculated by the Gibbs free-energy minimization method. Simulations have been carried out in two steps; first, the heat duty of the RGibbs reactor was determined to be zero, with no heat exchange with surroundings during the temperature calculations. Second, the outlet thermodynamic conditions of the RGibbs block have been investigated considering a typical temperature (810 °C) of CFB air combustion of EOS.

2.2. Oil Shale (OS) Characterization and Properties of Estonian Oil Shale (EOS). In a general description, OS is defined as a sedimentary rock, a type of fossil fuel that contains combustible organic matter in a mineral matrix. As a main difference between coal and OS, the organic part of OS accounts for <35% of the total mass, while coal usually consists of 75% organic matter. Thus, OS heating values are far lower than for coal, based on an equal amount of dry OS and coal.[1] EOS is defined as a highly heterogeneous fuel with complicated composition of organic and mineral matter. Besides, it is characterized by high contents of ash (45%−50%), moisture (11%−13%), and sulfur (1.4%−1.8%), with a net caloric value of 8−12 MJ/kg.[22] EOS is considered as a type of rich-grade (organic content) fuel among other shales with high conversion ratio into shale oil and gas. Although there are similar types of carbonate-rich fuels that have high mineral CO_2 content like EOS, such as Jordanian (Attarat Umm Ghudran) oil shale (JOS), and UOS), their heating values are not as high as those of EOS (see Table 1).

Table 1. Quick Comparison of Three (Carbonate-Rich) OS Fuels[a]

	EOS	JOS	UOS
high heating value, HHV[b] (MJ/kg)	11.86	5.11	6.15
total inorganic carbon, TIC (%)	4.55	5.8	4.79
CO_2[c] from TIC (%)	16.7	21.27	17.56

[a]EOS = Estonian oil shale; JOS = Jordanian oil shale; and UOS = Utah White River oil shale. [b]Per dry sample. [c]Mineral CO_2.

Comparison of the thermal behavior of some fuel samples in air combustion conditions has been presented by TG (mass change, %), DTG (mass change rate, %/min) and DTA (heat effect, μν) curves in Figure 1. Detailed information about the experimental method and fuel characterization can be seen from refs 15 and 16.

As a main difference, OS samples have two distinctive mass loss steps and these steps are related, first, to the oxidation of the organic part and second, to the decomposition of the mineral part. Mass loss of coal samples proceeds with one smooth step having a wide exotherm from 300 °C to 665 °C
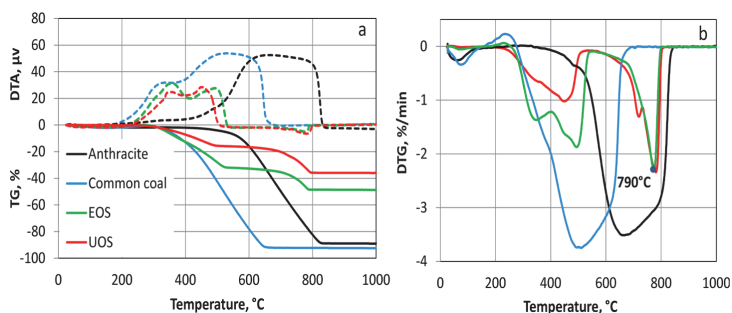
Figure 1. Air combustion of some selected fuels: (a) TG (straight lines)—DTA (dashed lines) and (b) DTG curves.

for common coal and from 450 °C to 830 °C for anthracite. In the case of OS samples, exothermic decomposition (organic part) occurs with two peaks at lower temperatures, which corresponds most likely to a devolatilization stage and a char oxidation stage, respectively. However, the chemistry is definitely more complex, because of numerous simultaneously occurring reactions.

The fuel used in air and OF combustion simulations is represented as a mixture of kerogen (a nonconventional fuel), the most important minerals (as solid ash), and moisture (as free water). The defined EOS contains 27% organics, 62% mineral part, and 11% moisture.[22,23] The simplified content of mineral part includes $CaCO_3$, $MgCO_3$, SiO_2 and FeS_2 for both fuels (Table 2). The average composition has been calculated

Table 2. EOS and UOS Composition Considered in the Modeling[a]

	EOS	UOS
kerogen		
C	77.45%	81.75%
O	10.01%	3.71%
H	9.7%	11.17%
S	1.76%	1.47%
Cl	0.75%	0%
N	0.33%	1.9%
mineral part		
$CaCO_3$	57.2%	37.3%
SiO_2	30.2%	45%
$MgCO_3$	7.8%	13%
FeS_2	4.8%	4.7%

[a]EOS = Estonian oil shale and UOS = Utah White River oil shale.

according to the data obtained from Estonian Energy S.C. for UOS and from refs 22 and 23 for EOS. The defined UOS contains 17% kerogen, 80% mineral part, and 3% moisture.

2.3. Combustion. Air combustion of EOS and UOS with 20% excess air and OF combustion with 3% excess O_2 in flue gases were simulated. The Ryield (Figure 2) reactor was used for the calculation of actual yield distribution from the entered ultimate analyses of the fuel (Table 2) to simulate decomposition of the feed. The RGibbs (Figure 2) reactor was used to predict the equilibrium composition of combustion products, according to the general reactions given in Table 3 (presented later in this work). RGibbs reactor calculates chemical equilibrium and phase equilibrium by minimizing the Gibbs free energy of the system.[24] The total Gibbs free energy of the system is defined as follows:[25]

$$G^t = \sum_{i=1}^{N} n_i \mu_i \tag{1}$$

$$\mu_i = G_i^0 + RT \ln\left(\frac{f_i}{f_i^0}\right) \tag{2}$$

where G^t is the total Gibbs free energy, n_i the number of moles of species i, and μ_i the chemical potential of species i. In eq 2, R and T are the universal gas constant and temperature, respectively, and G_i^0 is the standard Gibbs free energy, f_i and f_i^0 are fugacity and standard fugacity of species i, respectively.

$$\mu_i = G_i^0 + RT \ln\left(\frac{\theta P_i}{P^0}\right) \tag{3}$$

The chemical potential (μ_i) can also be written as a function of pressure P, as shown in eq 3, where θ is a fugacity coefficient.
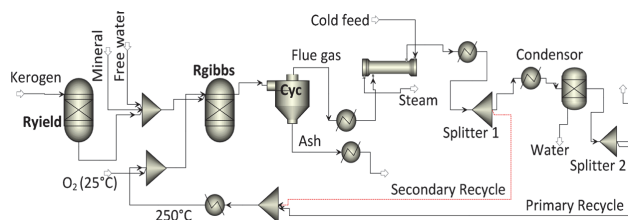
Figure 2. Process flow diagram for OF combustion with FGR system.

$$\mu_i = G_{fi}^0 + RT \ln(y_i) \tag{4}$$

If all gases are assumed as ideal gases at a pressure of 1 atm, the equation can be rewritten as described in eq 4, where y_i is the mole fraction of gas species i, which is defined as the ratio of n_i and the total number of moles in the reaction mixture. G_{fi}^0 is the standard Gibbs free energy of formation of species i, and it is set equal to zero for all chemical elements.

Substituting eq 4 into eq 1 gives

$$G^t = \sum_{i=1}^{N} n_i \Delta G_{fi}^0 + \sum_{i=1}^{N} n_i RT \ln\left(\frac{n_i}{n_{tot}}\right) \tag{5}$$

for the minimization of the Gibbs free-energy problem, the equation above can be applied with a Lagrange multiplier function. This method applies the elemental balance for each atom.

$$\sum_{i=1}^{N} a_{ij} n_i = A_j \quad j = 1, 2, 3, ..., k \tag{6}$$

where a_{ij} is the number of atoms of element j in a mole of species i. A_j is defined as the total number of atoms of element j in the reaction mixture. To form the Lagrangian function (L), the Lagrange multipliers (defined as $\lambda_j = \lambda_1, ..., \lambda_k$, are used by multiplying with elemental balance constraints, and those terms are subtracted from G^t as follows:

$$L = G^t - \sum_{j=1}^{k} \lambda_j \left(\sum_{i=1}^{N} a_{ij} n_i - A_j\right) \tag{7}$$

$$\frac{\partial(L)}{\partial n_i} = 0 \tag{8}$$

The partial derivatives of the Lagrange function (eq 7), with respect to each component, are set to zero, as shown in eq 8.

The general reaction model for organic and mineral parts of EOS and UOS, according to the defined components during the simulations, is presented in Table 3. Decomposition of

Table 3. General Reaction Model in the RGibbs Reactor Based on the Defined Components

organic part	mineral part
$C + O_2 \rightarrow CO_2$	$FeS_2 + 3O_2 \rightarrow FeSO_4 + SO_2$
$C + CO_2 \rightarrow 2CO$	$2FeS_2 + 5.5O_2 \rightarrow Fe_2O_3 + 4SO_2$
$C + H_2O \rightarrow H_2 + CO$	$MgCO_3 \rightarrow MgO + CO_2$
$H_2 + {}^1/_2 O_2 \rightarrow H_2O$	$CaCO_3 \rightarrow CaO + CO_2$
$CO + H_2O \rightarrow CO_2 + H_2$	$MgO + SO_2 + {}^1/_2 O_2 \rightarrow MgSO_4$
$S + xO_2 \rightarrow SO_x$	$CaO + SO_2 + {}^1/_2 O_2 \rightarrow CaSO_4$
$N_2 + xO_2 \rightarrow 2NO_x$	$CaCO_3 + SO_2 + {}^1/_2 O_2 \rightarrow CaSO_4 + CO_2$
$Cl_2 + H_2 \rightarrow 2HCl$	

$CaCO_3$ and $MgCO_3$, pyrite oxidation and sulfation of CaO and MgO have been specifically given, as they are the main characteristic reactions notably dependent on combustion atmosphere, reaction temperature and CO_2 partial pressure. Thus, the effect of combustion atmosphere and temperature on flue gas composition related to solid phase transformations has also been investigated considering the specific gas species that can affect the overall gas emissions.

2.4. FGR System for OF Combustion. Finding an optimum recirculation method and FGR ratio can be an important issue when it is considered for better combustion

efficiency. There can be variations on the FGR systems, depending on the fuel type and characteristics. Generally, in the OF combustion of coal, the recycled flue gas is split into primary stream (~30%−35% of the total RFG after condensation) and secondary stream (~65%−70% of the total RFG).[9] Using this approach, partially wet FGR can be carried out and that also would be suitable in the case of OF combustion of EOS, since the fuel has high moisture content and low heating value. Thus, two different FGR options have been considered in this study: dry FGR and partially wet FGR, as explained above. In the case of partially wet recycle, primary stream recycles ~30% of the total recycled flue gas (secondary ~70%) and it is found to be an optimum ratio. Since OF cases have been considered to target similar temperatures, compared to air combustion, the recycled flue gas temperature has a strong effect on the boiler heat duty and the furnace temperature; thus, it was kept constant at 250 °C, in order to analyze the effect of flue gas composition and FGR strategy. Figure 2 illustrates the OF combustion with both FGR systems.

In Figure 2, the secondary recycle stream is shown as a dashed red line, which is used for the wet flue gas recycle. In the case of dry FGR, only the primary recycle stream has been used. After splitting ash and flue gas with 100% separation efficiency, the streams are fixed to constant temperature at 250 °C as an optimum FGR temperature for both cases.

2.5. Heat Exchanger Design. Considering OF combustion technology in a retrofitted case or with flexi burn technology (air/oxy), the relative heat duty in different sections of a steam generator must be kept constant. By ensuring this, it would be possible to stay within temperature design limits to provide similar steam flux with similar properties to the steam cycle without considering any additional retrofit. However, because of the high CO_2 and H_2O fraction in flue gas in the case of OF combustion, the heat capacity of the flue gas can be higher, compared to flue gas in air combustion, which would cause redesign of heat exchangers and boiler temperatures for required heat-transfer areas.

As the driving force of the heat-transfer process in a heat exchanger is the temperature difference between the hot and cold sides, and by assuming that the specific heat of the media is constant, a logarithmic mean temperature difference (LMTD) method was used. LMTD is calculated as follows:

$$LMTD = \frac{(T_{H_{out}} - T_{C_{in}}) - (T_{H_{in}} - T_{C_{out}})}{\ln\left(\frac{T_{H_{out}} - T_{C_{in}}}{T_{H_{in}} - T_{C_{out}}}\right)} \tag{9}$$

With this method, the heat and mass balance of the heat exchanger, which is located at the exit of the combustion reactor (Figure 2), has been investigated. Both OF and air combustion cases have been simulated on the basis of producing 100 kg/s superheated steam (see Table 4); the required heat exchanger area has been calculated from eq 10, which gives the amount of heat transferred.

Table 4. Input Steam Properties for Inlet and Calculated Properties for Outlet Stream

	inlet	outlet
flow rate (kg/s)	100	100
temperature, T (°C)	250	538
pressure, P (bar)	130	130

Table 5. Summary of Simulation Results

| | Air | Oxyfuel, OF | | | |
	EOS/UOS	EOS		UOS	
fuel flow rate (kg/s)	100	100	100	100	100
FGR option		wet	dry	wet	dry
temperature (°C)	1556/1384	1558	1560	1387	1383
FGR ratio (%)		67.3	64.1	66.5	65.6
O_2 concentration (vol %)	21%/N_2	26.7	28.2	28.8	30.6
flue gas flow rate (kmol/s)	14.9/10.8	11.6	10.7	7.5	7.3
flue gas composition at 810 °C (vol %)					
CO_2	14.4/14.61	65.6	77.8	67.6	80.1
H_2O	12.8/10.2	30.1	17.5	28.1	14.9
O_2	3.4/3.1	3.09	3.01	3.03	3.08
N_2	69.3/71.9	1.01	1.1	0.94	1.15
$NO_{(ppmv)}$	2604/2875	355	381	345	393
$NO_{2\,(ppmv)}$	26.9/34.5	4.1	4.3	3.95	4.2
$SO_{3\,(ppmv)}$	0.01/0.01	0.02	0.024	0.021	0.016
$SO_{2\,(ppmv)}$	0.12/0.1	0.16	0.195	0.156	0.19
$CO_{(ppmv)}$	0.07/0.068	0.3	0.37	0.31	0.4
ash flow rate (kg/s)	47.9/65.5	61.7	61.7	76.9	76.9
ash composition (mass %)					
$CaCO_3$	0/0	50.5	50.5	33.8	33.8
CaO	36.8/22.1	0	0	0	0
$CaSO_4$	11/8.1	8.5	8.5	6.9	6.9
$FeSO_4$	7.8/7.2	6.1	6.1	5.8	5.8
recycled flue gas (RFG) composition (vol %)					
CO_2		74.6	94.57	76.1	95.1
H_2O		20.33	0	18.8	0
O_2		3.51	3.65	3.58	3.54
N_2		1.15	1.45	0.89	0.95
$SO_{2\,(ppmv)}$		0.12	0.23	0.23	0.21

$$Q = U \times A \times LMTD \tag{10}$$

Here, Q is the amount of heat transferred (given in watts), U the heat-transfer coefficient (assumed to be 100 W m^{-2} K^{-1}), and A the heat exchanger area (expressed in units of m^2).

3. RESULTS AND DISCUSSION

The process simulation for air and OF combustion of EOS and UOS with FGR was developed using the ASPEN PLUS simulator. Table 5 summarizes the most important system simulation results (O_2 concentration in oxidant, FGR ratio, flue gas composition and temperatures, RFG composition, etc.)

It can be seen that it is possible to reach similar temperature levels in both OF cases as that in the air combustion case by increasing the O_2 concentration in the oxidant. The calculated temperature for UOS air combustion is lower than the EOS air combustion, because of the lower combustible matter. For EOS, an ∼26% O_2/RFG mixture should be considered for the wet recycle case and ∼28% O_2/RFG for the dry FGR case. For UOS, a slightly higher O_2 concentration is required: ∼28% O_2/FGR for the wet FGR case and 30% O_2/RFG for the dry FGR case. Compared to the air combustion of EOS, a notable difference in the flow rate of flue gases has been identified in both FGR cases, being reduced by ∼23% and 29%, respectively, the same values for UOS being 31% for the wet FGR case and 33% for the dry FGR case. Two different FGR options have a small effect on the FGR ratio for both fuels, which gives slightly higher flue gas flux for wet FGR cases. After condensation and FGR setup, ∼87% less flue gas must be treated for EOS and 80% for UOS in wet and dry cases for flue gas cleaning and

CO_2 capture stages, as compared to air combustion case. For EOS, the volume fraction of CO_2 in the untreated flue gas increases up to 65.6 in the wet FGR case and 77.8% in the dry FGR case, giving the possibility to reach concentrations of ∼75% and 95% CO_2 in RFG, respectively. The CO_2 volume fractions are slightly higher for UOS as the carbon content of fuel is higher than that of EOS. NO_x emissions decrease considerably as can be seen from the flue gas composition of OF combustion cases, because N_2 enters the boiler only with the fuel. Although the CO fraction in the flue gas is increased due to the higher partial pressure of CO_2 in OF cases, compared to the air combustion case (the reaction between C and CO_2 is favored in OF combustion cases), CO emissions are rather low, because of the equilibrium-based calculation. Thus, when CO and CO_2 emissions from char combustion are estimated by using Gibbs free-energy minimization, one must remember that the results are also dependent on the kinetics, which could give slightly higher CO and lower CO_2 emissions, since the fixed carbon content of fuel is not high (∼7% for EOS).

3.1. Comparison of Modeling with Experimental Results.
Considering the experimental investigations on EOS and UOS (Figure 1) with TA methods,[15,16] there is an acceptable agreement between simulation results and previous investigations in the case of air combustion. The air combustion case has a very extensive decomposition of carbonates ($CaCO_3$, $MgCO_3$). Since the boiler temperature (810 °C) considered in the simulations was higher than the peak temperatures (Figure 1, 790 °C) of reaction rates determined by thermogravimetric (TG) tests, it was also expected that, in the simulations, a high

level of carbonate decomposition to CaO and MgO[15,16] would be observed for EOS and UOS. However, the extent of carbonate decomposition usually remains between 0.7−0.8 during the air combustion of EOS with CFB combustion technology, which considers boiler operation temperatures at 800−820 °C.[8] Since the amount of CO_2 released from carbonate minerals is dependent on furnace temperature, fuel particle size, partial pressure of CO_2, and residence time of the fuel particles, carbonate minerals should decompose to a smaller extent in the case of real CFB combustion. This high level of decomposition for the air combustion simulation arises due to the assumed general reaction model in the RGibbs reactor and also the simplified definition of mineral part of the fuel, which does not reflect the exact physical properties of the fuel. Thus, one must remember that the results are also strongly dependent on the kinetics and residence time of fuel particles in the CFB boiler.

As higher CO_2 partial pressure should result in a decreased calcination rate and higher thermal decomposition temperatures, OF combustion simulations show that if similar boiler temperatures are considered, there is a big difference in $CaCO_3$ decomposition. In both OF combustion cases for EOS, ~88% of the $CaCO_3$ is undecomposed in the ash and by increasing the boiler temperatures with sensitivity analysis, decomposition temperatures are shifted to above 834 °C for the wet FGR case and 855 °C for the dry FGR case. However, decomposition temperatures were expected to be above 900 °C.[15,16] In accordance with the TG air combustion tests, although there is an agreement on the amount of decomposed carbonates and ash values for both fuels (Figure 2), there is a big difference in the ash flow rates and the ash composition between air and OF cases including different concentrations of $CaCO_3$, CaO, $CaSO_4$, and $FeSO_4$, because of the increased amount of undecomposed $CaCO_3$ in OF combustion simulations. The FGR type has no effect on ash flow rates, and its composition for OF combustion simulations in the wet and dry FGR cases have identical ash properties.

$$CaCO_3 \rightarrow CaO + CO_2 \qquad (11)$$

$$CaO + SO_2 + \frac{1}{2}O_2 \rightarrow CaSO_4 \qquad (12)$$

$$CaCO_3 + SO_2 + \frac{1}{2}O_2 \rightarrow CaSO_4 + CO_2 \qquad (13)$$
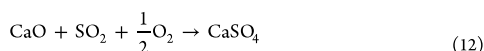
Decomposition of $CaCO_3$ (eq 11) and sulfation with the formed CaO (eq 12) or direct sulfation (eq 13) are the main reactions for SO_2 capture, since sulfation with MgO does not occur in the simulations. Although there is no big difference in $CaSO_4$ formation in both cases, OF cases have slightly increased SO_2 concentrations in the flue gas. The main impact for this can be the lowered flue gas flux and the FGR method— wet FGR is accompanied by lower SO_2 concentration in the recycled flue gas enabling to conclude that higher H_2O content enhances SO_2 binding into a solid phase.

3.2. Evaluation of Boiler Efficiency. In the case of EOS OF combustion, when the relative heat duty is kept constant for the heat exchanger in order to maintain the similar steam flux with similar properties as in air combustion case, it can be expected that the flue gas temperature leaving the heat exchanger in both cases can be lower than that in air combustion, because of the slightly reduced mass flow rate of flue gas. However, since flue gas in the OF combustion case has

a higher heat capacity than that in air combustion, the calculated temperatures are in alteration depending on the gas physical properties, higher for wet FGR case and lower for dry FGR case, as compared to air combustion (Figure 3).
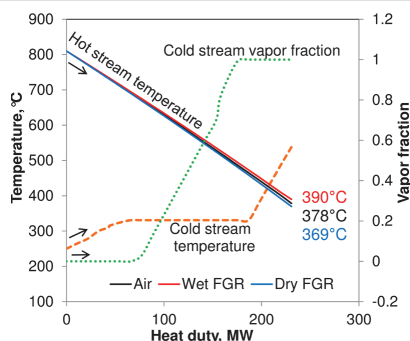
Figure 3. Temperature and heat duty profiles for air and OF combustion of EOS.

Therefore, the calculated heat-transfer areas, which are required for OF cases, are in accordance with the outlet flue gas temperatures as the heat capacity of the flue gas has a notable influence on the required heat-transfer area (Table 6).

Table 6. Summary of Operating Parameters and Physical Properties of Flue Gas

	air	wet FGR	dry FGR
exported heat (MW)	816	891	890
boiler efficiency (%)	81.6	89.1	89
flue gas heat capacity[a] (kJ kg^{-1} K^{-1})	1.28	1.41	1.33
flue gas density, (kg m^{-3})	0.32	0.39	0.43
flue gas mass flow rate, (kg s^{-1})	436	408.9	415.2
heat exchanger area (m^2)	9956	9620	10267
logarithmic mean temperature difference, LMTD (K)	379	389	369

[a]Computed ideal gas heat capacity for flue gas mixture (reference conditions: T = 810 °C, P = 1 atm).

Compared to air combustion, the heat duty in a combustion reactor is higher for OF combustion cases, showing that the amount of heat output and boiler efficiency can be increased when the system is converted to OF combustion. Compared to the air combustion case, heat duties in combustion reactor are higher for OF cases, which allow one to increase the boiler efficiency. OF cases have quite similar boiler efficiency due to the chosen FGR strategy and the assumed constant recycle temperature for both cases.

The same heat has been provided by the fuel for each simulation case, and the calculation of boiler efficiency can be expressed as

$$\text{boiler efficiency (\%)} = \frac{\text{heat released from boiler (MW)}}{\text{heat provided by fuel (MW)}} \times 100 \qquad (14)$$

3.3. Influence of Different Operating Temperatures on Flue Gas Species. In the case of OF combustion of EOS, the RGibbs reactor has been operated at different temperatures
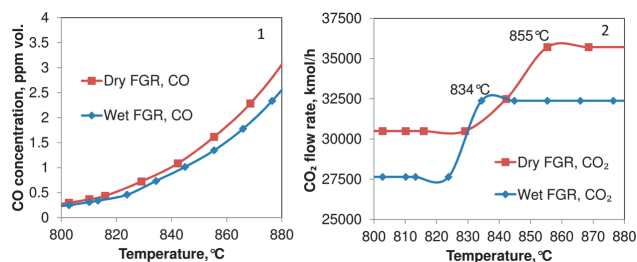
Figure 4. Influence of temperature on (1) CO and (2) CO_2 emissions from OF combustion of EOS.
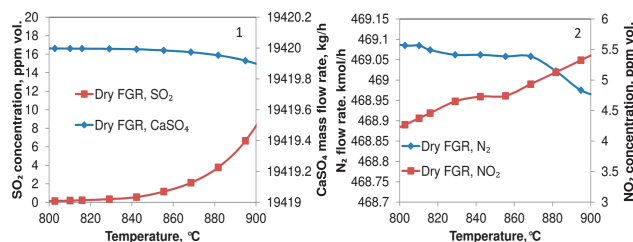
Figure 5. Influence of temperature on (1) $SO_2/CaSO_4$ and (2) NO_2/N_2 for OF combustion of EOS in the dry FGR case.

by sensitivity analysis and the influence of different operating temperatures on flue gas species have been presented in Figures 4 and 5. Generally, OF combustion simulations have almost the same volume fractions of gas emissions, since the main volume change occurs in correlation with water and the CO_2 content in the flue gas is related to the FGR method. However, because of the higher CO_2 partial pressure in the dry FGR case, CO emission is slightly higher than that observed for the wet FGR case. Since the reaction between C and CO_2 can be favored at high temperatures, CO levels increase as the temperature increases. The higher decomposition temperature at 855 °C for $CaCO_3$ in dry FGR case can be given as an additional visible effect of higher partial pressure of CO_2, compared to the wet FGR case. Temperatures below 834 °C for wet FGR cases and 855 °C for dry FGR cases should be considered, to avoid increased emission of mineral CO_2 via the decomposition of $CaCO_3$.

SO$_2$ emission levels are slightly higher for OF cases, and they increase when the boiler temperature is increased. In accordance with the relation of SO_2 and $CaSO_4$ given for dry FGR case in panel (1) of Figure 5, the possible release of SO_2 from $CaSO_4$ becomes more favorable above 860 °C. With regard to N$_2$-related emissions, although NO_x emission levels are quite low in both OF cases, high temperatures should still be avoided, to limit the conversion of N_2 to NO_x.

4. CONCLUSIONS

Three cases for combustion of Estonian oil shale (EOS) and Utah White River oil shale (UOS) (air combustion and two oxyfuel (OF) combustion cases with flue gas recycle (FGR)) were simulated using ASPEN PLUS process modeling software. Characteristic results, including volumetric flow rates of flue gases, flue gas composition, boiler efficiencies, emissions of selected gaseous components (CO_2, CO, SO_x, NO_x), and changes in mineral part of EOS were presented. Compared to the air combustion of EOS, the volume of flue gases is reduced

at the exit of the combustion reactor in both OF cases. After condensation and FGR processes, ~87% less flue gas needs to be treated in wet and dry FGR cases of EOS for flue gas cleaning and CO_2 capture, compared to the air combustion case, and ~80% for UOS. The effect of partial pressure of CO_2 on the decomposition of carbonates has been clearly presented, showing that the decomposition of calcite occurs at higher temperatures and higher CO_2 partial pressure decreases the calcination rate, compared to conventional combustion. Nevertheless, for further studies considering the mineral part of the EOS, the simulated model can be extended for specific solid processes by means of chemical kinetics. CO_2 emissions from carbonates of EOS and UOS can be diminished, to some extent, in the case of OF combustion with controlled temperature regimes. To minimize NO_x and, especially, SO_x emissions from OF combustion of EOS, high temperatures (above 840 °C) should be avoided. FGR options have no effect on the ash flow rates and its composition due to the simplified set of conditions for OF cases; however, for the air combustion case, there is notably lower ash flow rate with higher CaO content, because of the almost full decomposition of carbonates. Therefore, this can change the heat and mass balance of the system during the system transition from air to OF combustion of EOS. In order to maintain the heat flux similar to that observed in air combustion, slightly higher boiler temperatures should be considered in the OF cases. Accordingly, external heat exchangers will be more important in the case of OF combustion of EOS, which could be used to compensate the additional required heat-transfer area for operational adaptability, especially for the dry FGR case. Based on the FGR system and flue gas loadings, calculation of heat exchanger areas requires detailed investigations for optimization as various recycle options can alter the results. It is possible to reach temperature levels, in both OF cases, that are similar to those in the air combustion case by increasing the O_2 concentration in the oxidant with the applied modeling

approach. Compared to air combustion, the heat duty in the combustion reactor and the heat capacity of flue gases are higher for OF combustion cases, showing that the amount of heat output and boiler efficiency can be increased when air combustion is replaced with OF combustion.

■ AUTHOR INFORMATION

Corresponding Author
*Tel.: +372 6202872. Fax: +372 620280. E-mail: can.yoruk@ttu.ee.

Notes
The authors declare no competing financial interest.

■ ACKNOWLEDGMENTS

■ REFERENCES

(1) Qian, J.; Yin, L. Oil Shale: Petroleum Alternative; China Petrochemical Press: Beijing, China, 2010; pp 1−60.

(2) Altun, N. E.; Hiçyilmaz, C.; Hwang, J.-Y.; Bağcı, A. S.; Kök, M. V. Oil Shales in the World and Turkey; Reserves, Current Situation and Future Prospects: A Review. Oil Shale 2006, 23 (3), 211−227.

(3) Fei, Y.; et al. Evaluation of Several Methods of Extraction of Oil from a Jordanian Oil Shale. Fuel 2012, 92, 281−287.

(4) Xie, F.-F.; Wang, Z.; Lin, W.-G.; Song, W.-L. Study on Thermal Conversion of Huadian Oil Shale under N_2 and CO_2 Atmospheres. Oil Shale 2010, 27 (4), 309−320.

(5) Barkia, H.; Belkbir, L.; Jayaweera, S. A. A. Non-Isothermal Kinetics of Gasification by CO_2 of Residual Carbon from Timahdit and Tarfaya Oil Shale Kerogens. J. Therm. Anal. Calorim. 2004, 76 (2), 623−632.

(6) Kök, M. V.; Pamir, R. Pyrolysis Kinetics of Oil Shales Determined by DSC and TG/DTG. Oil Shale 2003, 20 (1), 57−68.

(7) Kök, M. V. Evaluation of Turkish Oil Shales—Thermal Analysis Approach. Oil Shale 2001, 18 (2), 131−138.

(8) Plamus, K.; Soosaar, S.; Ots, A.; Neshumayev, D. Firing Estonian Oil Shale of Higher Quality in CFB Boilers—Environmental and Economic Impact. Oil Shale 2011, 28, 113−126.

(9) Stanger, R.; Wall, T.; Spörl, R.; Paneru, M.; Grathwohl, S.; Weidmann, M.; Scheffknecht, G.; McDonald, D.; Myöhänen, K.; Ritvanen, J.; Rahiala, S.; Hyppänen, T.; Mletzko, J.; Kather, A.; Santos, S. Oxyfuel Combustion for CO_2 Capture in Power Plants. Int. J. Greenhouse Gas Control 2015, 40, 55−125.

(10) Lupion, M.; Diego, R.; Loubeau, L.; Navarrete, B. CIUDEN CCS Project: Status of the CO_2 Capture Technology Development Plant in Power Generation. Energy Procedia 2011, 4, 5639−5646.

(11) White Rose Carbon Capture & Storage Project. Capture Power; http://www.whiteroseccs.co.uk/your-questions-answered/construction; accessed Oct. 14, 2015.

(12) Croiset, E.; Thambimuthu, K. V.; Palmer, A. Coal combustion in O_2/CO_2 mixtures compared with air. Can. J. Chem. Eng. 2000, 78, 402−407.

(13) Liu, H.; Zailani, R.; Gibbs, B. M. Comparisons of Pulverized Coal Combustion in Air and in Mixtures of O/CO. Fuel 2005, 84 (7−8), 833−840.

(14) Tan, Y.; Croiset, E.; Douglas, M. A.; Thambimuthu, K. V. Combustion Characteristics of Coal in a Mixture of Oxygen and Recycled Flue Gas. Fuel 2006, 85 (4), 507−512.

(15) Yörük, C. R.; Meriste, T.; Trikkel, A.; Kuusik, R. Thermo-oxidation Characteristics of Oil Shale and Oil Shale Char Under Oxy-fuel Combustion Conditions. J. Therm. Anal. Calorim. 2015, 121 (1), 509−516.

(16) Meriste, T.; Yörük, C. R.; Trikkel, A.; Kaljuvee, T.; Kuusik, R. TG−FTIR Analysis of Oxidation Kinetics of Some Solid Fuels Under Oxy-fuel Conditions. J. Therm. Anal. Calorim. 2013, 114 (2), 483−489.

(17) Loo, L.; Maaten, B.; Siirde, A.; Pihu, T.; Konist, A. Experimental Analysis of the Combustion Characteristics of Estonian Oil Shale in Air and Oxy-fuel Atmospheres. Fuel Process. Technol. 2015, 134, 317−324.

(18) Sotudeh-Gharebaagh, R.; Legros, R.; Chaouki, J.; Paris, J. Simulation of Circulating Fluidized Bed Reactors Using Aspen Plus. Fuel 1998, 77 (4), 327−337.

(19) Onarheim, K.; Solantausta, Y.; Lehto, J. Process Simulation Development of Fast Pyrolysis of Wood Using Aspen Plus. Energy Fuels 2015, 29 (1), 205−217.

(20) Hu, Y.; Yan, J. Characterization of Flue Gas in Oxy-coal Combustion Processes for CO_2 Capture. Appl. Energy 2012, 90 (1), 113−121.

(21) Pei, X.; He, B.; Yan, L.; Wang, C.; Song, W.; Song, J. Process Simulation of Oxy-fuel Combustion for a 300MW Pulverized Coal-fired Power Plant Using Aspen Plus. Energy Convers. Manage. 2013, 76, 581−587.

(22) Ots, A. Estonian Oil Shale Properties and Utilization in Power Plants. Energetika 2007, 53 (2), 8−18.

(23) Arro, H.; Prikk, A.; Pihu, T. Calculation of Qualitative and Quantitative Composition of Estonian Oil Shale and Its Combustion Products. Part 1. Calculation on the Basis of Heating Value. Fuel 2003, 82 (18), 2179−2195.

(24) Aspen Plus User Guide. Getting Started Modeling Processes with Solids; 2010.

(25) Jarungthammachote, S.; Dutta, A. Equilibrium Modeling of Gasification: Gibbs Free Energy Minimization Approach and Its Application to Spouted Bed and Spout-Fluid Bed Gasifiers. Energy Convers. Manage. 2008, 49, 1345−1356.

APENDIX B. CURRICULUM VITAE

ELULOOKIRJELDUS

1. Isikuandmed

   Ees- ja perekonnanimi: Can Rüstü Yörük
   Sünniaeg ja -koht: 19.12.1985, Burdur, Türgi
   Kodakondsus: Türgi
   E-posti aadress: can.yoruk@ttu.ee

2. Hariduskäik

Õppeasutus (nimetus lõpetamise ajal)	Lõpetamise aeg	Haridus (eriala/kraad)
Tallinna Tehnikaülikool	2012	Tehnikateaduste magister
Karadenizi Tehnikaülikool	2009	Tehnikateaduste bakalaureus

3. Keelteoskus

Keel	Tase
Türgi keel	Emakeel
Inglise keel	Kõrgtase
Eesti keel	Algtase

4. Teenistuskäik

Töötamise aeg	Tööandja nimetus	Ametikoht
2016-	Tallinna Tehnikaülikool	insener

5. Kaitstud lõputööd

Tehnikateaduste magistrikraad: Põlevkivi hapnikus-põletamise alused, Tallinna Tehnikaülikool, 2012, juhendajad: Andres Trikkel ja Rein Kuusik

6. Teadustöö põhisuunad

Tehnikateadused: Keemiatehnoloogia ja –masinaehitus T350, Energeetika T140.

7. Uurimisprojektid

Lep12115 Põlevkivi termooksüdatsioon - hapnikus-põletamise alusnähtused, 1 ja 2 (1.08.2012−30.06.2016)

IUT33-19 Multikomponentsete mineraal-orgaaniliste süsteemide käitlemise alused: keemia, modelleerimine ja kestlik kasutus (1.01.2015−31.12.2020)

CURRICULUM VITAE

1. Personal data

   Name: Can Rüstü Yörük
   Date and place of birth: 19.12.1985, Burdur, Turkey
   Citizenship: Turkish
   E-mail: can.yoruk@ttu.ee

2. Education

Educational institution	Graduation year	Education (field of study/degree)
Tallinn University of Technology	2012	M.Sc. in Engineering
Karadeniz Technical University	2009	B.Sc. in Engineering (Mechanical)

3. Language competence/skills

Language	Level
Turkish	Native
English	Fluent
Estonian	Elementary

4. Professional employment

Period	Organization	Position
2016-	Tallinn University of Technology	engineer

5. Defended theses

M.Sc. thesis: Oxy-fuel combustion of oil shale. Tallinn University of Technology, 2012. Supervisors: Andres Trikkel and Rein Kuusik

6. Main areas of scientific work

Technological sciences: Chemical technology and engineering T350, Energy research T140.

7. Research projects

Lep12115   Thermo-oxidation of oil shale: fundamentals of oxy-combustion (1.08.2012−30.06.2016)

IUT33-19   Fundamentals of multicomponent mineral-organic systems: Chemistry, modeling and sustainable processing (1.01.2015−31.12.2020)

DISSERTATIONS DEFENDED AT
TALLINN UNIVERSITY OF TECHNOLOGY ON
CHEMISTRY AND CHEMICAL ENGINEERING

1. **Endel Piiroja**. Oxidation and Destruction of Polyethylene. 1993.

2. **Meili Rei**. Lihatehnoloogia teaduslikud alused. Fundamentals of Food Technology. 1995.

3. **Meeme Põldme**. Phase Transformations in Hydrothermal Sintering Processing of Phosphate Rock. 1995.

4. **Kaia Tõnsuaadu**. Thermophosphates from Kovdor and Siilinjärvi Apatites. 1995.

5. **Anu Hamburg**. The Influence of Food Processing and Storage on the N-Nitrosamines Formation and Content in Some Estonian Foodstuffs. 1995.

6. **Ruth Kuldvee**. Computerized Sampling in Ion Chromatography and in Capillary Electrophoresis. 1999.

7. **Külliki Varvas**. Enzymatic Oxidation of Arachidonic Acid in the Coral *Gersemia fruticosa*. 1999.

8. **Marina Kudrjašova**. Application of Factor Analysis to Thermochromatography and Promotion Studies. 2000.

9. **Viia Lepane**. Characterization of Aquatic Humic Substances by Size Exclusion Chromatography and Capillary Electrophoresis. 2001.

10. **Andres Trikkel**. Estonian Calcareous Rocks and Oil Shale Ash as Sorbents for SO_2. 2001.

11. **Marina Kritševskaja**. Photocatalytic Oxidation of Organic Pollutants in Aqueous and Gaseous Phases. 2003.

12. **Inna Kamenev**. Aerobic Bio-Oxidation with Ozonation in Recalcitrant Wastewater Treatment. 2003.

13. **Janek Reinik**. Methods for Purification of Xylidine-Polluted Water. 2003.

14. **Andres Krumme**. Crystallisation Behaviour of High Density Polyethylene Blends with Bimodal Molar Mass Distribution. 2003.

15. **Anna Goi**. Advanced Oxidation Processes for Water Purification and Soil Remediation. 2005.

16. **Pille Meier**. Influence of Aqueous Solutions of Organic Substances on Structure and Properties of Pinewood (*Pinus sylvestris*). 2007.

17. **Kristjan Kruusement**. Water Conversion of Oil Shales and Biomass. 2007.

18. **Niina Kulik**. The Application of Fenton-Based Processes for Wastewater and Soil Treatment. 2008.

19. **Raul Järviste**. The Study of the Changes of Diesel Fuel Properties a its Long Term Storage. 2008.

20. **Mai Uibu**. Abatement of CO_2 Emissions in Estonian Oil Shale-Based Power Production. 2008.

21. **Valeri Gorkunov**. Calcium-Aluminothermal Production of Niobium and Utilization of Wastes. 2008.

22. **Elina Portjanskaja**. Photocatalytic Oxidation of Natural Polymers in Aqueous Solutions. 2009.

23. **Karin Reinhold**. Workplace Assessment: Determination of Hazards Profile using a Flexible Risk Assessment Method. 2009.

24. **Natalja Savest**. Solvent Swelling of Estonian Oil Shales: Low Temperature Thermochemical Conversion Caused Changes in Swelling. 2010.

25. **Triin Märtson**. Methodology and Equipment for Optical Studies of Fast Crystallizing Polymers. 2010.

26. **Deniss Klauson**. Aqueous Photocatalytic Oxidation of Non-Biodegradable Pollutants. 2010.

27. **Oliver Järvik**. Intensification of Activated Sludge Process – the Impact of Ozone and Activated Carbon. 2011.

28. **Triinu Poltimäe**. Thermal Analysis of Crystallization Behaviour of Polyethylene Copolymers and Their Blends. 2011.

29. **Mariliis Sihtmäe**. (Eco)toxicological Information on REACH-Relevant Chemicals: Contribution of Alternative Methods to *in vivo* Approaches. 2011.

30. **Olga Velts**. Oil Shale Ash as a Source of Calcium for Calcium Carbonate: Process Feasibility, Mechanism and Modeling. 2011.

31. **Svetlana Jõks**. Gas-Phase Photocatalytic Oxidation of Organic Air Pollutants. 2012.

32. **Aleksandr Dulov**. Advanced Oxidation Processes for the Treatment of Water and Wastewater Contaminated with Refractory Organic Compounds. 2012.

33. **Aleksei Zaidentsal**. Investigation of Estonian Oil Shale Thermo-bituminization in Open and Closed System. 2012.

34. **Dmitri Šumigin**. Composites of Low-Density Polyethylene and Poly(Lactic Acid) With Cellulose and Its Derivatives. 2014.

35. **Aleksandr Käkinen**. The Role of Physico-chemical Properties and Test Environment on Biological Effects of Copper and Silver Nanoparticles. 2014.

36. **Ada Traumann**. Improvement of Work Environment through Modelling the Prevention of Health Risks Focusing on Indoor Pollutants. 2014.

37. **Marika Viisimaa**. Peroxygen Compounds and New Integrated Processes for Chlorinated Hydrocarbons Degradation in Contaminated Soil. 2014.

38. **Olga Budarnaja**. Visible-light-sensitive Photocatalysts for Oxidation of Organic Pollutants and Hydrogen Generation. 2014.

39. **Jelena Hruljova**. Role of Specifically Interacting Solvents in Solvent Swelling of Kukersite Oil Shale Kerogen. 2014.

40. **Irina Klimova**. Modification of Ammonium Nitrate Fertilizer. 2014.

41. **Julia Krasulina**. Upgrading of Liquid Products from Estonian Kukersite Oil Shale by Catalytic Hydrogenation. 2015.

42. **Irina Epold**. Degradation of Pharmaceuticals by Advanced Oxidation Technologies in Aqueous Matrices. 2015.

43. **Kadriann Tamm**. Leaching of the Water-Soluble Calcium Components of Oil Shale Waste Ash. 2016.

44. **Galina Sharajeva**. Thermochemical Destruction of Graptolite Argillite. 2016.

45. **Juri Bolubajev**. Effects of Organic Reducing Agents on the Fenton-like Degradation of Contaminants in Water with a Ferric Sludge Reuse. 2016.